



Departamento de Física

Electronic Modelling of Complex Dynamics

Alexandre Wagemakers

Universidad Rey Juan Carlos

Madrid, 2008

Miguel Ángel Fernández Sanjuán, Catedrático de Universidad del Área de Física Aplicada y Director del Departamento de Física de la Universidad Rey Juan Carlos

CERTIFICA:

Que la presente memoria de tesis doctoral, titulada “*Electronic Modelling of Complex Dynamics*”, ha sido realizada bajo mi dirección por Alexandre Wagemakers para optar al grado de Doctor por la Universidad Rey Juan Carlos.

Y para que conste que la citada tesis reune todos los requisitos necesarios para su defensa y aprobación, firmo el presente certificado en Móstoles a treinta de julio de dos mil ocho.

Móstoles, 30 de julio de 2008

Fdo. Miguel Ángel Fernández Sanjuán
Catedrático de Física Aplicada
Director del Departamento de Física
Universidad Rey Juan Carlos

Agradecimientos

Esta tesis no se hubiera podido crear sin el afortunado concurso de varias personas. No es nada más que el resultado del apoyo y de los esfuerzos de muchos compañeros con los que he podido contar para su realización. Sin embargo destacaré especialmente aquí, a mi Director de tesis, el Catedrático de Física Aplicada Miguel Ángel Fernández Sanjuán, el cual ha sido el iniciador y el incentivo constante para llevar a cabo el trabajo que aquí presento. En el transcurso de estos cuatro años me ha iniciado al mundo de la investigación y me ha proporcionado numerosos contactos y el todo el apoyo financiero para llevar a cabo mi tesis.

Además, durante el proceso de realización de la misma, he tenido la suerte de colaborar con distintos investigadores de prestigio, cuya valiosa ayuda ha sido imprescindible para la elaboración de los trabajos de investigación.

A Luís Vázquez Martínez quien me ayudó mucho cuando empecé la tesis y siguió apoyándome, en particular con el grupo especializado en Ciencias de la Vida de la Real Sociedad Española de Física.

A Kazuyuki Aihara por invitarme a trabajar en su Laboratorio en la Universidad de Tokyo, donde tuve la oportunidad de conocer a numerosos investigadores de renombre.

A Jordi García Ojalvo por haberme ayudado a empezar el tema de la Biología Sintética.

A Stéphane Binczak por recibirme en la universidad de Bourgogne en Dijon, donde hemos podido estudiar la implementación de modelos de neuronas en tiempo discreto en circuitos FPGA.

A José Manuel Casado que me aportó una ayuda muy valiosa para escribir mi primer artículo sobre el modelo de Morris-Lecar.

A Borja Ibarz con el que he podido colaborar en el marco de la acción integrada Hispano-Francesa con la universidad de Bourgogne.

A Antonio Coloma y Oscar de Luis del grupo de Biología Molecular de la

Universidad Rey Juan Carlos por el asesoramiento en redes de regulación genética y por el soporte experimental en Biología Sintética.

A Luís Vázquez, Inés Pérez, José Manuel Casado, Antonio Coloma y Ezequiel del Rio por haber aceptado ser miembros del Tribunal de esta tesis. También a mi compañero de departamento Samuel Zambrano que me ha hecho compartir su entusiasmo por la investigación a lo largo de estos cuatro años en la URJC.

A Jesús Seoane, Juan Antonio Almendral, Javier Buldú, Irene Sendiña, Inmaculada Leyva, Francisco Escribano, Inés Pérez, Jacobo Aguirre, y a todos los compañeros de la Universidad Rey Juan Carlos que me han transmitido su pasión por la ciencia y la docencia.

El trabajo de investigación que ha dado lugar a esta tesis doctoral se ha beneficiado de los siguientes proyectos de investigación: BFM2003-03081 del Ministerio de Ciencia y Tecnología, FIS2006-08525 del Ministerio de Educación y Ciencia, URJC-CM-2006-CET-0643 de la Comunidad de Madrid y Universidad Rey Juan Carlos y PPR-2004-28 de la Universidad Rey Juan Carlos, el proyecto PCI-Mediterráneo España-Túnez 2007 así como de la Acción Integrada Hispano-Francesa HF04-173 del Ministerio de Ciencia y Tecnología. Igualmente se ha beneficiado por parte de la Universidad Rey Juan Carlos de dos becas de ayuda a la movilidad para la realización de estancias predoctorales en Universidades y Centros de Investigación extranjeros dentro del Programa Propio de Investigación que tuvieron lugar en la Universidad de Tokio (Japón) de septiembre a diciembre de 2005 y en la Universidad de Boston (EEUU) de septiembre a diciembre de 2006.

Preface

This Ph.D. thesis focuses on the modelling and simulation of various nonlinear systems with complex behavior. One of the objectives of the work is to give a different point of view on the study of a class of nonlinear dynamical systems. We present several models that have been studied in detail with both non-linear circuits and numerical simulations. Some models presented here are biologically inspired, as it is the case in Chaps. 2 and 3, whereas the other circuits presented exhibit a chaotic dynamics. The variety of subjects discussed reflects the possibilities of this technique as a tool for the study of complex systems. We briefly describe the contents of the chapters forming this thesis.

- **Chapter 1** introduces briefly the concept of electronic simulation of complex dynamics. The concepts of dynamical systems and complex dynamics are presented with simple examples, followed by a short discussion on the advantages of using electronic circuits for the modelling of complex systems.
- In **Chap. 2** the dynamics of a neuron model is described by means of analog circuits. The Morris-Lecar model expresses the membrane voltage of a clam muscle fiber, which exhibits spiking oscillations under the action of an external excitation. The model lies on the mathematical representation with differential equations of the dynamics of the membrane ionic channels. The bifurcation structure of this model is explored as the parameters of the model are spanned in a two dimensional space. A complex bifurcation structure is found numerically and experimentally. Furthermore this work investigates how the model can be modified in order to obtain a bursting oscillatory pattern which is a periodic repetition of brief spiking activity followed by a silent period.

- **Chapter 3** deals also with a biologically inspired model. The electronic circuits are used in this chapter in order to reproduce the dynamics of a coupled genetic oscillator. The oscillator, called the repressilator, consists of three genes whose concentration of expressed proteins oscillates periodically. These oscillators can be coupled in such a way that a global synchronization is obtained. We demonstrate that the synchronization can be obtained with in-phase oscillations. It is also shown that a periodical forcing can synchronize a population of repressilators. We propose a plausible biological model which is simulated by the use of circuits. Finally, we discuss the simulation of other gene networks. In particular we describe the model of a genetic oscillator with delay whose oscillations are caused by the lag in the production of the proteins and the self-repression. Another system described here is a genetic switch made of two mutually repressive genes.
- In **Chap. 4**, the coupling of chaotic oscillators is treated and simulated with circuits. When we dealt with coupled systems in Chap. 3, we made the assumption about instantaneous transmission of the information which may not be true. We ask in this part about the role of the delay in this kind of synchronization. As two oscillators are coupled and synchronized, the introduction of a delay on the transmission line may destabilize this synchronization. We use chaotic oscillators in order to study the synchronization of two and three coupled units with delay. Different scenarios arise depending on the type of coupling. With two oscillators, synchronization is not possible. However as a feedback with delay is added to the oscillators, both circuits synchronize perfectly. When three units are coupled in a line, in some particular configuration of coupling the synchronization of the outer two is obtained whereas the central unit remains behind or in advance compared with the other oscillators. An experimental verification of this phenomenon is offered by using Chua's circuits.
- **Chapter 5** hints that it is possible to send an encrypted message as two chaotic circuits are coupled bidirectionally with delay on a transmission line. Moreover, the message can be sent and recovered by the two coupled units at the same time. We describe how it is possible to send and to receive a message with this experimental setup. This is the first experimental setup of this kind at the moment of the writing of this

Ph.D. thesis.

- In **Chap. 6** we summarize the most relevant points of this thesis.

Contents

Preface	v
1 Introduction	1
1.1 Simulation of complex dynamics	1
1.2 Dynamical systems	3
1.3 Why to use electronic circuits?	6
1.4 Modelling with circuits	8
1.5 The models	10
Bibliography	12
2 The electronic simulation of a neuron model	15
2.1 Introduction	15
2.2 The Morris-Lecar Circuit	18
2.3 Experimental bifurcation diagrams	22
2.3.1 $I - V_3$ diagram	23
2.3.2 $I - V_4$ diagram	25
2.3.3 $I - \tau$ diagram	26
2.4 The design of bursters	30
2.4.1 Square wave burster (“Fold/homoclinic” burster)	32
2.4.2 Elliptic burster (“subHopf/fold cycle” burster)	33
2.4.3 Circle/Fold cycle burster	34
2.5 Conclusions	35
Bibliography	37
3 The analog simulation of genetic networks	41
3.1 Molecular biology and nonlinear dynamics	41
3.2 Analog simulation of the repressilator	43
3.3 The electronic repressilator	46

3.4 Alternative implementation with operational amplifiers	49
3.5 Coupling electronic repressilators	51
3.6 Forcing electronic repressilators	53
3.7 Simulations of others genetic networks	59
3.7.1 The electronic toggle switch	59
3.7.2 The delay oscillator	64
3.8 Conclusions	66
Appendix I: Exact model of the repressor circuit	68
Bibliography	71
4 Synchronization of coupled systems with delay	75
4.1 Introduction	75
4.2 Mutually coupled chaotic circuits	76
4.3 Isochronous synchronization in three coupled circuit	83
4.4 Replacing the relay system	86
4.5 Conclusions	87
Appendix I: Coupling and delay board	89
Bibliography	90
5 Application of isochronous synchronization	93
5.1 Introduction	93
5.2 Experimental Setup	94
5.3 Isochronal synchronization	97
5.4 Bidirectional communication	100
5.5 Conclusions	103
Appendix I: Bifurcations of the Mackey-Glass model	104
Bibliography	110
6 Conclusions	113
Curriculum Vitae	115
Resumen	121

Chapter 1

Introduction

The diversity of subjects presented in this Ph.D. thesis is the result of discussions with scientists with different backgrounds and points of view. The interdisciplinary nature of the contents is a sign that a common methodology can be used with different systems. We propose a different insight to the modelling of complex dynamical systems by using analog electronic circuits. The common aspect to all the work collected in this Ph.D. thesis is the study of the dynamics of complex systems from different fields such as electronics, neurodynamics or genetic engineering.

1.1 Simulation of complex dynamics

Dynamics and the study of dynamical systems could be described as the science of motion. The word dynamics comes from the ancient Greek *δυναμικός*, which means power or force, and thus is related to the study of forces which originate the movement. The efforts made since the 17th century in giving a mathematical abstraction to these evolving objects gave the framework of the dynamical systems theory.

A physical system, in general, can be represented by a model based on a set of equations which is an abstraction of the reality. The study of this set of equations can give information on the object without making any further physical observations, in other words, we can draw conclusions on the behavior of the system without experimentation. The method by which the behavior of the system is studied through the set of equations is called simulation. This powerful method of prediction can also be used in another

context: the control of the dynamical system. The information on the system allows to develop a method to control undesired behaviors or to maintain the system in a desired dynamical regime.

These equations describing the model should be analyzed with some of the multiple techniques available to the experimenter. Here we present a method of simulation with electronic circuits that gives fruitful results in different fields of applications. Analog simulations have been used in different contexts such as chaotic dynamics [1], neuroscience [2, 3, 4], lasers [5], communication systems [6] and recently for the study of stochastic phenomena [7]. In this Ph.D thesis we introduce the simulation of complex systems by using analog circuits.

There are several definitions of a complex system in the scientific community and there are different definitions of the complexity depending on the subject of study. In our case, a complex system can be decomposed in simple components which can be modeled and simulated individually. These components can exhibit different dynamics, and even complex behaviors such as chaotic oscillations, that can be studied with all the available tools of the linear and nonlinear dynamics. However, these sub-units can interact with each other in a very complex and nonlinear way. The sum of all the individual behaviors can be dramatically different as they are connected into a network. In that case the study of the entire system is also necessary since new behaviors that were not present in the individual parts can now emerge in a connected system.

The methodology followed in this Ph.D. thesis consists in first studying the individual part and then growing in complexity by interconnecting different elements between them. This method is perfectly suited to the use of electronic circuits since the first step is to construct the basic elements with the available tools and studying them in order to characterize their behavior. These basic elements are then reproduced and interconnected for the analysis of the dynamics on different levels of complexity.

We must underline here that the method of studying a system from the smallest part to the most complex and organized one is called the bottom-up approach. This is the usual technique used in engineering during the design process of any system. The traditional scientific procedure is on the opposite side. It consists on studying an object from the highest level of detail to the smallest one. We propose here a different approach that gave fruitful results in different fields such as the synchronization of chaotic oscillators, neural systems modelling or even the genetic engineering.

1.2 Dynamical systems

The initial motivation of the study of dynamical systems comes from Classical Mechanics, where the need for a mathematical formalism to study the time evolution of the objects gave one of the most important theories in physics. Dynamics is strongly linked to the study of the trajectory of objects in space. However, it is now an abstract framework that can be applied to any evolution problem.

First, a dynamical system is represented by a set of variables, continuous or discrete, representing all the states of our system. This set is a description of the relevant quantities that are evolving, such as the space, temperature, speed or whatever. For convenience we will represent these variables in form of a vector

$$\mathbf{x} = \begin{pmatrix} x_1 \\ x_2 \\ x_3 \\ \dots \end{pmatrix}. \quad (1.1)$$

The number of variables and the set of definition depends on the system. The set of all possible states of the system is called the phase space, and a particular numerical value of this vector is a point of this space.

Now that the states are described by this set of variables, we need some rules to find out the evolution. In all the examples proposed in this Ph.D. thesis, we will refer to time evolution. This progression is determined by a differential equation which is a function of time and \mathbf{x} . It links the instantaneous variation of the system to its actual position \mathbf{x} . In other words, the position in the near future is a function of the actual position and eventually the time. It means that if we know the position at the time t with an infinite precision, we are able to reconstruct all the future states of the system. In this case we talk of a deterministic system. In general, a dynamical system can be written as:

$$\frac{d\mathbf{x}}{dt} = \mathbf{f}(\mathbf{x}, t) \quad (1.2)$$

$$\mathbf{x}(t_0) = \mathbf{x}_0. \quad (1.3)$$

The Eq. (1.2) determines the evolution of the system. The left term $d\mathbf{x}/dt$ is the instantaneous temporal variation of the variable \mathbf{x} , while the right term

is a function of the variable \mathbf{x} and time in the form:

$$\mathbf{f}(\mathbf{x}, t) = \begin{pmatrix} f_1(x_1, x_2, \dots, t) \\ f_2(x_1, x_2, \dots, t) \\ f_3(x_1, x_2, \dots, t) \\ \dots \end{pmatrix}. \quad (1.4)$$

This function and the initial condition $\mathbf{x}(t_0) = \mathbf{x}_0$ contain all the behavior of the system, this is the model of the system. A particular trajectory $\mathbf{x}(t)$ with the precedent initial condition is called a solution of the differential equation (1.2). This is the first type of differential equation that we will study in this work. The function \mathbf{f} generally depends on a set of parameters $\mu = \{\mu_1, \mu_2, \dots\}$ that links the variable $\{x_1, x_2, \dots, t\}$ in a linear or nonlinear manner. This set of parameters can strongly influence the dynamics of the system. The dynamics in function of a parameter is studied through the bifurcation diagram. This diagram represents the different possible regimes of the system as one or several parameters are varied. These plots provide a substantial knowledge on the system if we are looking for a particular dynamical regime. In Chap. 2, we present such diagrams as two parameters of the system are varied. In this case oscillatory regimes can appear or vanish.

The differential equations will appear where an evolution problem has to be solved. Solving this equation analytically in most cases is an impossible task. This is one of the purposes of the presented work to propose methods to obtain such solutions.

Later on in this thesis, we show how to simulate differential equations when a delay is present in the problem. In the case of the equation with delay the instantaneous variation of the variable depends on the present state and also from the past states at an previous time τ . The differential equation becomes:

$$\frac{d\mathbf{x}}{dt} = \mathbf{f}(\mathbf{x}(t), \mathbf{x}(t - \tau), t) \quad (1.5)$$

$$\mathbf{x}_0 = \{\mathbf{x}(t) \text{ for } -\tau \leq t \leq 0\}. \quad (1.6)$$

The initial conditions of Eq. (1.6) in this case should be defined for the values of the trajectory during the time $t \in [-\tau, 0]$. This dependence on the past states can have a dramatic effect on the evolution of the system. To illustrate these effects we will take a very simple example of differential equation:

$$\frac{dx}{dt} = -ax + b, \quad (1.7)$$

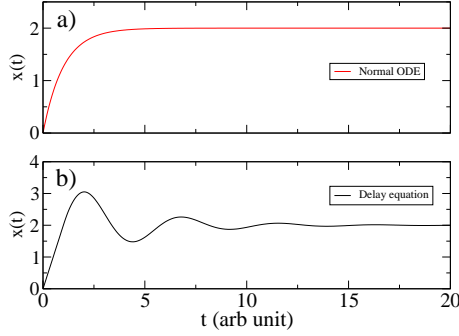


Figure 1.1: *Time evolution of two differential equations. (a) The solution of the equation without delay is plotted. (b) The solution of the same equation with delay is shown. In this second case the oscillations appears due to the effect of the delay.*

with $x(0) = 0$. The solution of this equation is straightforward:

$$x(t) = \frac{b}{a}(1 - e^{-at}). \quad (1.8)$$

The time evolution of this equation is shown in the Fig. 1.1 (a). Now suppose that the system has a memory of its past state and the system depends on a delay:

$$\frac{dx}{dt} = -ax(t - 1) + b. \quad (1.9)$$

The time evolution of this equation is no longer so simple. In Fig. 1.1 we show the difference for the time evolution of the two equations. When a delay is introduced in the system, the trajectory oscillates before stabilizing to the steady state value. Different tools are necessary to find the solution of this kind of equation. The electronic circuits are good candidates for the implementation of differential equations with delay.

Nevertheless, the use of electronic circuits as a tool of simulation can be questioned for such systems, and specifically, which are the advantages of using this particular kind of simulation technique. A short discussion about the benefits and the inconveniences is necessary before starting the description of any particular system. In the section (1.3), we expose the main arguments of the discussion.

1.3 Why to use electronic circuits?

Here we give a small discussion about the possible advantages and drawbacks of using electronic circuits:

1. First of all, an analog circuit is a physical system. It means that the behavior of the system, which is reflected by the electrical variable, can be observed with a measurement. The system ceases to be a mathematical object and becomes a physical object.
2. The fact that the system can be implemented in a electronic circuit means that it is robust to small parameter changes. The components are not perfect and their nominal values change from component to component which implies that if the circuit works the model is not sensitive to these small differences.
3. The mathematical models of the components are not perfect, they may be subjected to nonlinearities and influenced by external factors such as the temperature. The noise is present in all the variables of the circuit and it may affect the dynamics of the circuit in one way or another. The resistance to noise is another kind of robustness. The noise due to the thermal agitation of the carriers is present in every electronic component and increases with the number of parts.
4. For the practical benefits of using electronic circuits, we can comment that building an electronic circuit from a theoretical model can lead to interesting applications. The most striking example is perhaps the electronic circuits which interact with real systems, *e.g.*, neurons by reproducing their behavior [2], or even neurocomputers which are inspired by the information processing of real neurons.
5. In order to explore the dynamics of the model, the electronic circuits can have several advantages compared with the numerical simulations. For example, the numerical integration of complex models may last minutes, or even hours, while it is really faster with the electronic circuits.
6. Another interesting point is that it is possible to change the parameter directly. For example, if a resistor controls the time constant of an integrator, a simple variation of this resistor changes the dynamics in real

time. In many cases, the exploration of the parameter space is faster than using numerical simulations, however the analysis of the corresponding time series may be longer. To overcome this difficulty, it is possible to develop electronic tools, useful when the dynamical system has a chaotic dynamics, such as automatic analysis of the bifurcation diagram and the Poincaré sections [8].

7. The construction of the circuit by itself is a very instructive process. One can see how the dynamics of the system appears as the elements are connected. Moreover, as the parameters are changed the experimenter can see unexpected results in the dynamics. Seeing chaos in a electronic circuit and observing the route to chaos is a wonderful experience.

On the other hand, the realization of electronic circuits may be subject to several criticism. The inconveniences can also be separated in two parts, mainly practical and theoretical.

1. Often, there is nothing that you see in the circuit that you cannot see with the numerical simulation. In this case, the electronic circuit is nothing more than a practical confirmation of the theoretical results. One can say that this is not a “real experiment”, that it is just an analog integrator of a mathematical model. This is in part true, but we stress on the fact that it remains an experiment in a physical system.
2. The robustness to noise mentioned before can also be regarded as a problem if we are looking for a particular behavior in a small range of parameters. These mismatches may be a problem if we want to observe this particular dynamical regime.
3. Constructing circuits may have also some inconveniences on the practical aspects. Building a circuit may be a hard task of design and assembly. The time spent to construct the circuit may be longer than programming the numerical simulations. as long as some systems are difficult to implement. For example when they include multipliers the complexity of the design may increase.

Still, the analog circuits are a good tool for the simulation of certain equations, such as systems with delay, since they can integrate accurately very complex equations in a very short time. The use of circuits is a potential alternative, or at least a complement, to the numerical simulation of complex systems.

1.4 Modelling with circuits

Before describing the models which are at the core of this work, we present the motivations of the use of the analog circuits for the simulation and modelling.

The basic components used in analog electronic circuits, such as resistors, capacitors and transistors, can be described with the laws of electromagnetism. Deduced from these fundamental laws, a model of the component describes its macroscopic behavior which is the relation between current and voltage. The model consists, in general, in a linear (or nonlinear) differential equation. An association of these components would represent a set of differential equations which can be solved by letting the circuit evolving freely, after setting the initial conditions.

Fairly simple models are used for these components in order to express the relation between the voltage and the current. In the case of the transistor the models are rather more complex, which will be treated later on. Here we present the simplest components (resistors and capacitors) needed to simulate a differential equation. The resistor from the point of view of dynamical systems is a simple linear gain, more precisely, it can be considered from a physical point of view as a dissipative device. The equation of a simple resistor expresses the relation between the current and the voltage in function of the resistance R by using Ohm's law:

$$V = Ri. \quad (1.10)$$

We have a linear relation between the current and the voltage which depend on the physical characteristics of the resistance. The second elementary component that is commonly used is the capacitor. A simple model of the capacitor is two conductive plates opposed to each other and connected to a different electric potential.

In this configuration charges are accumulated on each plate. More generally, the relation between the voltage difference between plates and the flow of charges, which is the current, is

$$C \frac{dV}{dt} = i. \quad (1.11)$$

The current that flows across the device is the derivative of the voltage and C is the capacity of the capacitor which is a physical property of the device. The capacitor can also be viewed as a current integrator:

$$V(t) = \frac{1}{C} \int_{-\infty}^t i(x) dx. \quad (1.12)$$

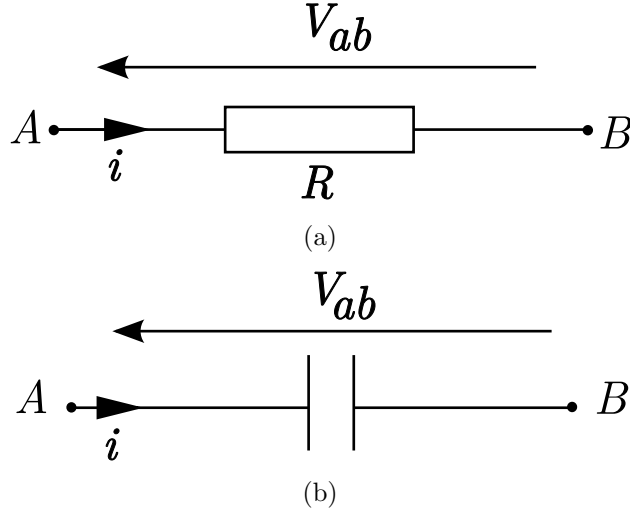


Figure 1.2: Normalized schemes of a resistance and a capacitor, the voltage across the component is V_{ab} and the current is i . (a) represents a resistor and (b) a capacitor.

These are the basic necessary elements to construct a circuit that simulates a differential equation. In order to illustrate the method to simulate such equations, we present a very simple example of a first order differential equation:

$$\frac{dy}{dt} = -\alpha y + \beta. \quad (1.13)$$

The equivalent circuit of this equation is presented in Fig. 1.3. The capacitor integrates the current i as written in Eq. (1.11). By using the Kirchhoff law and the Ohm law we deduce that the current is proportional to the voltage drop in the resistance:

$$i = \frac{(E - V)}{R}. \quad (1.14)$$

The complete differential equation of the circuit can now be written as:

$$RC \frac{dV}{dt} = E - V. \quad (1.15)$$

To simulate the Eq. (1.15) it is now necessary to identify the constants β and α :

$$\alpha = \frac{1}{RC},$$

$$\beta = \frac{E}{RC}.$$

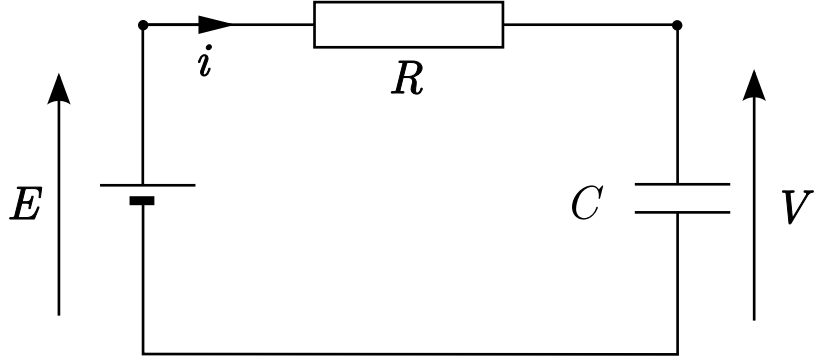


Figure 1.3: *Simple example of the simulation of a first order differential equation. The circuit is composed of a resistor, a capacitor and a DC voltage source.*

The initial conditions of the equation are more delicate to choose. However it is easy to start with the capacitor discharged and the voltage source turned off, that is, with $V = 0$ and $i = 0$.

The voltages and currents in the circuit simulate the variables that can later be observed, recorded and analyzed by using a standard laboratory equipment. Several classes of differential equations can be simulated by this mean:

- Ordinary differential equations (ODEs).
- Non autonomous differential equations.
- Delay differential equations.

For each class of equation we propose several examples along this work, as for instance, the ODEs which are simulated in Chap. 3, correspond to a small genetic network. The non autonomous equations with a forced oscillator and the delay equations are treated in Chap. 5.

1.5 The models

The first work presented in this Ph.D. thesis is centered in the neuroscience context. The nervous system is a typical example of a complex system where the interconnection of the basic units (which are the neurons) gives birth to very complex dynamics and behaviors.

The purpose of this first work is the exploration of the parameter space of a simple neuron-model. The Morris-Lecar model expresses the membrane voltage of a clam muscle fiber, which exhibits spiking oscillations under an external excitation. The spiking activity is a typical electrical activity of the neurons by which the information is transmitted and it travels along the axons, which are the links between the neurons. The spikes are brief pulses of current that circulate along the membrane of the neuron. The modelling of the neuron is based on differential equations which describe accurately the dynamics of the system. The dynamical properties of the system are explored with circuits and later on used to construct a new neuron type: a burster, which is a neuron with periodic repetition of brief spiking activity followed by silenced period. This is an example of how the circuits can be useful to construct a system with a different dynamics.

In the following chapters a different biological system is studied. In Chap. 3 we deal with the simulation of a genetic process. In this chapter, we propose a new approach for the simulation of a genetic network with the modelling of a biological oscillator with analog circuits. A single oscillator is constructed with electronic components, as an analogy to the genetic one. Next, this unit is connected to similar circuits in order to observe the effects of the coupling in a population of oscillators. As in biological clocks, which consist in coupled oscillators with an external forcing due to environmental changes, we introduce a periodical forcing in the coupled system and we determine the conditions in which the system is entrained. Several other genetic systems can be modeled as shown in Chap. 3, where we also analyse the influence of the delay on the dynamics of the system.

The coupling between oscillators has been extensively investigated during many years and it is still a hot topic. As we mentioned before the coupling of oscillators appears not only in many biological processes but also in mechanical/electronic/physical/social phenomena. Chapter 4 deals with the study of the synchronization of oscillators when the coupling is not instantaneous, *i.e.*, when a delay is present in the transmission of the information. The classical concept of synchronized state is modified in this context. When two chaotic oscillators are coupled with delay, there is a case where the system is alternatively forcing and forced by its counterpart. This state is called achronal synchronization. Chaotic circuits are used in order to measure the effect of this peculiar synchronization, however the conclusions can be extended to any other system. When a feedback is introduced in the oscillator, another kind of synchronization appears, the isochronous state. In this case

we observe exactly the same dynamics at the same moment despite the delay on the transmission line. This isochronous state is observed not only in two coupled systems but also in an array of three coupled oscillators. We give an experimental observation of the isochronous synchronization between two circuits with a third relaying circuit in the middle.

As a possible application of this peculiar synchronization, we demonstrate experimentally that a message can be transferred between two peers with a chaotic masking scheme. The message is sent along with a chaotic carrier that hides the information within the broad spectrum of the chaotic signal. The bidirectional communication is possible in the sense that the message can be sent in both senses at the same time. This configuration may be used in some particular application as for example the negotiation of secret keys.

References

- [1] L.O. Chua , “The Genesis of Chua’s Circuit”, *AEU* **46**, 250 (1992).
- [2] A. Szûcs, P. Varona, A.R. Volkovskii, H.D.I. Abarbanel, M.I. Rabinovich and A.I. Selverston, “Interacting biological and electronic neurons generate realistic oscillatory rhythms”, *Neuroreport* **11**, 563-569 (2000).
- [3] S. Le Masson, A. Laflaquiere, T. Bal and G. Le Masson, “Analog circuits for modeling biological neural networks: design and applications”, *IEEE Trans. on Biomed. Eng.* **46**, 638-645 (1999).
- [4] G. Roy, “A simple electronic analog of the squid axon membrane”, *IEEE Trans. on Biomed. Eng.* **19**, 60-63 (1972).
- [5] F. T. Arecchi, L. Fortuna, M. Frasca, R. Meucci, and G. Sciuto, “A programmable electronic circuit for modelling CO₂ laser dynamics” , *Chaos* **15**, 043104 (2005).
- [6] K.M. Cuomo and A.V. Oppenheim, “Circuit implementation of synchronized chaos with applications to communications”, *Phys. Rev. Lett.* **71**, 65-68 (1993).
- [7] T. Stemler, J. P. Werner, H. Benner, and W. Just, “Stochastic Modeling of Experimental Chaotic Time Series”, *Phys. Rev. Lett.* **98**, 044102 (2007).

- [8] C.K. Tse, in *Chaos in Circuits and Systems*, Edited by G. Chen and T. Ueta, (World Scientific, Singapore, 2002).

Chapter 2

The electronic simulation of a neuron model

2.1 Introduction

Nowadays the interface between electronic circuits and biological systems is attracting a great deal of research due to the enormous variety of potential applications of electronic devices to the general field of biomedical sciences. Even a connection of an electronic circuit with biological neurons is now possible [1, 2]. As a consequence of this fact, new disciplines such as biomedical engineering or bionics are reviving. From a theoretical viewpoint, the modelling of neurons is becoming more and more accurate, and the electrical behavior of neurons is well reproduced at a quantitative level by the increasingly complex mathematical models that are used in computational neuroscience. In this context, the modelling of neurons by means of electronic circuits is a steady growing field that presents rich potentialities for the design of specific hardware that is able to display some useful characteristics for the processing of information in real time.

Experimentation on real neurons is a hard and expensive task, nevertheless part of these difficulties can now be solved to some extent with the help of artificial neurons. Computational neuroscientists can profit from the use of electronic devices as a tool for the exploration in real time of the behavior of neuron models [3, 4]. As a consequence, a network of artificial neurons can be emulated this way and tested in a real time environment. The devices connecting such circuits with biological neurons are called hybrid networks

[5, 6], and the achievements of these tools in the biomedical sciences are immense. Artificial vision and audition [7] or spinal cord stimulation for hemiplegic patient are some examples.

Neurons are cells forming part of the nervous system of the evolved multicellular living being. This particular cells are capable of the processing and the transmission of the information by mean of electric impulses which are called spikes. Depending on the kind of animal we are looking at, the neurons will have different shapes and properties. However most of them are composed of three main sections. The soma is the main part of the cell which contains the nucleus and the components necessary for the survival of the cell within the body. Joint to the soma, the dendrites are the receptor of the nervous activity of other neurons. These received signals are processed, and if the condition are matched then a nervous response is produced. This response takes the form of a electrical pulse, called a spike, transmitted along the axon which is the afferent ending of the neuron. This spikes will then activates other neurons and so forth. The information is processed through this large amount of connections among neurons. The shape and the frequency of the spikes can be very different from one neuron to another. In the general case, the duration of this pulses is of a few milliseconds of duration and a few milivolts of amplitude. They can be generated individually (with a resting time before the following spike), or in burst of several spikes with a silent period before the next burst of pulses. The cell generating these patterns are called bursters. Bursters are a class of neurons which are present in many areas of the brain and whose autonomous activity displays periods of fast spiking alternated with resting or silent intervals. Furthermore, an external current can modulate the bursting response of those neurons and the coupling between bursters can lead to very complex synchronization patterns [8]. An extensive review on the dynamics of the neurons can be found in [9].

In this chapter we propose an electronic implementation of a simple model of the giant barnacle muscle fiber developed by Morris and Lecar in 1981 [10]. The Morris-Lecar model is a characteristic example of a simple dynamical system presenting a rich and wide variety of dynamical behaviors (see for instance [10] and [11]). It uses only two dynamical variables to describe the state of the neuron and thus allows us a straightforward observation of the phase plane. In fact, with the help of an oscilloscope it is possible to visualize the attractors in real time. Moreover, depending on the parameters of the model, it presents Hopf (subcritical and supercritical), saddle-node and tangent bifurcations which can be easily observed. By examining these bi-

furcations, when two parameters are varied, we can observe some interesting codimension-2 bifurcations taking place in the system. A similar experimental work with electronic circuits has been achieved by [12] with a modified FitzHugh-Nagumo neuron model and in [13] in which a bifurcation diagram varying only one parameter for the Morris-Lecar neuron model is carried out. The phase plane of the Morris-Lecar model has been extensively explored in [14] with bifurcation analysis and numerical simulations. This work investigates the bifurcations in a five-dimensional space. Nevertheless the method proposed here is experimental.

We have analysed the Morris-Lecar phase plane to develop a method to obtain bursting behavior. The rather complex behavior of a burster is due to the coexistence of multiple attractors so that the phase point passes through a succession of different pseudo-attractors as it traces a closed orbit through the phase space [15]. By finding out regions showing bistable behavior in the Morris-Lecar model, we can construct a great variety of bursters [16]. To do that, we take advantage of the hysteretic behavior of the system, leading to paths in the phase plane that are different depending in the way the parameter is varied. In our case the fundamental control parameter will be an external excitatory current delivered to the neuron. By choosing an appropriate dynamics for this current we can allow the system to hop between coexisting states thus giving rise to bursting activity patterns. In [17] a design of a burster neuron based on the FitzHugh-Nagumo model has been proposed, where an external forcing current is applied so that the model exhibits bursting activity. The parameters of the perturbation are based on the analysis of a two-parameter bifurcation diagram. In our work, since the excitation current is an internal variable of the system, the burster is autonomous. As examples of our methodology we present a square wave (or fold/homoclinic) burster, an elliptic (sub-Hopf/fold cycle) burster and a cycle/fold burster, all of them obtained from the dynamics of the Morris-Lecar neuron model [16].

The organisation of the chapter is as follow. In Sec. 2.2 we present the Morris-Lecar model and its electronic implementation. The bifurcations of the circuit are analysed in Sec. 2.3. In Sec. 2.4 we present a method for the design of electronic bursters and finally we summarize our results in Sec. 2.5.

2.2 The Morris-Lecar Circuit

The Morris-Lecar model was originally developed as a mathematical model of the giant barnacle muscle fiber [10]. It belongs to the class of the so-called conductance models and uses a calcium current, a potassium current and a leaky ohmic current to phenomenologically describe the behavior of the muscle fiber. As the dynamics of the calcium channels is much faster than that of the potassium channels, we will consider the former always in the equilibrium state, thus reducing the model to the following system of two first order differential equations:

$$C \frac{dV_m}{dt} = -g_{Ca}^* M(V_m)(V_m - V_{Ca}) - g_K^* N(V_m - V_K) - g_L(V_m - V_L) + I, \quad (2.1)$$

$$\frac{dN}{dt} = \lambda_N(V_m)(-N + G(V_m)), \quad (2.2)$$

where V_m is the membrane voltage, N is the activation variable of the slow potassium channels, and I is an external tonic current delivered to the neuron. Notice the voltage dependence on V_m of the time constant λ_N in Eq. (2.2), where its expression takes the following form:

$$\lambda_N(V_m) = \frac{1}{\phi} \cosh((V_m - V_3)/2V_4). \quad (2.3)$$

On the other hand, g_{Ca}^* and g_K^* are the maximal conductances of the calcium and potassium channels, respectively, and g_L is a constant leak conductance. The conductances of the potassium and calcium channels vary in a sigmoidal way with the membrane voltage V_m . This dependence is introduced by the following functions $M(V)$ and $G(V)$:

$$M(V) = 0.5(1 + \tanh((V - V_1)/V_2)), \quad (2.4)$$

$$G(V) = 0.5(1 + \tanh((V - V_3)/V_4)), \quad (2.5)$$

where V_1, V_2, V_3 , and V_4 will be considered as adjustable parameters .

As many other mathematical systems describing the electrical activity of the nerve membrane, a strategy based on the use of electronic circuits is well suited to implement its dynamical behavior. The above set of equations can be represented in a block diagram as shown in the Fig. 2.3 (a). This figure represents the equations of the model schematically and it will be the

basis of the electronic circuit design that is presented in Fig. 2.3 (b). In this figure we can see the three ionic currents which are generated by using the feedback of the voltage membrane V_m into the functional blocks. The calcium current has only one element, the sigmoidal shaped function $G(V)$, whereas the potassium channel includes an integrator for the slow dynamics of this channel and also the variable time constant which depends on V_m . That means that the channel does not open and close instantaneously as the calcium channel does, but rather gradually, with a certain inertia. From the viewpoint of the electronics, this means a first order filter. These three currents are summed up and fed into an integrator to generate the membrane voltage.

In order to further reduce the complexity of the model we can make a strong approximation. Equation (2.2) representing the dynamics of the potassium channel includes a voltage-dependent time constant $\lambda_N(V_m)$. Implementing this parameter in the electronic circuit represents a difficulty. The hard point is to construct a voltage controlled resistor in order to modify the value of the time constant of a RC filter (or the first order filter). These components are mainly nonlinear and they introduce noise and undesirable harmonic components. Furthermore, this time constant has a complex influence in the equation. Nevertheless, when this function is set to a constant, the Morris-Lecar system of equations still exhibits interesting features like a Hopf bifurcation and spiking capabilities. Based on this observation we have reduced the original set of equations to a new set given by

$$C \frac{dV_m}{dt} = -g_{Ca}^* M(V_m)(V_m - V_{Ca}) - g_K^* N(V_m - V_K) - g_L(V_m - V_L) + I, \quad (2.6)$$

$$\frac{dN}{dt} = \tau^{-1}(-N + G(V_m)), \quad (2.7)$$

with the same functions $G(V_m)$ and $M(V_m)$ as in Eqs. (2.4) and (2.5). Here the parameter τ has a *constant* value, that is, it does not depend on the membrane voltage. This parameter has a critical role in the stability of the system because the Jacobian matrix of the linearized system around an equilibrium point has its eigenvalue depending on the parameter τ .

The proposed circuit is displayed in Fig. 2.3 (b). It uses mainly linear components excepts for the analog multipliers and diodes. With this circuit we can now describe the experiments. The main logical blocks are delimited by dashed lines. The calcium block is made of a sigmoidal function, implemented with pn-junction diodes, an operational amplifier, and an amplifier

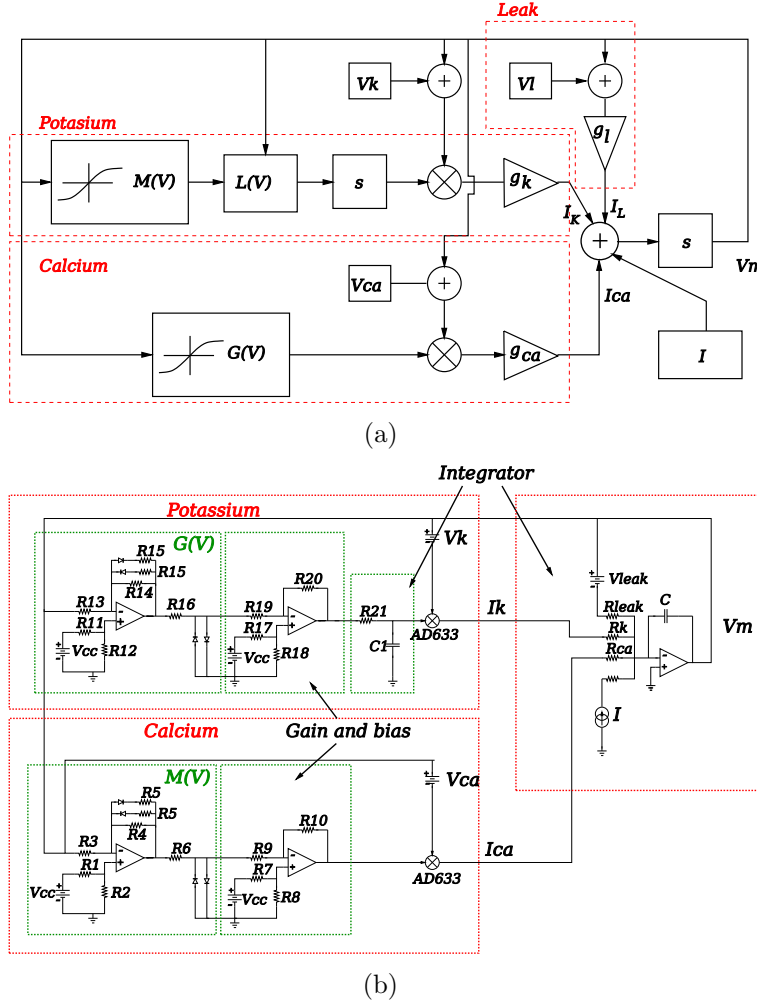


Figure 2.3: (a) Block representation of the Morris-Lecar model. We represent the differential equations in a schematic way; the blocks symbolize integrator, gains, transfer functions and multipliers. This logical representation is the basis of the implementation of the circuit. The blocks representing the ionic currents are delimited by dashed-lines; the Eqs. (2.8) and (2.9) correspond to the currents I_{Ca} and I_K . All the currents are summed and fed into an integrator; the sum of the currents is comparable to the Eq. (2.11). (b) Electronic scheme of the circuit simulating the Morris-Lecar model. The ionic currents are delimited by red dashed lines and correspond to the equivalent blocks in Fig. (a). The ionic currents I_{Ca} , I_K , and I_L are summed and fed into an integrator so that the output is the membrane voltage V_m of the neuron model. The functions $G(V)$ and $M(V)$ are implemented with 1n4148 diodes and with UA741 OP-Amps.

Parameter	Values	Units
τ	$R_{21} \times C_1$	s
V_1	$-V_{cc} \times R_1 / (R_1 + R_2)$	V
V_2	$-0.5V \times R_3 / R_4$	V
V_3	$-V_{cc} \times R_{11} / (R_{11} + R_{12})$	V
V_4	$-0.5V \times R_{13} / R_{14}$	V
V_L	V_{leak}	V
g_{Ca}^*	$1/R_{Ca}$	S
g_K^*	$1/R_K$	S
g_L	$1/R_{leak}$	S
OPAMP	UA741	—
V_{cc}	10	V
Mutiplier	AD633	—

Table 2.1: *Equivalence between the parameters of the model and the parameters of Eqs. (2.6) and (2.7).*

to adjust the gain and the bias. The output signal is fed into an analog multiplier (AD633) and multiplied by the tension V_m . Except for the explicitly specified cases, the parameters used for all the experiments are shown in the Tab. 2.1. The output of this block is the current I_{Ca} which expression is

$$I_{Ca} = g_{Ca}^* M(V_m) \times (V_m - V_{Ca}). \quad (2.8)$$

The potassium current is quite similar, but now we use an analog integrator (a simple RC circuit). The expression of the ionic current can be described with the following two equations:

$$I_K = g_K^* N(V_m - V_K), \quad (2.9)$$

$$\frac{dN}{dt} = \tau^{-1}(-N + G(V_m)). \quad (2.10)$$

The last block, the integrator, sums all the ionic currents and integrate them into a capacitor. The output of this circuit is the membrane voltage V_m . Thus, this variable is the solution of the following differential equation,

$$C \frac{dV_m}{dt} = -I_K - I_{Ca} - I_L + I, \quad (2.11)$$

where I_L is a simple ohmic leak. In the following section we will explore the properties of this circuit.

2.3 Experimental bifurcation diagrams

In this section the equations used for the implementation of the circuit are slightly different. We have scaled the voltage in Eqs. (2.6) and (2.7) so that the observation of the voltage variable is made much easier. The scaling factor is a non-dimensional number $\alpha = 0.120$. We can give the values of the fixed parameters that will be used next, the other parameters will be specified in each case: $V_{Ca} = 1V$, $V_K = -0.66V$, $V_L = 0.5V$, $C = 20\mu F$, and $C_1 = 1\mu F$.

The experimental setup for the measurements of the bifurcation diagram is a simple ADC converter board. For a fixed set of parameters we construct the bifurcation diagram as a function of a varying external current. We slowly

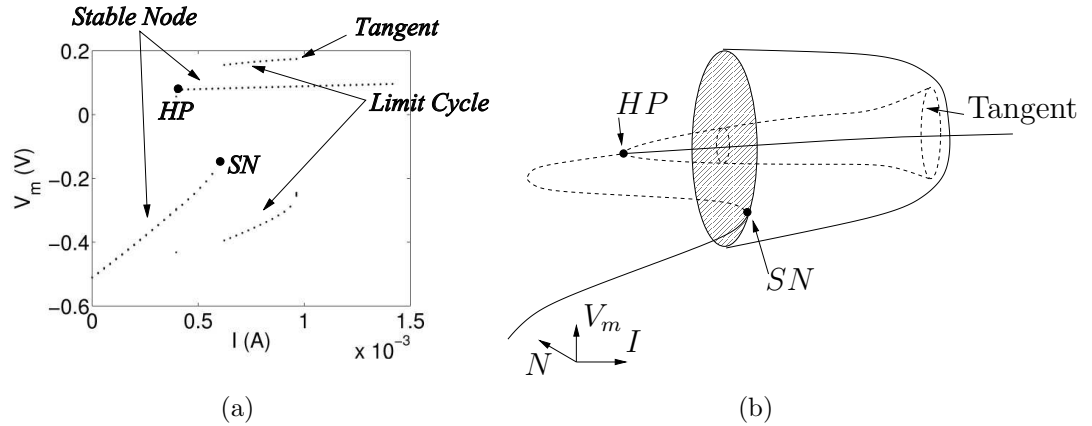


Figure 2.4: (a) *Experimental bifurcation diagram example in one dimension obtained by plotting the maxima and minima of the membrane voltage V_m as a function of the excitation current I . There we can observe three different attractors: two branches of stable fixed points, one of them starting from the left and another from the right of the panel, and a stable limit cycle (spiking behavior) coexisting with them between 0.5 and 1 mA.* (b) *This schematic diagram is the three dimensional phase space (N, V_m, I) which corresponds to the experimental bifurcation diagram in (a). We can observe a saddle-node bifurcation (SN), a subcritical Hopf bifurcation (HP) and a tangent bifurcation of a limit cycle. The stable branches appear in solid lines while dashed lines represent unstable branches or unstable limit cycle.*

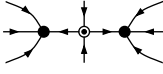
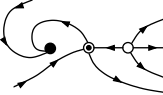
	<i>Saddle point with two stable points</i>
	<i>Saddle point with one stable point and one unstable point</i>
	<i>Sink</i>
	<i>Stable fixed point coexisting with a stable limit cycle</i>
	<i>Stable limit cycle</i>

Figure 2.5: *Legends of the notation on the bifurcation diagrams.*

increase the current step by step and observe the changes of the membrane voltage V_m .

In Fig. 2.4 (a) we plot the maxima and minima of the membrane voltage to visualize the oscillatory behavior and stable states of the system. In this figure there appears a saddle-node bifurcation on an invariant cycle (point SN), a subcritical Hopf bifurcation (point HP) and a limit-cycle (the spiking regime of the neuron), for clarity we schematically draw the corresponding three dimensional phase space (N, V_m, I) in Fig. 2.4 (b). By collecting a great amount of these diagrams varying only one parameter and joining these one-dimensional diagrams in a two-parameter plot we can visualize how the bifurcations in the system evolve when a parameter is varied. Due to the complexity of the whole high dimensional bifurcation diagram, we have used two-dimensional diagrams with one axis being I and the other one being another parameter of the model. Notice that in the case of the experimental bifurcation diagrams the unstable states cannot be observed. It is only possible to capture the stable steady states as well as the stable limit-cycles.

We have chosen three types of bifurcation diagrams which exhibit interesting features, (a) $I - V_3$ plane, where V_3 is the activation threshold of the potassium channel, (b) $I - V_4$ plane, where V_4 is the slope of the activa-

tion function for the potassium channel and, (c) $I - \tau$ plane, where τ is the time constant of the potassium channel. These parameters have a large influence on the model behavior as we describe below in each case. The Fig. 2.5 explains the principal notations used on the bifurcation diagrams for the representation of the phase plane of each zone.

2.3.1 $I - V_3$ diagram

In the Fig. 2.6 (a) we have plotted the corresponding bifurcations observed in the circuit when the parameter I and V_3 are varied. The different attractors and behaviors of the model are specified on the graphics with oscillations and stable nodes. The bifurcation diagram shows interesting global bifurcations, such as a Bogdanov-Takens bifurcation (BT point on the panel) and a cusp bifurcation close to it. In fact, these two bifurcations are so close that at the selected scale they cannot be clearly differentiated. The first one represents the transition from a saddle-node bifurcation to a sub-critical Hopf bifurcation, where this last bifurcation always lie near a cusp bifurcation. The cusp bifurcation appears when three equilibrium points, a saddle point and two nodes, collapse. In the Fig. 2.6 (b) we have plotted the bifurcation diagram obtained with the software XPP-AUTO; we have simulated the Eqs. (2.6) and (2.7) with the parameters obtained from the circuit. Both diagrams are very similar albeit some little differences in the location of the bifurcations, for example the experimental diagram is shifted left from 0.5mA in comparison with the numerical diagram. There are several other differences due to the imprecisions and the noise in the circuit. The fine bifurcation structure detailed in Fig. 2.6 (b) is too narrow to be observed in the circuit. The system in the magnified region displays two homoclinic bifurcations. The first one is the homoclinic bifurcation of a stable limit cycle along the line H1 and the second one is the bifurcation of an unstable limit-cycle along the line H2. In the shaded region we have a stable limit cycle. The Hopf bifurcation starts with a Bogdanov-Takens bifurcation on the saddle-node branch. The general aspect and the bifurcations are conserved which manifest that the circuit is robust. In spiking neurons we have basically two types of excitability. The excitability represents the way the neurons begin to spike when an external current is gradually increased. In the first type of neurons, the class I neurons, the neuron begins to spike with an almost zero frequency when the current is increased. In the class II neurons, the spiking begins at nonzero frequency. The change in the excitability of the neuron can be explained

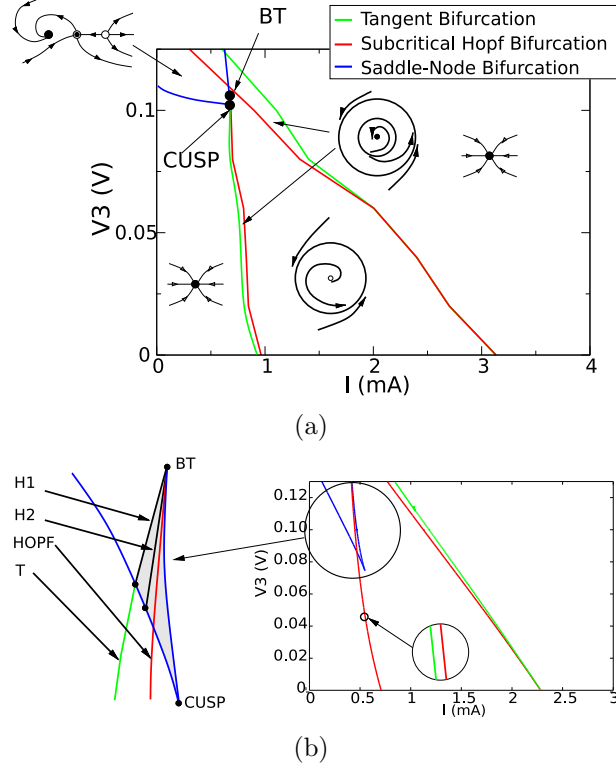


Figure 2.6: (a) *Experimental bifurcations in the I - V_3 plane. We observe a Bogdanov-Takens bifurcation (BT point) and a cusp bifurcation close to it.* (b) *The numerical results obtained from the Eqs. (2.6) and (2.7) with the XPP-AUTO software. The color used for the bifurcations are the same as in the Fig. (a). Both diagrams look very similar despite some differences on the place of the bifurcations due to the natural errors and distortions introduced by the circuit. The general aspect is conserved and also does the type of bifurcations, which manifests that the circuit is robust. We schematize the region of the circle which presents a complex bifurcation structure. In the inset of the figure we enlarge a part of the subcritical Hopf bifurcation. The numerical simulation and the analog simulation correspond to the following parameters: $\tau = 2$ ms, $V_4 = 0.2$ V, $V_2 = 0.15$ V, $V_1 = 0$ V, $g_K^* = 8$ mS, $g_{Ca}^* = 4$ mS and $g_L = 2$ mS.*

considering these bifurcations. As is well known, the Morris-Lecar model

is able to support both class I and class II excitabilities. The change from the class I to class II excitability comes from a Bogdanov-Takens bifurcation which set the transition from a saddle-node bifurcation (class I excitability) to a sub-critical Hopf bifurcation (class II). In our circuit we can control this parameter easily and so we can switch the type of excitability by only changing the parameter V_3 .

2.3.2 $I - V_4$ diagram

This bifurcation diagram which is shown in Fig. 2.7 is quite similar to the previous one in its structure. We observe the same characteristics and the same Bogdanov-Takens and cusp bifurcations (the BT bifurcation always lies near a cusp bifurcation). Moreover, a new type of codimension-2 bifurcation appears. This is a generalized Hopf bifurcation (also called a Bautin bifurcation) that corresponds to a transition from a sub-critical to a super-critical Hopf bifurcation [18]. Once again the BT bifurcation changes the excitability of the neuron. We have two parameters that permit the control of the excitability of the model: V_3 and V_4 . As in the Fig. 2.6 we also present the numerical result for the same set of parameters in Fig. 2.7 (b). The numerical simulation obtained with XPP-AUTO agrees with the experimental diagram in Fig. 2.7 (a). Moreover, the bifurcations are the same and their positions in the phase plane are similar in both diagrams. Some discrepancies appear between the two diagrams due to the approximations and the nonlinearities in the circuit as well as experimental noise. Nonetheless the diagram obtained with the circuit is satisfactory and illustrates well the model.

2.3.3 $I - \tau$ diagram

As it was mentioned before the parameter τ is very important for the stability of the system because the dynamics of the potassium current is crucial to the stability of the model. It represents the time of repolarization of the membrane, or in other words, the time necessary for the membrane to return to the resting state after firing of a spike. In fact, by varying this parameter we can change dramatically the dynamics of the system. The position in the phase space of the equilibrium points does not depend on τ , but the stability of each point is affected by this parameter. Figs. 2.8 (a) and 2.9 (a) show experimental bifurcation diagrams where we observe bistable regimes. In Fig. 2.8 (a), we have a big zone of bistability. On one side we have the

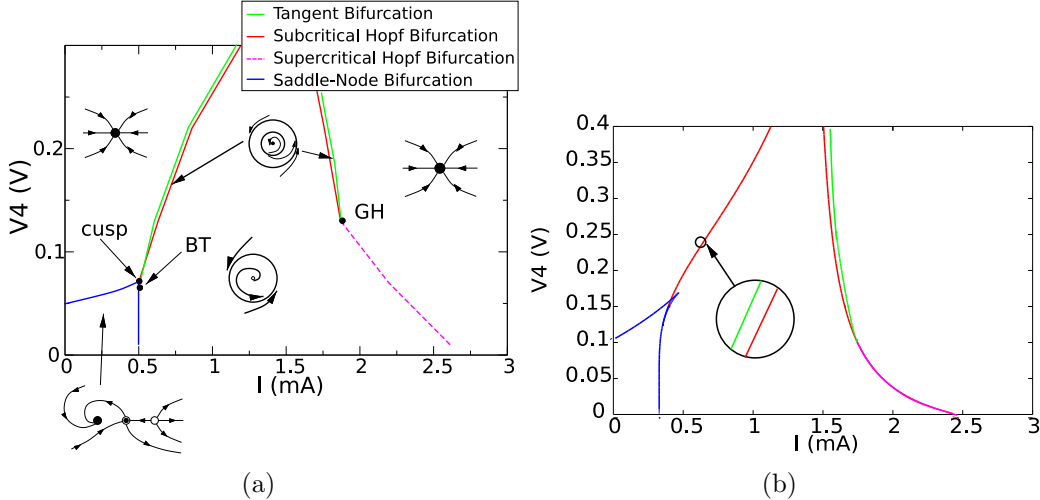


Figure 2.7: (a) *Experimental bifurcations in the $I - V_4$ plane. A Bogdanov-Takens lies in the plain and a cusp bifurcation is close to it. We found also a generalized Hopf bifurcation which represents the transition from a subcritical to a supercritical Hopf bifurcation.* (b) *This diagram represent the numerical simulation of Eqs. (2.6) and (2.7) for the same set of parameters. It is clear that the experimental diagram and the simulated diagram are very similar. Some mismatches between the two diagrams are due to the nonlinearities and to the experimental noise. The parameters are as follows: $\tau = 2$ ms, $V_3 = 0.06$ V, $V_2 = 0.15$ V, $V_1 = 0$ V, $g_K^* = 8$ mS, $g_{Ca}^* = 4$ mS and $g_L = 2$ mS.*

bistability with a stable node and a limit cycle and on the other side one with two stable nodes (along the line l_1). This particularity can be used for the design of a burster neuron as we will see next. Figure 2.8 (b) shows the numerical simulation of Eqs. (2.6) and (2.7). This simulation validates the diagram obtained with the circuit, and the results are very close.

By modifying the parameter V_4 we obtain the new bifurcation diagram shown in the Fig. 2.9 (a). This diagram displays similar characteristics as the previous one. The saddle-node bifurcation on the limit-cycle is independent of the parameter τ . In this figure we have an interesting bistable zone along the line l_2 where a limit-cycle and a stable node coexist. The transition from one to another occurs through a subcritical Hopf bifurcation and a fold bifurcation. By using this particularity an elliptic burster can be constructed

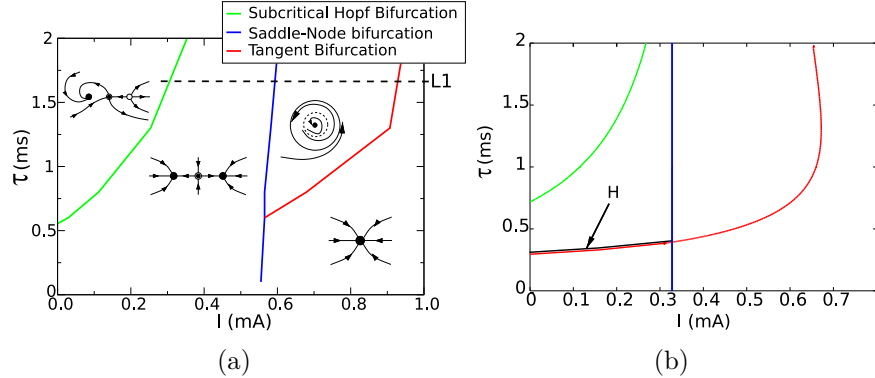


Figure 2.8: (a) *Experimental bifurcations in the $I - \tau$ plane. We have a large bistable zone represented by the coexistence of a stable node and a limit-cycle (spiking behavior) due to a subcritical Hopf bifurcation.* (b) *This figure is the numerical result of Eqs. (2.6) and (2.7) with the same parameter set. The figures are almost identical but there is a systematic difference on the place of the bifurcations. The saddle-node bifurcation obtained with the circuit is shifted from 0.3mA to the right. The black line marked as **H** on the diagram is the homoclinic bifurcation of a stable limit-cycle, which bifurcation is difficult to observe in the circuit. This limit cycle region is too narrow. The parameters are as follows: $V_4 = 0.06\text{ V}$, $V_3 = 0.12\text{ V}$, $V_2 = 0.15\text{ V}$, $V_1 = 0\text{ V}$, $g_K^* = 8\text{ mS}$, $g_{Ca}^* = 4\text{ mS}$ and $g_L = 2\text{ mS}$.*

as it will be described in the next section. Along the line l_3 we have a bifurcation pattern identical to the one shown in Fig. 2.8 (a) along the line l_1 . On one side we have a bistability between a limit-cycle and a stable node and on the other between two stable nodes, although the transition from one to another in this case occurs through a saddle-node bifurcation. We have verified also this diagram with the numerical simulation presented in Fig. 2.9 (b) and both graphics correspond well.

The bifurcation diagram appearing in Fig. 2.10 (a) presents a small bistable zone (the small triangle) where a stable node and a limit cycle coexist. If the system is on the stable branch for example at the point 1 on the diagram, when we increase the external current the attractor changes to a spiking regime after a saddle-node bifurcation (see the point 2). On the other hand, when the current decreases the stable limit cycle collapses with an saddle point. The system describes a hysteresis loop as the trajectory is

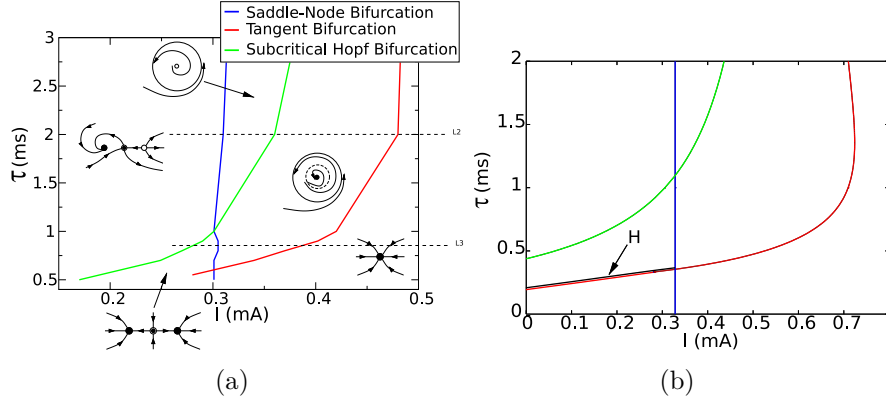


Figure 2.9: (a) Experimental bifurcations in the $I - \tau$ plane. This diagram is very close to Fig. 2.8 (a). In this figure we have changed slightly the parameters V_4 of the model and plot a new bifurcation diagram. We have the bistable zone with a stable node and a limit-cycle, and a new zone appears where a single limit-cycle (spiking behavior) is present. (b) The diagram plotted is the numerical result of the model equations with the same parameters used in the circuit. The two diagrams are very similar, while some differences appear in the diagram owing to the noise and the nonlinearities present in the circuit. The black line marked as **H** on the diagram is the homoclinic bifurcation of a stable limit-cycle. This limit cycle region is too narrow to be observed with the circuit. The numerical values of the parameters are as follows: $V_4 = 0.1$ V, $V_3 = 0.12$ V, $V_2 = 0.15$ V, $V_1 = 0$, $g_K^* = 8$ mS, $g_{Ca}^* = 4$ mS and $g_L = 2$ mS.

different if we increase or decrease the external current. Although this region of bistability always remains in a narrow range of parameters it can be a good candidate for the design of the square wave burster. The numerical simulation displayed in Fig. 2.10 (b) with XPP-AUTO matches the result obtained experimentally. The homoclinic bifurcation seems longer than in the experimental diagrams and this region remains small but it is sufficient for our purpose.

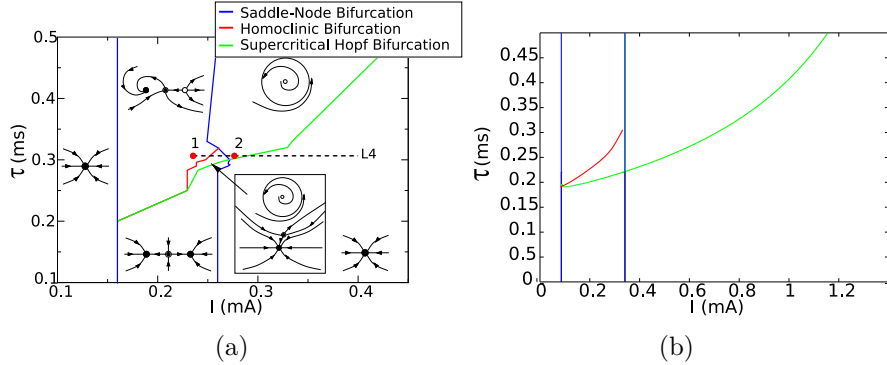


Figure 2.10: (a) In this diagram we have a bistable zone with a limit cycle and a stable point. The transition from the limit cycle to the resting state occurs through a homoclinic connection to an unstable point. We can observe in the insets the different phase portrait and the attractors of the regions of the bifurcation diagram. The zone of bistability remains very small and is difficult to find out experimentally. (b) The figure shows the numerical result of Eqs. (2.6) and (2.7) with the same parameter set. The region of bistability in the triangle appears to be larger than in the experimental diagram, but in numerical simulations the noise is not present. So the region appears greater. The numerical values of the parameters are as follows: $V_4 = 0.07$ V, $V_3 = 0.032$ V, $V_2 = 0.15$ V, $V_1 = -0.028$ V, $g_K^* = 8$ mS, $g_{Ca}^* = 2.6$ mS and $g_L = 2$ mS.

2.4 The design of bursters

The previous experiments are the basis for the implementation of some models of bursting behavior. Since a burster works by switching with two pseudo-stable attractors (a limit-cycle and a stable node for example), we have to spot the bistable zones of the parameter space. Here the previous experimental work is essential, since we can visually find out the bistable regimes of the neuron model. So, the first step is the search for bistable states where we can switch easily from one attractor to another by simply varying the external current. In the previous diagrams we have to look for a bistable regime along a horizontal line. For example, following the line l_2 in Fig. 2.9 (a) we have a bistable behavior between a stable node and a stable limit-cycle. When the external current is moved a hysteresis loop appears between the resting state

and the spiking state (Fig. 2.11). This hysteresis loop leads to transitions from the resting state to the spiking regime and back. Once we have chosen two coexisting states as good candidates for the switching, we introduce a new differential equation in our system to allow this switching to take place autonomously. This new equation governs the slow current I , and is given as follows:

$$\frac{dI}{dt} = \frac{1}{R_a R_b C_2} (V_m - V_{th}), \quad RC \gg \tau. \quad (2.12)$$

The introduction of the new variable $I(t)$ allows us to switch the whole dynamics from one attracting state to another one by a suitable election of values of R_b and V_{th} . Observe that now I is really an “internal” variable of the extended dynamical system. Equation (2.12) is implemented by using a simple operational amplifier in integrator mode. In order to develop our method, we start by marking the interesting bistable zone on the bifurcation diagram (horizontal line l_1 on Fig. 2.8 (a) and extracting the corresponding projection in one dimension (current vs amplitude on Fig. 2.4). Setting the voltage threshold V_{th} in Eq. (2.12) is a rather difficult task because the integrated current must decrease when the burster is spiking and must increase when the burster is in its resting state. The parameter is tuned manually so

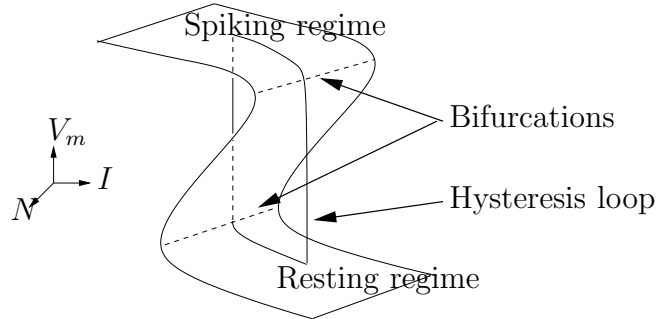


Figure 2.11: *Hysteresis loop of the burster. Observe that the system switches from a resting state to a spiking regime and back when the current I is changed. When the system is in the spiking regime, the current changes so that the state approaches the edge. As the system crosses the bifurcation on the edge the system returns in a resting state. The current in this state changes its direction and the state approaches the lower edge. The burster oscillates between these two states.*

that we obtain the desired behavior. The resulting waveform of this current for the square-wave burster is shown in Fig. 2.12. Notice that the current I is increasing when $\langle V_m \rangle$ (where $\langle \cdot \rangle$ holds for the mean value) is above the threshold and decreasing when it is below V_{th} . The second parameter R_b is important for the time constant of the equation; it determines the speed of the slow driving current. If this parameter is set too high, the oscillations are weak. If the constant is too low the system can switch to another attractor.

We present in the next sections three different kind of bursters whose differences are due to the bifurcations involved. Biological equivalence exist for two of the three bursters. The square-wave behaves like the pancreatic β -cells and the Hindmarsh-Rose model. The elliptic bursting phenomena have been observed in rodent trigeminal interneurons.

2.4.1 Square wave burster (“Fold/homoclinic” burster)

First, we have built the well-known square-wave (or fold/homoclinic) burster [16, 19]. This burster displays oscillations between a stable limit cycle and a stable node. In Fig. 2.10 (a) we have found a small region of bistability between an oscillatory state with an homoclinic connection and a stable node. If we sketch the behavior of V_m along the line l_4 drawn in Fig. 2.10 (a), a graph similar to the one displayed in Fig. 2.12 (a) is obtained. The bistable regime can be seen on the bifurcation diagram appearing in Fig. 2.12 (a). Although this bistable regime only occurs in a narrow range of the variable I we can apply the technique to this case. Here the transition between the two states takes place through a fold bifurcation for the passage from the resting point to spiking activity and through a homoclinic connection of the saddle point for the transition from firing to resting.

In Fig. 2.12 (b) we have an example of a bursting oscillation between two attractors in the three dimensional phase space. We also plot the corresponding time series of the voltage in Fig. 2.12 (c), where the temporal characteristics of the bursting are clear.

2.4.2 Elliptic burster (“subHopf/fold cycle” burster)

We have simulated also the elliptic burster. Once again the bistability is the key point. But in this case the nature of the bifurcation is totally different. In Fig. 2.13 (b) we have a representation of the oscillation in the full three dimensional phase space. The solid red line corresponds to the trajectory

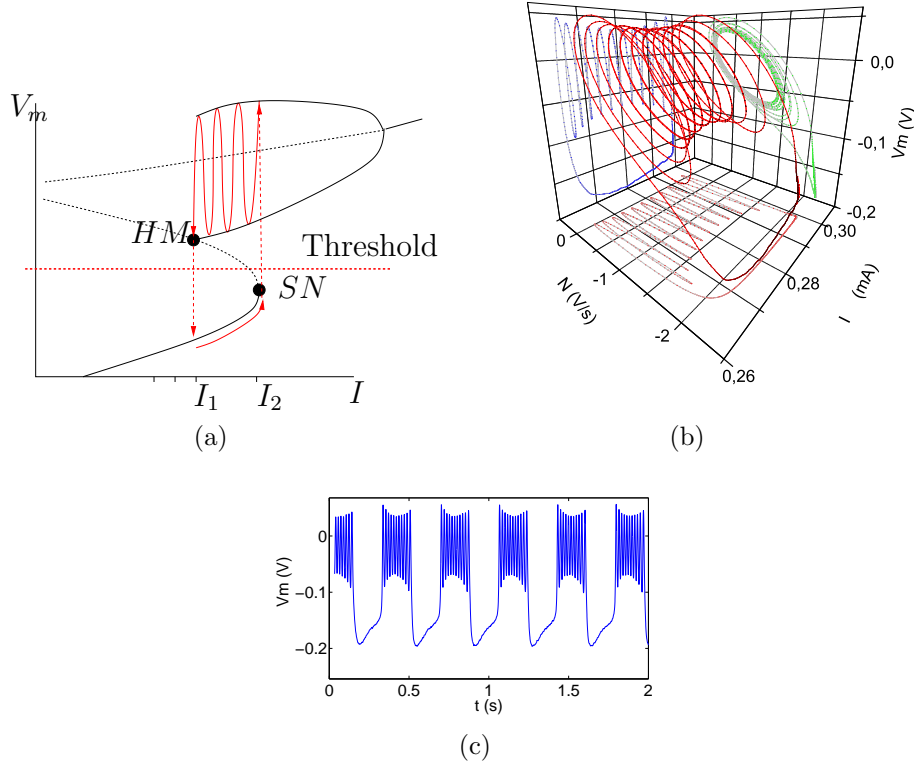


Figure 2.12: (a) Dynamical behavior of the square-wave burster. The figure represents the bifurcation diagram of the Morris-Lecar model as a function of I . The bursting regime appears through a fold bifurcation for the passage from the stable node to the limit cycle and through a homoclinic connection when the cycle loses its stability and gets back to the resting state; (b) 3D view of the orbit in the space (I, N, V_m) . The parameter values are as follows: $\tau = 0.03$ s, $V_4 = 0.07$ V, $V_3 = 0.028$ V, $V_2 = 0.15$ V, $V_1 = -0.032$ V, $g_K^* = 8$ mS, $g_{Ca}^* = 1.38$ mS, $g_L = 2$ mS, $C_2 = 1\mu F$, $R_a = 4.3$ k Ω and $R_b = 13.7$ k Ω . (c) Time series of the membrane voltage corresponding to the output of the circuit.

in phase space. The transition from the resting to the spiking regime takes place through a subcritical Hopf bifurcation and the reverse transition occurs through the tangent bifurcation where the unstable limit cycle collapses with

the stable cycle. This bifurcation is also called a “fold cycle”. This kind of behavior can be seen along the line l_2 in the figure 2.9 (a), where we can see a bistable region due to the sub-critical Hopf bifurcation. We can configure this system to oscillate along the line l_2 .

In Fig. 2.13 (b) we represent the experimental phase space, which consists in a three dimensional space spanned by the membrane voltage, the current and the potassium channel activation. In Fig. 2.13 (c) we have plotted the time series of the voltage V_m . The Fig. 2.13 (d) depicts the variation of the excitation current.

2.4.3 Circle/Fold cycle burster

This kind of bursters is slightly different from the previous one. There are three different transitions. We have drawn the line l_3 on the bifurcation diagram in Fig. 2.9 (a). Along this line we have some different bistable states. First we observe the bistability with two stable nodes and then with a stable node and a stable limit cycle.

The bursting starts after a saddle-node bifurcation on a limit-cycle. The electric current goes increasing until the tangent bifurcation (the fold-cycle bifurcation) takes place and then the system gets back to a new stable node. The current is now decreasing and is reduced until the sub-critical Hopf bifurcation occurs. Once this bifurcation is crossed the system returns to the first stable state and the cycle starts over. We summarize this complex behavior in Fig. 2.14 where we can clearly see how the sequence of attractors is followed by the dynamical system. In panel (a) we have plotted a schematic view of the phase space. In (b) a view of the experimental attractor in the three-dimensional phase space is depicted. The panel (c) shows the temporal evolution of the membrane voltage as the system carries out some cycles of bursting.

2.5 Conclusions

We have designed and built a circuit that approximates the main dynamical regimes of the well-known Morris-Lecar neuron model. By analyzing the behavior of this system in the phase space in terms of some of the parameters of the model we have been able to obtain different bursting behaviors where each one of them is characterized by the visiting of a particular succession of

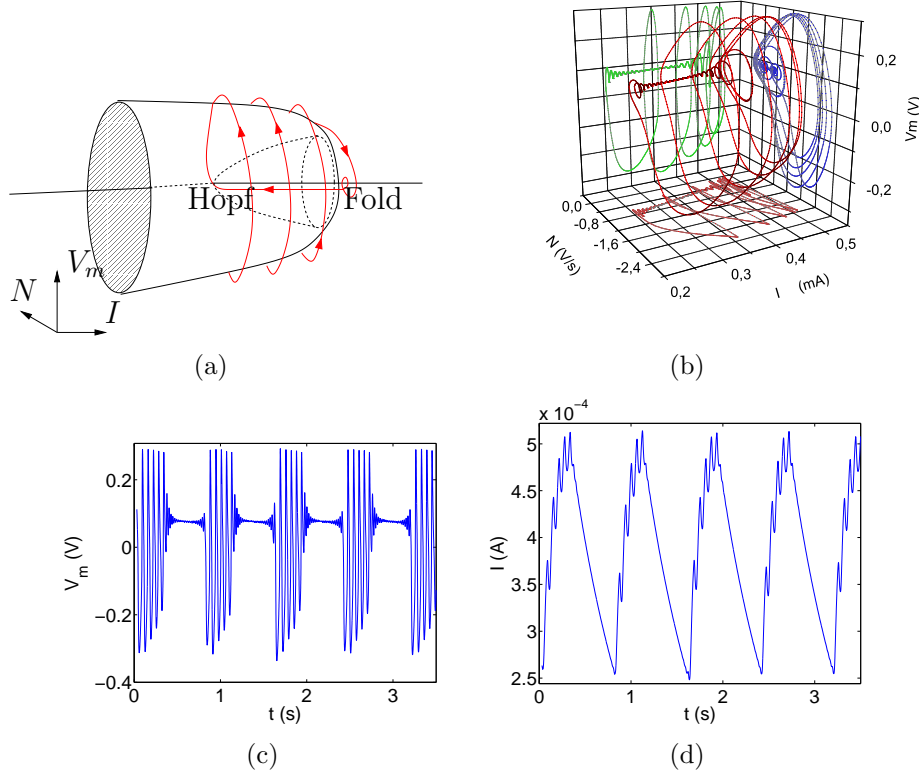


Figure 2.13: (a) *Bursting behavior of the elliptic burster. The bursting is produced through a sub-critical Hopf bifurcation. The gray shade represents the limit cycle and the solid line the stable state.* (b) *View of the phase space of the system, the variables are (V_m, N, I), parameter are as follows: $\tau = 0.079$ s, $V_4 = 0.07$ V, $V_3 = 0.12$ V, $V_2 = 0.15$ V, $V_1 = 0$, $g_K^* = 8$ mS, $g_{Ca}^* = 4$ mS, $g_L = 2$ mS, $R_a = 174$, $C_2 = 1\mu F$, $k\Omega$ and $R_b = 10$ k Ω .* (c) *Time series generated by an elliptic burster built from the Morris-Lecar circuit. Observe the growing of the oscillation as the sub-critical Hopf bifurcation is approached.* (d) *Time series of the current I .*

attractors of the subsystem by the evolving phase point. Thus, our strategy provides a method to investigate the features of relatively simple dynamical systems giving rise to rather complex cycles in the phase space that appear as the phase point transiently visits a given set of the stable attractors of the

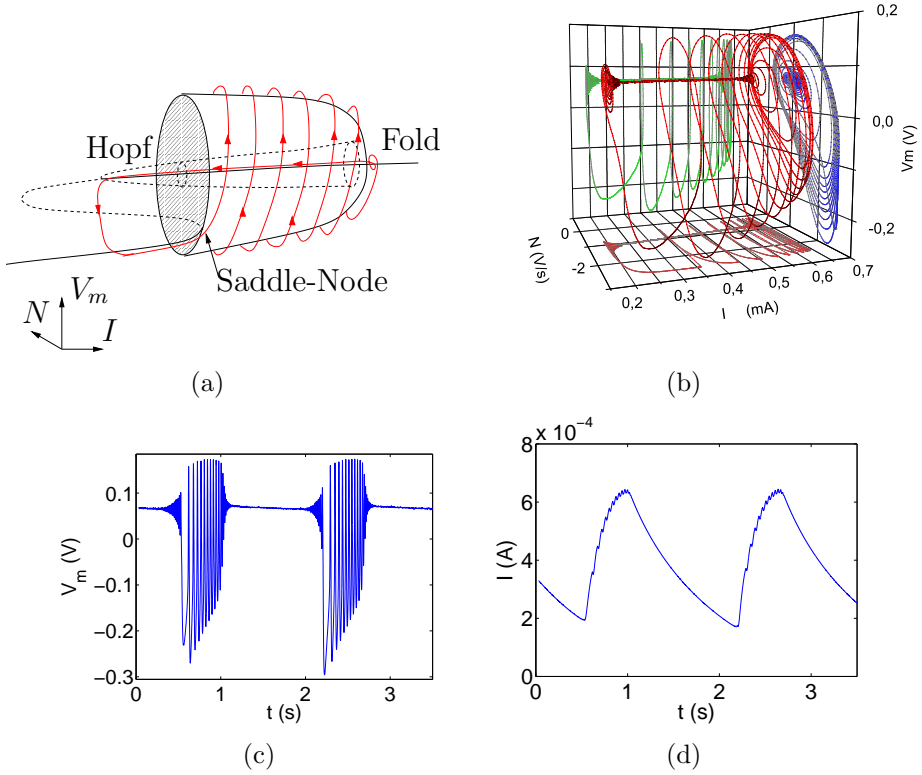


Figure 2.14: (a) Dynamical behavior of the circle/fold burster. The transition from the resting to the oscillatory state is made through a saddle-node bifurcation on a limit-cycle. The cycle collapses by a fold bifurcation and the system remains on a stable state until it returns to the resting state through a subcritical Hopf bifurcation. (b) Experimental measurement of the attractor as viewed in the three-dimensional phase space (V_m , N , I). The parameter values are as follows: $\tau = 0.026$ s, $V_4 = 0.07$ V, $V_3 = 0.12$ V, $V_2 = 0.15$ V, $V_1 = 0$, $g_K^* = 8$ mS, $g_{Ca}^* = 4$ mS, $g_L = 2$ mS, $C_2 = 1\mu F$, $R_a = 4.3$ k Ω and $R_b = 10$ k Ω (c) Time series of V_m . (d) Time series of the current I

dynamical subsystem.

We have explored the bifurcation diagram of the simplified ML model to point out and extract the dynamical behaviors. We are looking for bistable states and hysteretic phenomena in the system. An appropriate selection of

the attractors and a slow drive current forms a complex oscillator with the characteristics of a bursting neuron. Such a circuit can be implemented in a VLSI circuit with some modifications, in such a way that a large assembly of coupled bursting neurons can be simulated.

The implementation of the method by means of an electronic circuit introduces a great flexibility in the real time control of the characteristics of the system. In particular, this method allows us to carry out a continuous control of the behavior of the system by allowing the continuous observation of the system's output as the parameters are changed. The use of electronic circuits is an advantage in this context because they are physical devices that operate in a real environment and thus they are subject to a great deal of uncontrollable noise. This is in fact the environment in which evolve real dynamical systems as neurons and so, our method could provide an approach to analyze the robustness of the dynamics of neuronal models under real situations.

References

- [1] S. Le Masson, A. Laflauiere, T. Bal and G. Le Masson, "Analog circuits for modeling biological neural networks: design and applications", *IEEE Trans. on Biomedical Engineering* **46**, 638 (1999).
- [2] A. Szucs, P. Varona, A.R. Volkovskii, H.D.I. Abarbanel, M.I. Rabinovich and A.I. Selverston, "Interacting biological and electronic neurons generate realistic oscillatory rhythms", *Neuroreport* **11**, 563 (2000).
- [3] T. Kohno and K. Aihara, "A MOSFET-based model of a class 2 nerve membrane", *IEEE Trans. on Neural Networks* **16**, 754 (2005).
- [4] Y. Horio and K. Aihara, "Chaotic Neuro-Computer", in *Chaos in Circuit and Systems*, eds. Chen, G. & Ueta, T. (World Scientific) 237 (2002).
- [5] G. Zeck and P. Fromherz, "Noninvasive neuroelectronic interfacing with synaptically connected snail neurons immobilized on a semiconductor chip", *Proc. Natl. Acad. Sci. USA* **98**, 10457 (2001).
- [6] M.F. Simoni, G. S. Cymbalyuk, M.E. Sorensen, R.L. Calabrese and S.P. DeWeerth, "A multiconductance silicon neuron with biologically

- matched dynamics”, *IEEE Trans. on Biomedical Engineering* **51**, 342 (2004).
- [7] A. Van Schaik, “Building blocks for electronic spiking neural networks”, *Neural Networks* **14**, 6 (2001).
 - [8] J. M. Casado, B. Ibarz and M.A.F. Sanjuán, “Winnerless competition in networks of coupled map neurons”, *Modern Physics Letters B* **18**, 1347 (2004).
 - [9] M.I. Rabinovich , P. Varona, A.I. Selverston and H.D.I. Abarbanel, “Dynamical Principles in Neuroscience”. *Reviews of Modern Physics* **78** 1213 (2006).
 - [10] C. Morris and H. Lecar, “Voltage oscillations in the barnacle giant muscle fiber”, *Biophys. J.* **35**, 193 (1981).
 - [11] J. Rinzel and B. Ermentrout, “Analysis of neural excitability and oscillations”, *Methods in Neuronal Modeling*, Koch, C. & Segev, I. (eds.) (MIT press) 1359 (1989).
 - [12] S. Binczak, V. Azantsev, V. Nekorkin and J.-M. Bilbault, “Experimental study of bifurcation in modified Fitzhugh-Nagumo cell”, *Electronic Letters* **39**, 961 (2003).
 - [13] G. Patel, G.S. Cymbalyuk, R.L. Calabrese and S.P. DeWeerth, “Bifurcation analysis of a silicon neuron”, *Proceedings of NIPS’1999, MIT press* **12**, 731 (2000).
 - [14] K. Tsumoto, H. Kitajima, T. Yoshinaga, K. Aihara and H. Kawakami, “Bifurcation in Morris-Lecar neuron model”, *Neurocomputing* **69**, 293 (2006).
 - [15] T. R. Chay, Y. S. Fan and Y.S. Lee, “Bursting, spiking, chaos, fractals, and universality in biological rhythms”, *International Journal of Bifurcation and Chaos* **3**, 595 (1995).
 - [16] E.M. Izhikevich, “Neural excitability, spiking and bursting”, *International Journal of Bifurcation and Chaos* **10**, 1171 (2000).

- [17] S. Tsuji, T. Ueta, H. Kawakami and K. Aihara, “A design method of bursting using two-parameters bifurcation diagrams in Fitzhugh-Nagumo model”, *International Journal of Bifurcation and Chaos* **14**, 2241 (2004).
- [18] Y.A. Kuznetsov, *Elements of applied bifurcation theory*, (Springer, Berlin, 1998).
- [19] F.C. Hoppensteadt and E.M. Izhikevich, *Analysis of neural excitability and oscillations* (Springer, Berlin, 1997).

Chapter 3

The analog simulation of genetic networks

3.1 Molecular biology and nonlinear dynamics

The cells are systems with a great complexity due to the existing high number of interactions of diverse nature between their numerous components, particularly between proteins and genes. The understanding of these interactions is important, since they regulate the fundamental cellular processes. Many years of experimentation have been necessary to reveal the molecular bases of these processes. Recently, a new complementary way for the study of the interactions between genes and proteins based on the design of synthetic genetic networks began. The creation of these artificial genetic networks, much more simple than those operating in the cell, is contributing to decipher the existing relation between the coordinated activity of groups of genes and the cellular functions. This has given birth of the so-called synthetic biology, where nonlinear dynamics, physics of complex systems, engineering and molecular biology play an important role.

The climax of the genome project, which most notable success has been the complete sequencing of the human genome, among other species important for the experimental biologists, is the knowledge of all the genes that compose the genetic material of an organism. Moreover it led to a new phase of the project: the postgenomic era.

The interest is now focused on the discovering of the organization and

the type of the interactions amongst the proteins, which are the product of the expression of the genes. Each protein is in charge of a function which can induce changes in other molecules in the cell, as for example the enzymes or even hormones. These molecules can be viewed as the nodes of a network where the interactions are the links. It forms a complex network of regulation interaction which are responsible for the functioning of the cell. The works on the regulation and the expression of the genes in the cellular processes received a strong impulse in the 1960's decade with the publication of the work of the French scientists François Jacob and Jacques Monod. With the establishment of the operon theory, some of the fundamental mechanisms of the gene regulation has been unveiled, as for example the differential expression of the genome in different biological process, such as the cellular development and differentiation.

The introduction of the recombinant DNA technique produced a noticeable change in the biochemistry and in the experimental molecular biology due to the possibility to clone, design and synthesize new genes. These genes can be introduced later in an organism in order to be expressed. Another important technology is the analysis of the the genetic expression profiles in DNA microarray which allows the observation of the expression level of all the genes in some particular metabolic conditions. This kind of analysis allows to define groups of genes which are coordinated (coreregulated genes). This experimental setup improved the knowledge of the regulation of the genetic expression. Nevertheless, the structure and the function of this natural genes networks needs new techniques and new tools for the study.

Recently, the design and the construction of artificial networks has been proposed to study biological processes, such as oscillations of the metabolism. These networks, simpler than the natural ones, can contribute to the understanding of the molecular bases of a specific function. For its simplicity, the synthetic genetic networks can be synthesized in a laboratory and simple mathematical models can be constructed in order to obtain qualitative and numerical analysis. These works, among others, gave birth to the so-called synthetic biology which integrates several scientific fields such as non-linear dynamics, complex systems physics and bio-molecular engineering. This is a new emerging field with a strong interdisciplinary component in which the future advances seems promising.

In this context, we propose an alternative way to design and analyze the genetic networks. The approach of the analog circuit allows to view the logical units of the network but with a determined dynamics. The interesting

point here is that instead of using the boolean approach, we can interconnect unit with a specific dynamics in order to design the objective dynamical system.

The organization of the chapter is as follows. In Sec. 3.2, we introduce the electronic repressilator. It is a simple analog electronic circuit that mimics the behavior of a well-known synthetic gene oscillator, the repressilator, which represents a set of three genes repressing one another. In Sec. 3.3, synchronization of a population of such units is thoroughly studied, with the aim to comparing the role of global coupling with that of global forcing on the population in Sec. 3.4. In the Sec. 3.5, we propose the implementation of two different genes network. The first one is a simple electronic version of a genetic toggle switch, which is a simple network of two mutually repressor genes, where control by external forcing is also analyzed. The second one is a auto-repressive gene network in which the delay of the self-repression induce oscillations.

3.2 Analog simulation of the repressilator

One of the main advances brought about by the advent of synthetic biology is the design of artificial gene regulation networks that mimic the behavior of natural ones. One could think that this simplifies the analysis of cell behavior by isolating in a modular way relevant network modules, which can therefore be studied independently of other complex cellular processes that in the natural case are intermingled with the module of interest. This is certainly the case, and it has been the main motivation behind the design of certain synthetic gene networks, such as oscillators and switches. A paradigmatic example is the repressilator, a set of three genes (and their respective proteins) which repress one another in a circular way, leading to clear-cut oscillations in the protein expression. In spite of their doubtless advantages, experimental studies of these synthetic systems are still difficult, due both to the inherent complexity of molecular biology experiments and to our lack of knowledge of the kinetic parameters of the specific network components. For example, mutual synchronization of globally coupled populations of repressilators has not yet been observed, in spite of theoretical predictions and of the interest of the phenomenon as a model of synchronized rhythm generation in multicellular circadian clocks. Here we take another approach, reproducing the dynamical behavior of the repressilator via a simple analog electronic

circuit, and using it to investigate experimentally the synchronization of a set of repressilators, with an emphasis on the comparison between the effect of global coupling and global external forcing, two ingredients that can realistically be expected to exist in natural multicellular clocks. The usefulness of the approach is further demonstrated by the design of an even simpler circuit representing a genetic toggle switch, and its use to study the effect of forcing on a population of such devices.

Genetic regulatory networks have been well studied in living microorganisms such as bacteria or viruses since the early 1960s [1]. They rely on the fact that certain specific proteins are able to influence and regulate the activity of DNA transcription. The final product of this DNA transcription is another protein, which could influence in turn the expression of yet another gene (or of its own gene, or even that of its transcription factor). This process leads to networks of genetic interactions, where proteins and genes can be interpreted as nodes, and the interactions between them as links [2]. These regulatory networks provide the essential control of protein expression in the cell.

Transcription regulation can arise in a positive or negative way. Negative regulation occurs when a protein hinders, or even blocks, the transcription process, as illustrated in the Fig. 3.1. For instance when a protein binds at a certain location of the DNA chain, called *promoter*, it blocks the access of RNA polymerase, which is the enzyme that transcribes DNA into messenger RNA. This kind of proteins are called *repressors*. An example of repressive regulation is the tryptophan *trp* operon in the bacterium *Escherichia coli* (*E. coli*), where the presence of tryptophan proteins inhibits the transcription of the *trp* operon [3]. On the other hand, positive regulation results from biochemical processes that enhance protein transcription, or at least allow it. The regulation of the lactose operon in *E. coli* is a good example of positive regulation [1]. The presence of β -galactosidase in the bacteria's medium speeds up the transcription of the operon, and consequently the bacteria can transform lactose in glucose.

These mechanisms of positive and negative regulation are similar to control mechanisms in electronic engineering. Negative feedback regulation is a basic system of control that enhances the stability and the resistance to noise in gene expression [4] .

Gene regulation is the basis of the design of synthetic regulatory pathways. In our context, synthetic means that the genetic network does not exist in a natural form. The first synthetic genetic networks, a genetic toggle

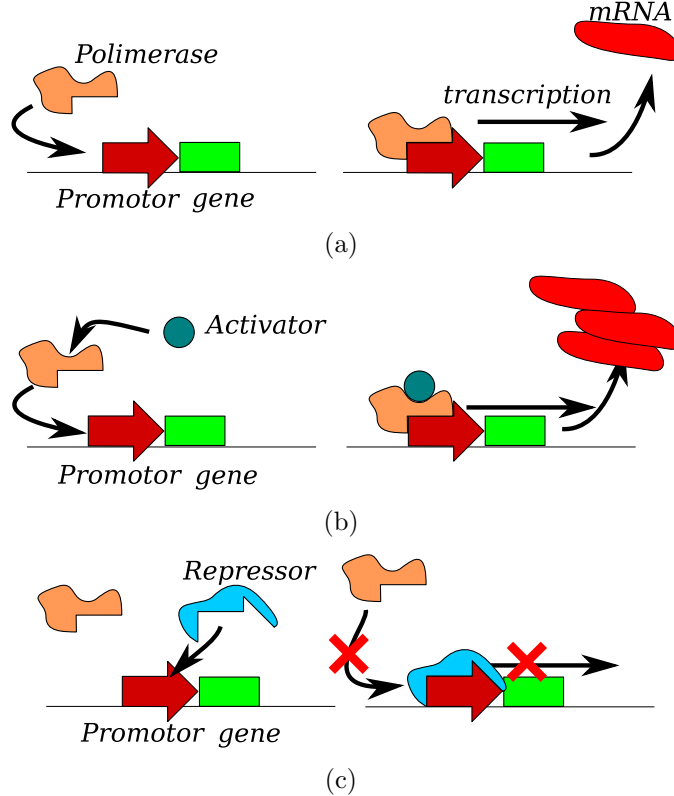


Figure 3.1: Graphical illustration of the transcription process (a), the activation of a particular gene (b) and the repression of the same gene (c).

switch [5] and a genetic oscillator [6], have been presented in two seminal articles. In Ref. [5], the combination of two mutually repressing genes forms a bistable system whose state can be changed due to an external inducer (e.g. a protein or a temperature shift). When one of the transcribed proteins is produced, the other one remains silenced. The switching occurs when the inducer (external influence) is applied beyond a certain threshold, making the system jump to the opposite state. After a jump between states, which consists in a variation of the protein concentration, the system maintains the protein level. One can say that this genetic switch has memory, since it remains in its current state until an external inducer acts again.

The second paradigmatic system is the repressilator [6], which is in fact a genetic oscillator and where three repressor genes are placed in a ring,

with each repressor inhibiting the production of the following protein with a certain delay. In Fig. 3.2 (a) we show a schematic representation of the interactions of this genetic network, where blue arrows represent promoters. The product of each repressor gene (in green) binds to the next promoter and inhibits production of the corresponding protein. This configuration leads to oscillations in the expression of the three proteins, with a $2\pi/3$ phase delay. Driven by this network motif, different bacteria oscillate independently, with different phases and slightly different frequencies (due to intrinsic cell variability) [6]. Synchronization of these rhythms would allow global oscillations in the cell population, thus simplifying the observation of the phenomenon, which currently requires single-cell tracking. Intercell communication through quorum-sensing has been proposed as a mechanism of synchronization [7], but no experimental verification has been made so far.

In this chapter, we propose an analysis of the dynamics of these two genetic regulatory networks (repressilator and toggle switch), making use of nonlinear analog electronic circuits. Our circuits allow a one-to-one correspondence between the structure of the genetic and electronic networks, and their analog character extends this correspondence to the full dynamical behavior. An evident benefit is that the electronic circuits are easier to implement experimentally than genetic circuits. The natural parameter mismatch in the living cell is reproduced by component dispersion in the electronic circuits. We study the synchronization of a population of repressilators due to global coupling. Additionally, in order to improve the synchronization of the genetic oscillators we add an external periodical forcing to every repressilator. We analyze the influence of external forcing on synchronization when the frequency and the amplitude of the external signal are modified. The results obtained with electronic circuits should be extensible to synthetic genetic networks, where external forcing could be implemented via a temperature periodic shift, or by periodic injection of a repressor protein.

3.3 The electronic repressilator

Previous work on electronic genetic networks used hybrid digital-analog circuits based on AND and OR functions [8]. Here we propose the use of all-analog circuits whose structure and dynamics are as similar as possible to that of the corresponding genetic network. Fig. 3.2 (b) shows the electronic setup of the analog repressilator. The output of the three MOS transistors

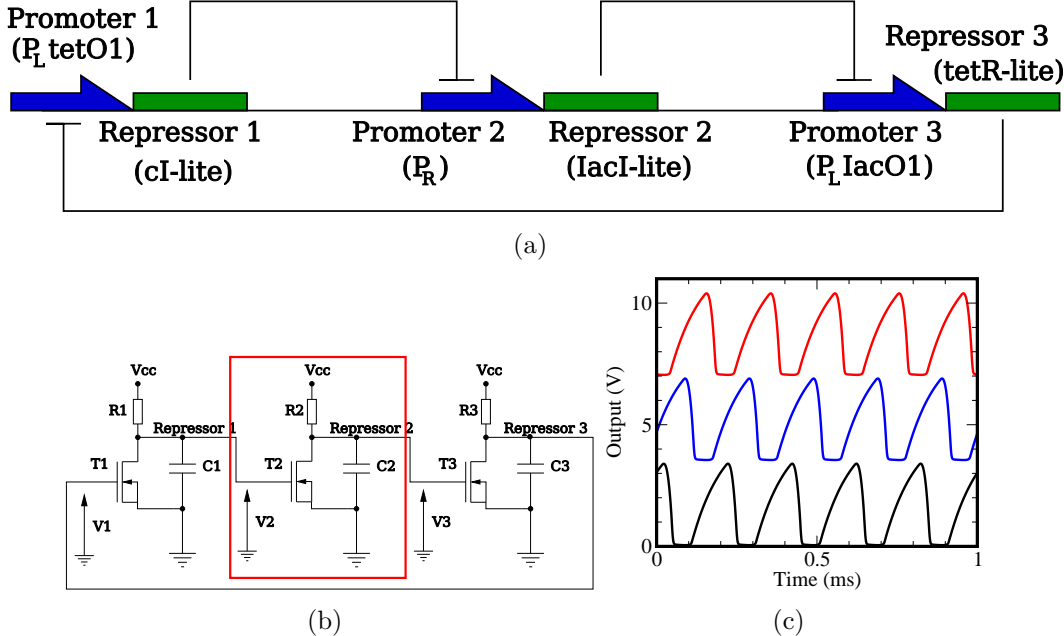


Figure 3.2: (a) Network architecture of a synthetic oscillator, the repressilator. Three repressor genes are consecutively connected by negative feedback. Promoters (in blue) of each gene (in green) are repressed by proteins (cI , $LacI$ and $TetR$) transcribed from the previous gene. (b) Electronic setup of the analog repressilator. Only three kind of elements are required: resistances, MOS transistors and capacitances. The output of each transistor corresponds to the level of each repressor protein. (c) Dynamics of the electronic repressilator. Time series (displaced in the vertical axes to allow comparison) of the three analog protein concentrations. They oscillate at the same frequency but phase shifted by $2\pi/3$.

correspond to the level of the three repressor proteins of the repressilator. The numerical values of the resistances, and capacitances are indicated in Table 3.1. Two reasons have motivated this particular design. First, the simplicity of the circuit, which is composed of basic electronic components. Second, the fact that the MOS technology allows the use of the analog repressilator in integrated circuits.

The N-channel MOSFET transistors of Fig. 3.2 (b) can be viewed as controllable switches. If the tension applied to the gate exceeds a certain

Symbol	Parameter	Values	Units
R_i	Internal resistance	$1.0 \pm 10\%$	$\text{k}\Omega$
C_i	Internal capacitance	$1.0 \pm 20\%$	μF
T_i	Transistor 2N7000	—	—
V_{cc}	Voltage source	3.227	V
R_i^c	Coupling resistance	from 0.130 to 30	$\text{k}\Omega$

Table 3.1: Numerical values of the electronic components used in the experiment

threshold voltage, the transistor switches off its output, leading to an output voltage close to zero (the transistor has very low output impedance). In this case, the tension on the gate acts as a repressor of the output voltage, similar to what happens with a repressor protein. When the gate voltage V_2 falls below the threshold, the voltage V_3 associated to transistor T2 begins to increase and the transistor T2 acts as a high-level impedance, that is, we have an open circuit. The protein level is represented by the output voltage of the transistors (and capacitors). In the absence of repression (no tension on V_2), the transistor voltage V_3 , which in turn will be the repressor of the following transistor, grows until it reaches its maximum value (the supply voltage V_{cc}). On the other hand, if repression rises, due to an increase of voltage at the previous transistor, the output voltage falls to zero. Summarizing, we can say that the three transistors are repressing themselves in the same way as it happens in the repressilator genetic network. This kind of configuration is responsible of the oscillations at the three output voltages/protein levels and is known as a *ring oscillator*.

We can derive the differential equations of this model by considering a basic unit (equivalent to a single repressor gene), which is made of a *RC* circuit connected to a voltage source and a transistor [see red square at Fig. 3.2 (b)]. Without any voltage V_2 on the gate of the transistor T2, it will behave as a simple *RC* circuit. The transistor will be turned off and the capacitor will be charged until it reaches its maximum value. If the gate voltage increases and reaches a certain threshold V_{th} , the transistor T2 “cuts” the output tension and the capacitor discharges rapidly through the transistor. From this simple circuit we can derive the differential equation of the variable V_3

$$R_2 C_2 \frac{dV_3}{dt} = -V_3 + V_{cc} f(V_2), \quad (3.1)$$

where the function $f(x)$ depends on the transistor parameters and should be sigmoidal shaped if we want to obtain oscillations at the transistor's output. A good candidate for $f(x)$ is

$$f(x) = \frac{\alpha}{1 + \beta x^n}, \quad (3.2)$$

where α , β and n are parameters depending on the MOSFET transistor. This corresponds to the Michaelis-Menten equation of growth of order n .

The complete set of equations of the repressilator reads

$$R_1 C_1 \frac{dV_2}{dt} = -V_2 + V_{cc} f(V_1) \quad (3.3)$$

$$R_2 C_2 \frac{dV_3}{dt} = -V_3 + V_{cc} f(V_2) \quad (3.4)$$

$$R_3 C_3 \frac{dV_1}{dt} = -V_1 + V_{cc} f(V_3). \quad (3.5)$$

And the time series of the circuit can be seen in Fig. 3.2 (c), where the three repressor levels evolve with a phase difference of $2\pi/3$. When a repressor is active (e.g. T1 voltage), the following repressor (T2) is inhibited and the third increases (T3). The increase of T3 leads, in turn, to the decrease of T1 voltage. The chain repression is responsible of the oscillations of the whole system, both in electronic and genetic repressilators.

3.4 Alternative implementation with operational amplifiers

Operational amplifiers are common components in a wide variety of electronic circuits. One of their applications is the construction of modules which compute basic operations such as addition and subtraction. Within this framework we propose an electronic circuit that reproduces the global behavior of the repressilator. The design is shown in the left plot of Fig. 3.3 and is based on the same principles as the biological repressilator, namely three dynamical elements coupled in chain with an inhibitory interaction. The electronic implementation consists on three basic units made of one RC integrator circuit and one UA741 operational amplifier (OP-Amp). Each voltage measured at the output of the RC circuits (marked as V_i in Fig. 3.4) is equivalent to the concentration of each repressor protein. This voltage is further fed into

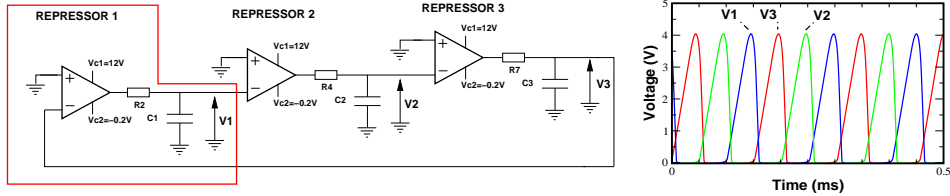


Figure 3.3: (a) Electronic setup of the analog repressilator. We used $C_i = 1\mu F$, $R_i = 1k\Omega$ and UA741 Op-Amps. (b) In the right plot we show the dynamics of the system.

the OP-Amp representing the promoter of the following gene. The output voltage V_i is connected to the negative input and the positive input is set to ground, therefore the OP-Amp is used as a voltage comparator. The output of the amplifier can take only two values: V_{c1} and V_{c2} which are the positive and negative power supply of the OP-Amp. The outputs V_i are linked through the RC circuits in a closed chain, in the same way as the genetic network shown in Fig. 3.2. The differential equations describing the behavior of the voltage of each unit is expressed by:

$$R_1 C_1 \frac{dV_1}{dt} = -V_1 + H_v(-V_3) \quad (3.6)$$

$$R_2 C_2 \frac{dV_2}{dt} = -V_2 + H_v(-V_1) \quad (3.7)$$

$$R_3 C_3 \frac{dV_3}{dt} = -V_3 + H_v(-V_2), \quad (3.8)$$

where $H_v(x)$ represents the comparator function of the OP-Amp, which can be represented ideally by a step function:

$$\begin{aligned} H_v(x) &= V_{c2} & \text{if } x < 0 \\ H_v(x) &= V_{c1} & \text{if } x > 0. \end{aligned} \quad (3.9)$$

The supply voltage is asymmetric, in our case the lower voltage V_{c2} is set to a value slightly below 0 V. In this way the behavior of the circuit is closer to the original genetic oscillatory network and does not display negative voltages. The positive supply is set to $V_{c1} = 12$ V. When an output voltage (for example V_2) increases, it induces a reduction of the following output voltage (V_3), since it is injected at the negative input of the corresponding Op-Amp (3 in this case), crossing the threshold $V_{th} = 0V$. Following the

chain, V_3 , which is decreasing, will enhance the value of V_1 which in turn will decrease V_2 . This mechanism leads to an oscillatory behavior (see right plot of Fig.3.3) with a frequency and amplitude that depend on the OP-Amp internal parameters but also on the value of R_i and C_i .

3.5 Coupling electronic repressilators

One of the questions raised by the seminal paper of Elowitz *et al.* [6] is the way in which a population of repressilators might be synchronized. It has been observed that each cell of a colony of repressilators oscillates at its own frequency and phase, preventing the occurrence of global oscillations. Intercellular communication via quorum sensing [9, 10] has been proposed as

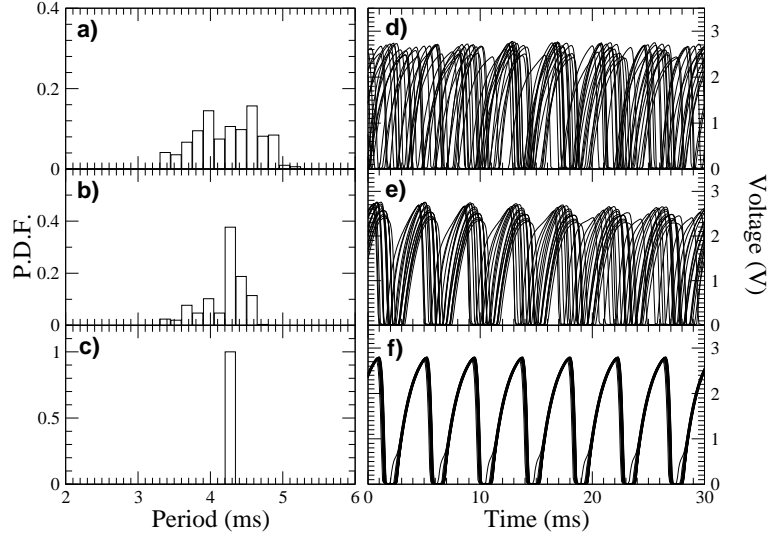


Figure 3.4: *Experimental time series (d,e,f) and probability distribution function (pdf) of the oscillation periods (a,b,c) for a population of 16 repressilators. The coupling strength increases when the resistance decreases (the currents between the coupled circuits flow easier). In this figure we show three cases starting from low coupling (upper figures) to high coupling (lower figures). From upper figure to lower figure we have: low $R_i^c = 5.1 \text{ k}\Omega$ (a,d), intermediate $R_i^c = 2.2 \text{ k}\Omega$ (b,e) and high $R_i^c = 0.24 \text{ k}\Omega$ coupling (c,f). Note that the coupling is measured by the inverse of R_i^c in such a way that when R_i^c decreases the coupling increases.*

a way of coupling repressilators [7], with the aim of observing global oscillations of the colony. In this section, we reproduce the numerical observations of [7] using a collection of globally coupled electronic repressilators. The internal parameters of the circuits are adjusted to make them oscillate at different frequencies, and a global coupling is introduced through a resistance R_i^c placed at the output of the first transistor (T1) of each repressor. All coupling resistances are connected to a common point, allowing an exchange of information about the dynamical state of the repressilators through the intensities of each branch. The coupling intensity is controlled by adjusting the values of R_i^c , which are set to be the same: coupling increases as the coupling resistance decreases. The experimental setup is composed of 16 coupled electronic repressor as shown in the Fig. 3.6. One of the dynamical variable of the 16 circuits is recorded with a A/D converter board with 16 inputs.

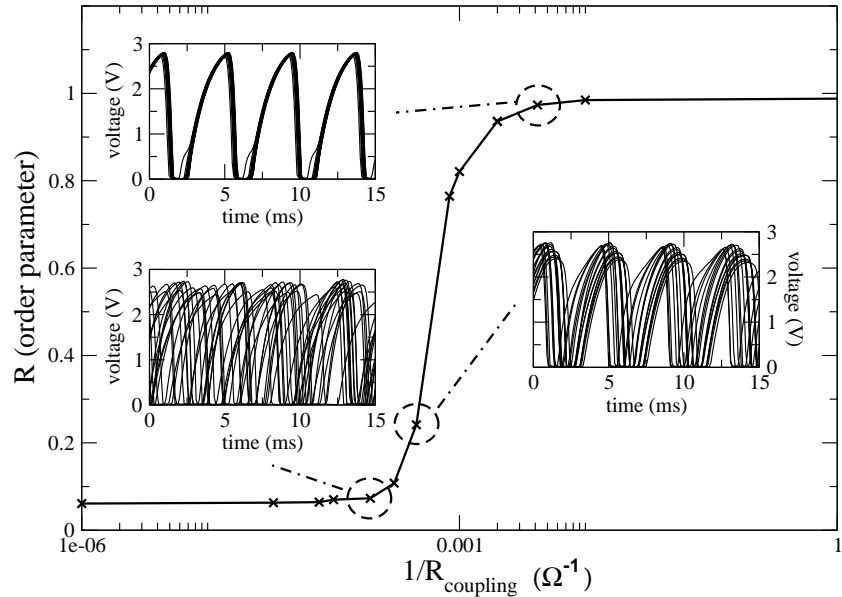


Figure 3.5: *Synchronization transition of a population of electronic repressilators for increasing values of the coupling parameter. An order parameter R (see Eq. (3.10)) close to one indicates synchronization of the population of repressilators for values of $1/R_i^c > 0.001\Omega^{-1}$. This figure shows the characteristic transition to synchrony of a population of coupled oscillators when the coupling is increased.*

Figure 3.4 (d,e,f) shows the temporal evolution of a population of 16 electronic repressilators for increasing coupling (that is decreasing coupling resistance R^c). Time series correspond to the voltage at the output of the first transistor. Panels (a,b,c) of the figure show the probability distribution function (pdf) of the period between oscillations. For low coupling ($R_i^c = 5.1 \text{ k}\Omega$), repressilators oscillate unsynchronized at their own frequency (upper plots), and the pdf has a wide distribution of periods. Intermediate values of coupling ($R_i^c = 2.2 \text{ k}\Omega$), show a partial entrainment (central plots), which is reflected by the appearance of a peak at the pdf. Finally, when coupling is further increased ($R_i^c = 0.24 \text{ k}\Omega$), we achieve synchronization of all repressilators (bottom plots), denoted by the unique peak at the pdf. It is worth noting that repressilators oscillate not only at the same frequency but also at the same phase, a fact that can only be observed at the time series of the voltage as shown in Fig. 3.4 (e). Our experimental observations agree qualitatively with the numerical simulations of [7] and confirm that global coupling would be a suitable way of obtaining synchronization of a colony of repressilators. Figure 3.5 shows a systematic study of the influence of coupling in the synchronization of the population of repressilators. We have evaluated the order parameter R given by the expression

$$R = \frac{\overline{\langle V_{2,i}^2 \rangle} - \overline{\langle V_{2,i} \rangle}^2}{\overline{\langle V_{2,i}^2 \rangle} - \overline{\langle V_{2,i} \rangle}^2}, \quad (3.10)$$

where $V_{2,i}(t)$ corresponds to the voltage at the T1 output of repressor i , $\langle \dots \rangle$ indicates time average and $\overline{\dots}$ denotes average over the population of repressilators. Low values of R correspond to the absence of coherent fluctuations of the system, while R close to the unity indicates a high coherence of the oscillations. Figure 3.5 corresponds to the classic synchronization phase transition predicted by Kuramoto [11] in coupled phase oscillators [12], and has been reported experimentally in coupled electrochemical oscillators [13] and in numerical simulations of a population of repressilators [7].

3.6 Forcing electronic repressilators

Synchronization of a population of repressilators by global coupling, reported above for our analog electronic circuits, has not yet been reproduced in a real

biochemical setting. In this section we propose a parallel source of entrainment, which can be provided by external influences [14]. An extra motivation in our case arises from the behavior of circadian rhythms, biochemical rhythms with a period close to 24 hours that have been observed ubiquitously among living organisms [15]. In the absence of external cues, the internal rhythms of such organisms drift with periods close to (but different from) 24 hours, but in the presence of external forcing they become perfectly entrained to the external period. In many organisms, the source of external forcing has been identified to be a variation of the light due to night and day cycles. Indeed, the molecular basis of the effect of light on different circadian biochemical networks has been unraveled [16]. The question on whether such

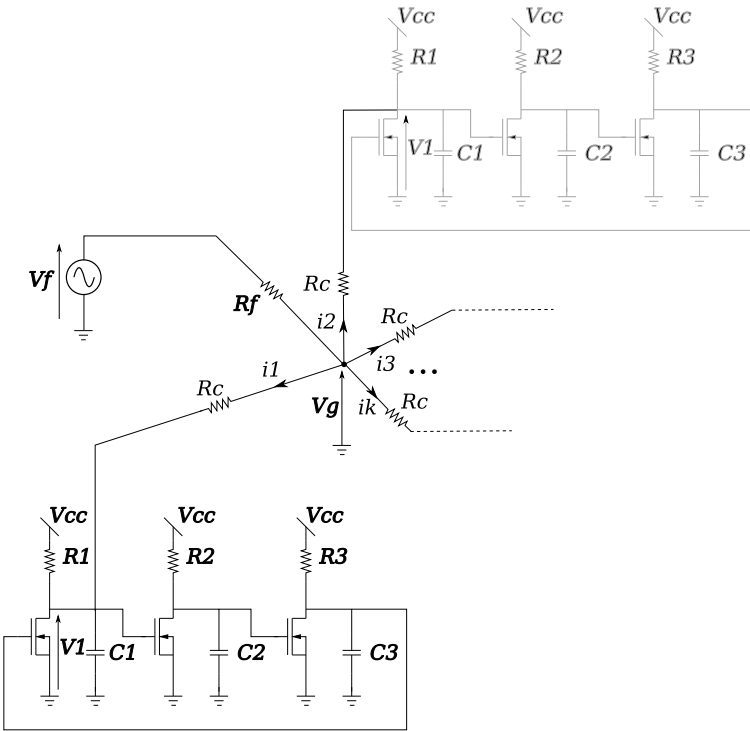


Figure 3.6: Schematic representation of the repressilator population. The coupling among the repressilators is controlled with the resistance R_c . A function generator is connected to the central node so that all units receive the same forcing. The amplitude of the forcing can be controlled with the amplitude of the generator V_f or with the resistance R_f .

external forcing is enough to induce the synchronization between circadian cells usually observed in experiments [17], or if coupling between the cells is needed, is still open. This is precisely what we address here, with the help of electronic circuits. We consider a population of electronic repressilators oscillating within a certain range of frequencies, i.e., in the absence of global oscillations. When a periodic external forcing is applied to the whole population, all repressilators would be affected by the same external frequency, leading to global oscillations. In our case, the electronic repressilators are forced by modulating the common point of the coupling resistances. An intermediate coupling resistance $R_f = 0.24 \text{ k}\Omega$ is placed between the common point and an external forcing voltage. The intensity of the forcing is controlled by the amplitude of the external voltage. Fig. 3.6 shows a schematic representation of a repressilator population where forcing and coupling are controlled.

This configuration allows to adjust both the coupling and the forcing of the system and analyze its combined effect on the synchronization of a population of repressilators. Figure 3.7 plots the time series (insets) and the power spectra of the whole system (16 repressilators) for three different forcing amplitudes A_f , and a given forcing frequency $f_f = 240 \text{ Hz}$. We have chosen the forcing frequency to be within the frequency range of the unsynchronized repressilators (150 Hz...300 Hz). In order to study only the influence of forcing, the coupling resistance is set to $R_i^c = 5.1 \text{ k}\Omega$, which corresponds to a negligible coupling [see Fig. 3.4 (a)]. For low values of forcing $A_f = 1 \text{ V}$ [Fig. 3.7 (a)], repressilators keep their oscillating frequencies, as shown by the time series and the wide power spectrum. If the forcing amplitude is increased $A_f = 2.4 \text{ V}$, we observe a reduction of the spectrum amplitude and an appearance of a central peak at the forcing frequency $f_f = 240 \text{ Hz}$ [Fig. 3.7 (b)]. At the same time, some repressilators seem to be frequency locked (inset of Fig. 3.7 (b)). Finally, for high enough values of the forcing amplitude, $A_f = 4 \text{ V}$, the power spectrum shows a unique peak, indicating that oscillators are frequency locked [Fig. 3.7 (c)]. Nevertheless, a phase shift is kept between them, as can be observed at the temporal evolution of their output voltages (inset of Fig. 3.7 (c)).

Now we consider different forcing frequencies, since it is well known that nonlinear oscillators can adjust their period of oscillations within a certain range of frequencies [18]. In Fig. 3.8 we plot the power spectrum and the corresponding time series for three different forcing frequencies f_f and a given forcing amplitude $A_f = 4 \text{ V}$. We have chosen the forcing frequencies to be

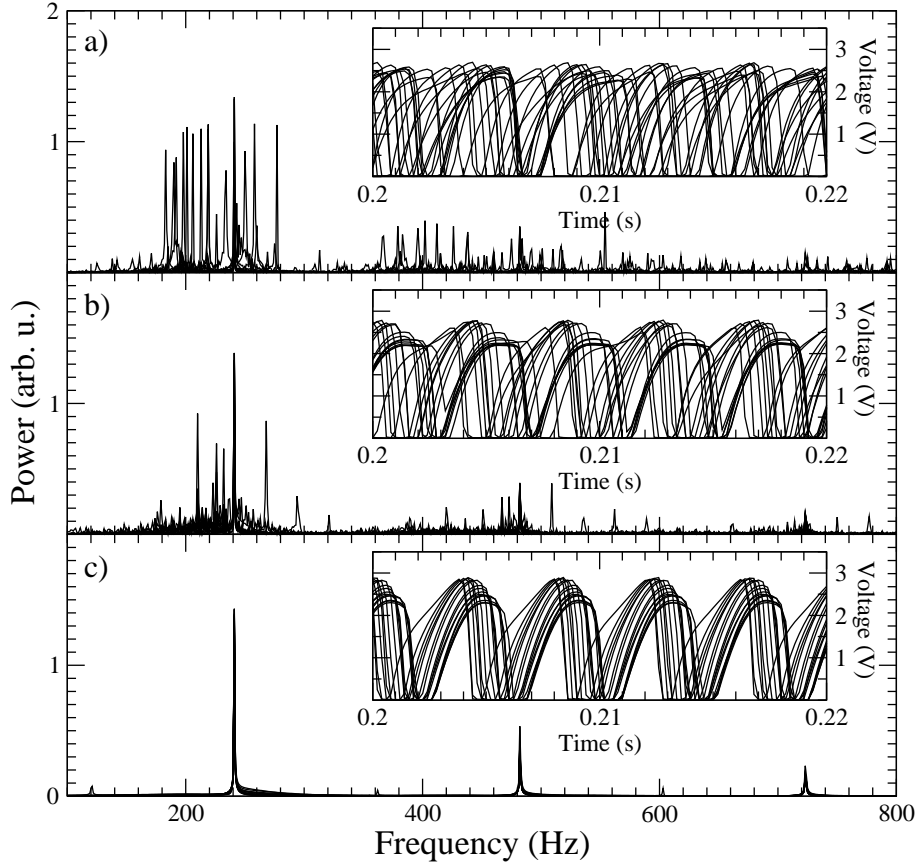


Figure 3.7: *Transition to synchronization by an external forcing of frequency $f_f = 240$ Hz: power spectrum of 16 repressilators for varying values of external forcing and their corresponding time series (inset).* The coupling between the units is set to a low value, so that we focus on the influence of forcing. The three figures show the power spectrum for increasing values of the forcing: (a) weak forcing $A_f = 1V$; (b) intermediate forcing $A_f = 2.4V$; (c) strong forcing $A_f = 4V$. For a weak forcing each unit present a different frequency of oscillation. At intermediate coupling some of the repressilators locked their frequency. At strong coupling values the system is synchronized.

inside (b) and outside (a,c) the frequency distribution range of the population of repressilators. When the forcing frequency is too low, repressilators do not follow it, and the power spectrum does not show any peak at the forcing frequency [Fig. 3.8 (a)]. If the forcing frequency enters a region close to

the natural frequencies of the repressilators, the system is entrained by the forcing frequency [Fig. 3.8 (b)]. Nevertheless we still observe a phase shift at the time series (inset). The entrainment is optimum for a central frequency $f_f = 240$ Hz and it is gradually lost when the frequency is further increased [Fig. 3.8 (c)].

At this point it is worth noting the differences between forcing and coupling. Figure 3.9 shows the synchronization of the population of repressilators for the two different techniques. We can see that despite of having the same power spectrum, i.e., the same oscillating frequency, the time series show a phase shift between repressilators only for the case of forcing. In fact, we must distinguish between two different synchronized states. In the case of a coupled population, we achieve both frequency and phase locking leading to an order parameter R close to the unity. Nevertheless, when we introduce external forcing in an uncoupled system, we observe only frequency locking and the phases of each oscillator depend on its initial conditions. This fact slightly reduces the efficiency of this technique, decreasing the amplitude of the global oscillations.

If coupling and forcing are considered at the same time, a better entrainment of the global oscillations would be expected. To check this conjecture we scan the amplitude and frequency of the forcing signal in the absence or presence of coupling. In Fig. 3.10 we plot the results obtained with a frequency step of $\Delta f = 20$ Hz and an amplitude step of $\Delta A = 0.5$ V. Two cases are shown; the left plot corresponds to negligible coupling between repressilators, whereas coupling and forcing are jointly considered in the right plot. For the latter case, we set the coupling to intermediate values [$R_i^c = 2.2$ k Ω , see Fig. 3.4 (b)].

At first sight, a resonance region appears in both cases, although some differences exist. In the absence of coupling (left plot), the synchronization region is reduced, showing a sharp peak. In addition, we observe low peaks at the first harmonic of the resonance frequency. Nevertheless the highest value corresponds to $R = 0.46$, which is considerably low compared with the highest peak of the coupling case $R = 0.92$. Such differences are caused by the phase shift, since the order parameter R measures correlations between series at zero lag (i.e. without phase shift). If coupling is considered (right plot), R has high values even for the case of forcing at low/high frequencies. Synchronization is increased when the forcing frequency enters the region of natural frequencies of the system. Furthermore, resonances at the first harmonic of the natural frequencies are also observed.

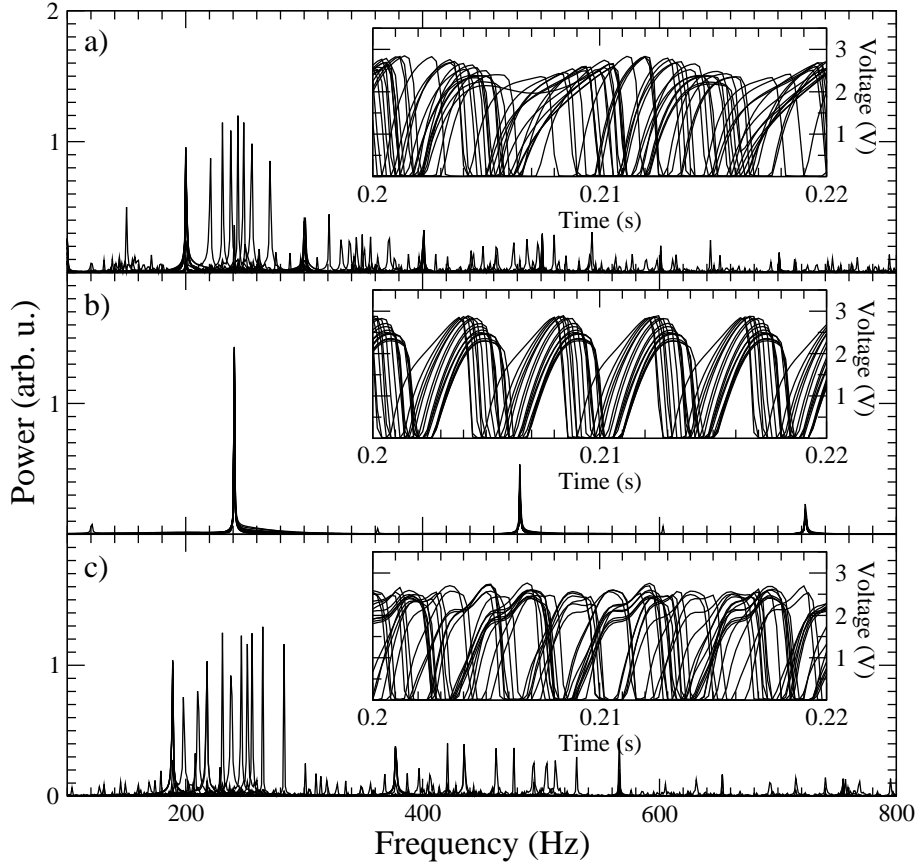


Figure 3.8: *Influence of the external frequency on the synchronization of analog repressilators.* We fix the amplitude of the external forcing to a high enough value $A_f = 4V$ while its frequency f_f is modified in a range close to the natural frequency of the repressilator population. In (a) although the forcing strength is high, synchronization is not observed for low values of the forcing frequency $f_f = 100$ Hz. In (b) the entrainment is achieved when the forcing frequency $f_f = 240$ Hz is close to the natural frequency of the electronic repressilators. In (c) we lose again synchronization if the forcing frequency is further increased, $f_f = 560$ Hz.

These results indicate that external forcing enhances synchronization in a population of globally coupled repressilators. However, these results are not so good when the coupling is suppressed or reduced to a negligible part. With only the forcing acting, a phase shift between the repressilators appears as in

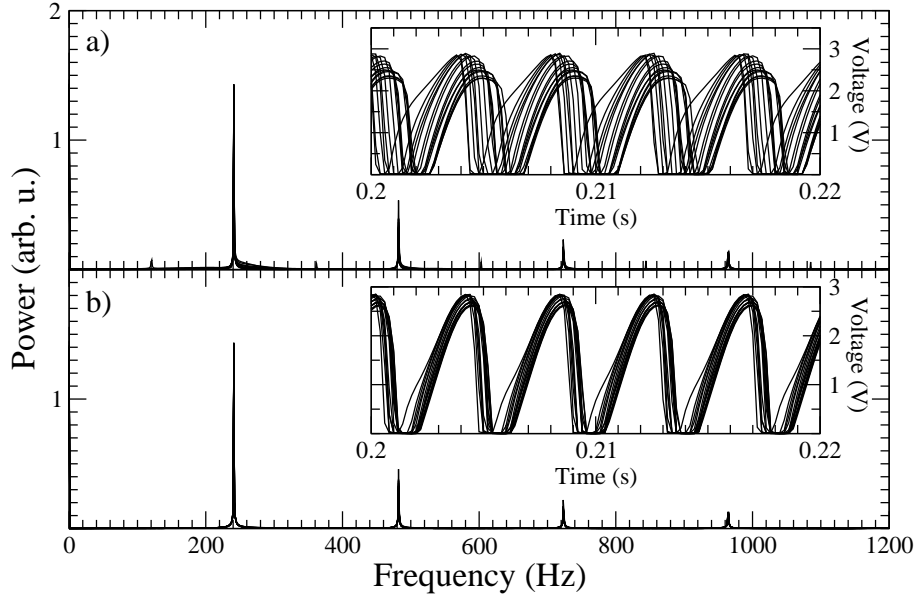


Figure 3.9: *Comparison between synchronization by forcing (a) and coupling (b).* We can observe that although both spectra are similar, which means that there is an entrainment to the external frequency, the phase difference only disappears when repressilators are coupled (b). The population of repressilators oscillates at the forcing frequency nevertheless when the coupling between units disappears a phase deviation appears between the units.

the inset of Fig. 3.7 (c) and the total coherence R of the system decreases.

3.7 Simulations of others genetic networks

3.7.1 The electronic toggle switch

Following the same procedure as in the electronic repressilator, we can build other electronic-circuit representation of genetic networks. For example, removing one transistor from the repressilator circuit leads to a bistable system similar to the toggle switch developed in [5] by Gardner *et al.*. The toggle switch is a simple network of two repressor genes, where each of the repressor proteins binds to the promoter of the other one, see Fig. 3.11 (a). In this way, when a repressor dominates, the system remains at the same state unless an external effect changes it, by degrading artificially one of the repressors, so

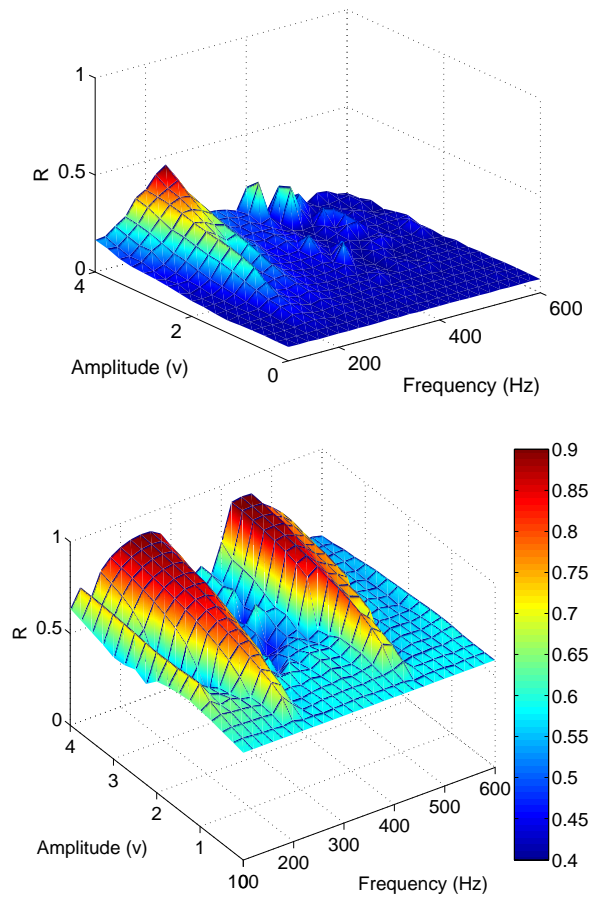


Figure 3.10: Synchronization efficiency of external forcing in the presence (lower plot) and absence (upper plot) of coupling. The axes correspond to the forcing frequency (X), forcing amplitude (Y) and the corresponding order parameter (Z). In the absence of coupling (left plot), we observe a maximum (resonance) close to the region of the natural frequency of the repressilators. We can also observe a low peak close to the first harmonic of the resonance frequency. When coupling and forcing are considered, we can observe an increase of the order parameter. Nevertheless we can still observe a region where the system enters resonance with the external forcing. The peak at the first harmonic has increased (compared with the uncoupled case) and both resonance regions are now wider.

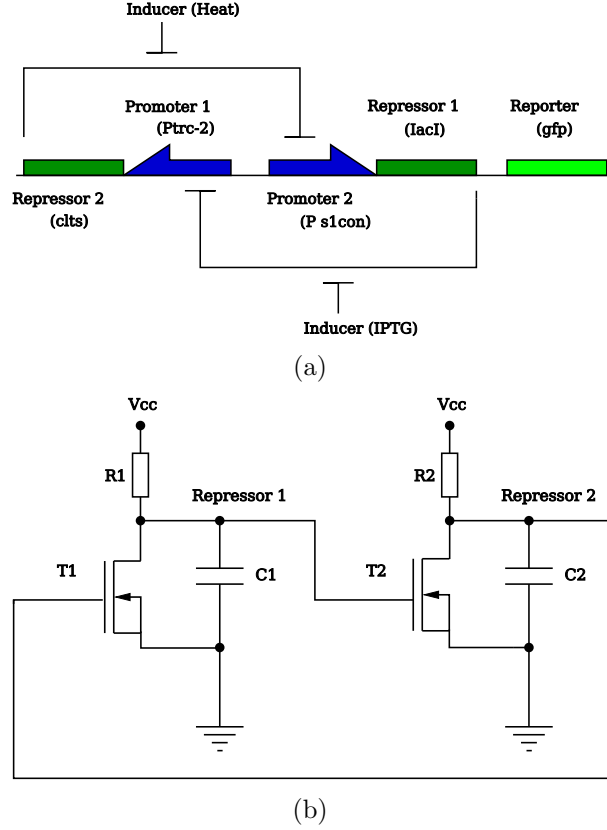


Figure 3.11: (a) Network architecture of a bistable genetic network toggle-switch. Two repressor genes are mutually connected by negative feedback. Promoters (in blue) of each gene (in green) are repressed by proteins transcribed from the previous gene. A green fluorescent protein (GFP), associated to a protein (cI) level, acts as the reporter of the system state. (b) Electronic setup of the analog toggle-switch. The output of each transistor corresponds to the level of the two repressor proteins.

the other one takes over and the state is changed.

The design of the circuit is similar to the electronic repressilators, but it contains only two basic units, each one consisting of a transistor and a RC circuit. We assume that the voltage of one component (T1) is large. Since it is applied at the gate of the other transistor (T2), it inhibits the second component, whose output voltage is switched off. The differential equations

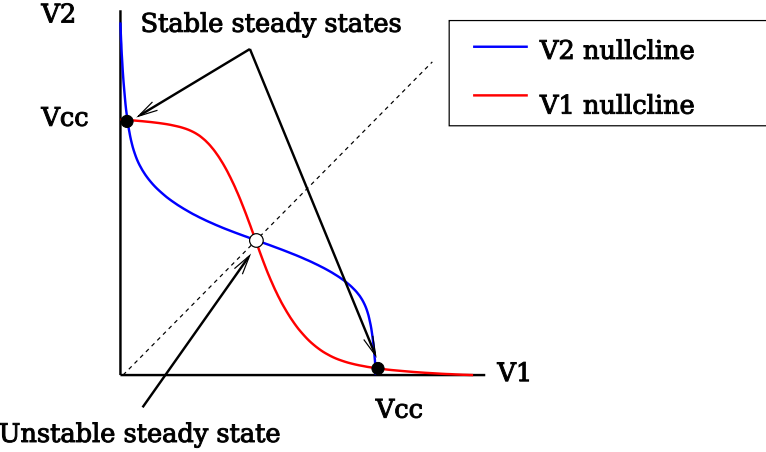


Figure 3.12: Phase portrait of the system described in the Eqs. (3.11) and (3.12). There are three steady states in the system: two stable and one unstable. The nullclines are in solid red and blue lines. The separatrix dividing the two basins of attraction is drawn in dashed lines.

of the system are:

$$R_1 C_1 \frac{dV_1}{dt} = -V_1 + V_{cc}(1 - f(V_2)), \quad (3.11)$$

$$R_2 C_2 \frac{dV_2}{dt} = -V_2 + V_{cc}(1 - f(V_1)), \quad (3.12)$$

where the function $f(x)$ was given in Eq. 3.2. The phase diagram of the system is displayed in the Fig. 3.12. The phase portrait of the system contains three stable states, two of them stable and the other one unstable. Moreover it is divided into two parts with a separatrix marking the boundary between the two basins of attraction. When the state of the system crosses the separatrix after being forced, it jumps to the other basin of attraction and a switching occurs.

First of all, we must check the switching properties of the Electronic Toggle Switch (ETS). In bistable systems, switching between states must be produced by external induction. In our case, the inducer is an external voltage source, whose potential is applied through a discharge resistance R_d . Since the system is bistable, we first turn off the output voltage of transistor T1 (i.e. turn on T2). Next, we turn off T2, leading to a turn-on of T1.

Figure 3.13 shows the evolution of a population of toggle switches in

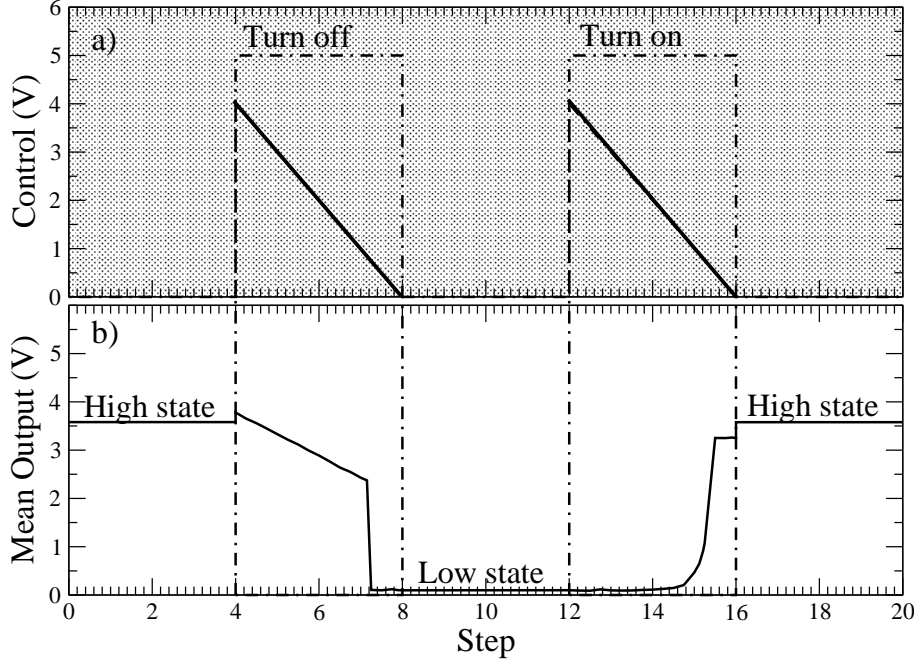


Figure 3.13: *Control of an electronic toggle-switch population by external forcing. Starting from all bistable switches at the high state, we induce a jump by forcing repressor 1 of each toggle-switch with an external potential (steps 4 to 8). In the absence of forcing the toggle-switch population keeps its state (steps 8 to 12). We can turn on the system again by forcing the opposite repressor (step 12 to 16). The system keeps its state when external forcing is removed (step 16 to 20).*

response to a global external driving. The upper plot depicts the inducing voltage, and the lower plot shows the mean voltage of T1 for the whole population of repressilators. The system, which is initially at the high state, suffers the action of an external inducer at step 4. The output voltage of the population of repressilators decreases until the system jumps towards the off state. At step 8 we stop the inducing action and the system remains off. The turning-on process begins at step 12, where a forcing potential is applied, in this case, at the T2 output. A jump to the high state is observed after step 15, remaining at this point even when the external inducer is removed.

The results obtained with the ETS match with those reported in a real genetic network [5]. The advantage of using ETS is that its simplicity allows

to test different configurations of coupling. It can be easily coupled with other circuit like a repressilator so that the study of the dynamics of these complex systems results simple.

3.7.2 The delay oscillator

In this section we present a different kind of genetic oscillator present in many living beings. The principle of the oscillator is shown in Fig. 3.14 (a). It consists in a simple autorepressive loop which is a self-inhibitory gene network. The gene produces its own repressor but this one acts only after a time delay τ due to the successive steps of the processing of the mRNA and the proteins. Similar oscillators have been observed in circadian oscillators and in the early development of the chicken and zebrafish embryos called the segmentation oscillator [19, 20, 21, 22]. The transcriptional oscillator works as follow. First, the genetic information is transcribed into mRNA and then transported from the nucleus to the cytoplasm with a delay τ_m . Once the mRNA is in the cytoplasm the translation and the processing of the protein begins. Several operations take place during this time τ such as the phosphorylation, dimerization, folding and so on. The time delay accumulated during the translation is τ_p . Following this step, the protein is transported to the nucleus in order to interact with the promoter of the gene producing an additional time delay τ_t . The total time lag between the beginning of the process and the return of the protein to the nucleus can be summed into a single delay $\tau_d = \tau_m + \tau_p + \tau_t$. The simple autoregulated genetic network can be formulated by two ordinary differential equations:

$$\frac{dm}{dt} = \frac{k_m}{1 + (\frac{p(t-\tau_d)}{p_0})^2} - \gamma_m m \quad (3.13)$$

$$\frac{dp}{dt} = k_p m - \gamma_p p, \quad (3.14)$$

where m is the mRNA level and p is the corresponding protein level. The conditions on τ_d for the oscillations of the system can be derived analytically. We build an analog electronic circuit composed of a negative feedback loop with a MOSFET transistor. The circuit is represented in Fig. 3.14 (b). The voltage V holds for the level of proteins, which increases as the capacitor charges from the resistor R . This signal is delayed through a digital delay line. The delayed signal is applied onto the gate of the MOSFET transistor, which

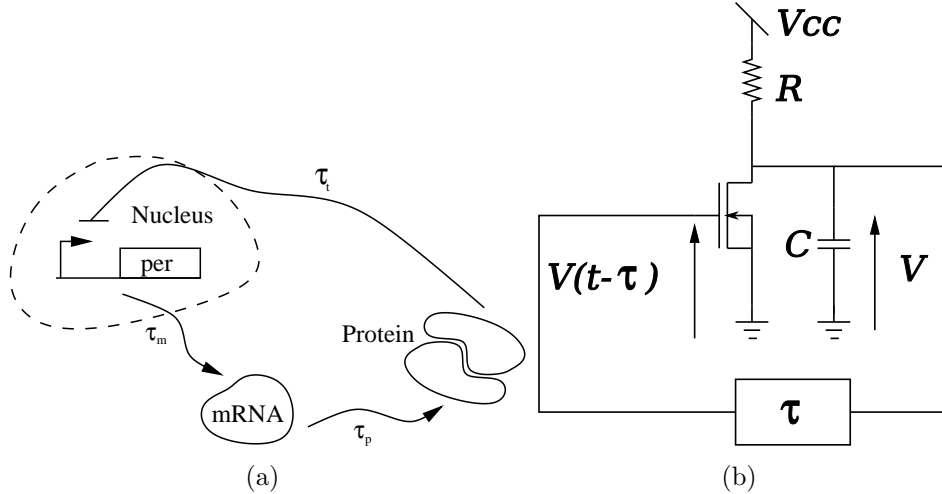


Figure 3.14: *Schematic of the genetic oscillator with delay. At each step of the process, during the transcription, the protein synthesis and nucleus translation a time lag is generated. The total delay of the negative feedback loop is $\tau_d = \tau_m + \tau_p + \tau_t$. The accumulation of the delays in the repression process can lead to oscillations when τ_d is large enough. The Fig. (b) shows the equivalent electronic circuit designed for the simulation of the dynamics of this kind of genetic oscillators. The voltage V represents the protein level. This level grows when the RC circuit connected to V_{cc} begins to charge. This tension is delayed through a digital delay line. The delayed voltage $V(t - \tau)$ is fed back to the MOSFET transistor. When the delayed tension exceeds the threshold V_{th} the output of the MOSFET transistor is switched off and the protein production is inhibited. For sufficiently large delays, oscillations of the protein level arise. Parameters: $V_{cc} = 10\text{ V}$, $C = 22\mu\text{F}$, $R = 5\text{k}\Omega$, $V_{th} = 2.3\text{ V}$, MOSFET 2N7000.*

acts as a promoter. When the level of $V(t - \tau_d)$ exceeds the threshold V_{th} the output of the transistor is switched off, which means that the production is stopped. In other words the gene is inhibited. With small delays the system reaches a stable state. However when the delay of the feedback loop is increased, the stability of the stable state is affected and oscillations arise for a sufficiently large time delay. For the simplicity of the circuit we consider that the time delay is large in comparison to the protein translation so that we consider this reaction instantaneous. With this assumption Eq. 3.13 can

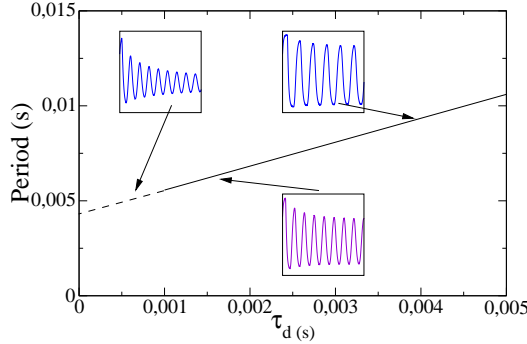


Figure 3.15: *Dynamics of the circuit represented with the period of the oscillations and with time-series for some values of the time delay of the negative feedback loop. The period grows almost linearly with the time delay as shown in the inset. The dashed line represent the period of the damped oscillations, in this region the system is stable.*

be simplified into a single equation and we can rewrite the equation of the circuit as:

$$RC \frac{dV}{dt} = \frac{V_{cc}}{1 + \left(\frac{V(t-\tau_d)}{V_{th}}\right)^n} - V \quad (3.15)$$

this equation is an autonomous oscillator since the delayed variable inhibits its own production. Moreover the differential equation representing the circuit has the same form than the Mackey-Glass model [22]. More on this model can be found in Chap. 5 in the appendix I. The experimental results of the circuit are shown in the Fig. 3.15. This figure shows the bifurcation diagram of the circuit as the delay in the feedback loop increases. The period of the circuit increases almost linearly with the time-delay as shown in the inset. The role of the time delay in the genetic oscillator can be very important since time delays tend to destabilize the system and help the system to oscillate. We showed here that a very simple electronic circuit with a digital delay line reproduces the dynamics of this class of oscillators.

3.8 Conclusions

In this chapter, we have proposed the use of nonlinear electronic circuits to analyze the dynamics of populations of synthetic genetic networks. An

electronic repressilator have been designed under the same operating conditions as the *genetic repressilator*. Experimentaly we showed that the global coupling in the synchronization locks the frequency and the phase of a population of electronic repressilators. Next, we have studied the influence of an external forcing in the synchronization of the system and we have seen that despite that we obtain frequency locking, phase locking is not achieved. The results indicate that external forcing is a suitable technique to enhance synchronization in combination with coupling between repressilators, but is less efficient when applied by itself. The methodology has been shown to be also efficient for the simulation of different gene network such as auto-repressive network with delay and toggle genetic switches. We showed that the dynamics of this population of genetic networks can be reproduced with simple electronic circuits.

Appendix I: Exact model of the repressilator circuit

The basic unit of the repressilator like circuit can be viewed in the Fig. 3.16.

The core of the model is a MOSFET circuit which behave as a switch controlled by the gate voltage. Based on the MOSFET enhancement n-channel model we have the following expression for the drain current i_d :

$$i_d(V_i, V_{i-1}) = \begin{cases} 0 & \text{for } V_{i-1} < V_{th} \\ K(2V_i(V_{i-1} - V_{th}) - V_i^2) & \text{for } 0 < V_i < V_{i-1} - V_{th} \\ K(V_{i-1} - V_{th})^2 & \text{for } 0 < V_{i-1} - V_{th} < V_i, \end{cases} \quad (3.16)$$

with K a parameter depending on the MOSFET particular model. Other models can also be used for the drain current. A simpler model can be approximated in the form of a continuous function:

$$id(V_i, V_{i-1}) = K(V_{i-1} - V_{th})^2 \left(\frac{V_i}{V_i + V_{i-1} - V_p} \right) \left(\frac{(V_{i-1}/V_p)^n}{1 + (V_{i-1}/V_p)^n} \right).$$

However this function is less accurate than the exact model.

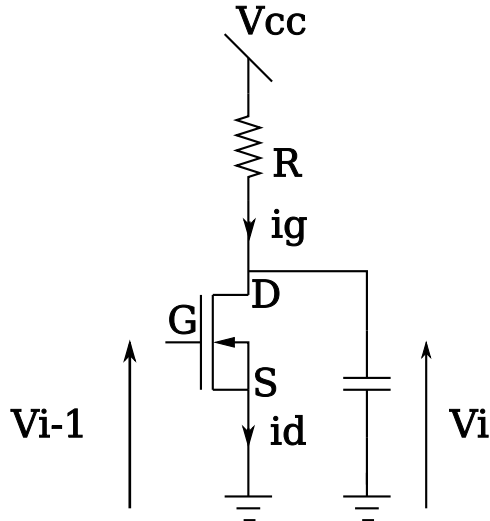


Figure 3.16: Basic cell of the repressilator circuit.

The equation that rules the dynamics of one basic cell can be written as:

$$C_i \frac{dV_i}{dt} = \frac{(V_{cc} - V_i)}{R_i} - i_d(V_i, V_{i-1}). \quad (3.17)$$

Which is the sum of the currents in the transistor C_i . The complete model of the repressilator circuit is set of ODEs that can be written as:

$$C_2 \frac{dV_2}{dt} = \frac{(V_{cc} - V_2)}{R_2} - i_d(V_2, V_1), \quad (3.18)$$

$$C_3 \frac{dV_3}{dt} = \frac{(V_{cc} - V_3)}{R_3} - i_d(V_3, V_2), \quad (3.19)$$

$$C_1 \frac{dV_1}{dt} = \frac{(V_{cc} - V_1)}{R_1} - i_d(V_1, V_3). \quad (3.20)$$

The coupling between the units is achieved through a common resistor to all circuits as shown in Fig. 3.8. The voltage V_1 of each circuit is connected to a common point through a resistor R_c . We obtain this way a global coupling of the system.

To obtain the equation of the coupled circuit we have to consider first the voltage V_g of the common point were all the resistors R_c are connected. The current flowing from this point to one of the voltage V_1 of the repressilator n is:

$$i_n = \frac{(V_g - V_1^n)}{R_C}, \quad (3.21)$$

with V_1^n the voltage V_1 of the circuit n . On the other hand we have the sum of all the current at this point:

$$\sum_{n=1}^N i_n = 0, \quad (3.22)$$

which leads to:

$$\sum_{n=1}^N (V_g - V_1^n) = 0. \quad (3.23)$$

We deduce that V_g is the mean of all the voltages:

$$V_g = \frac{1}{N} \sum_{n=1}^N V_1^n. \quad (3.24)$$

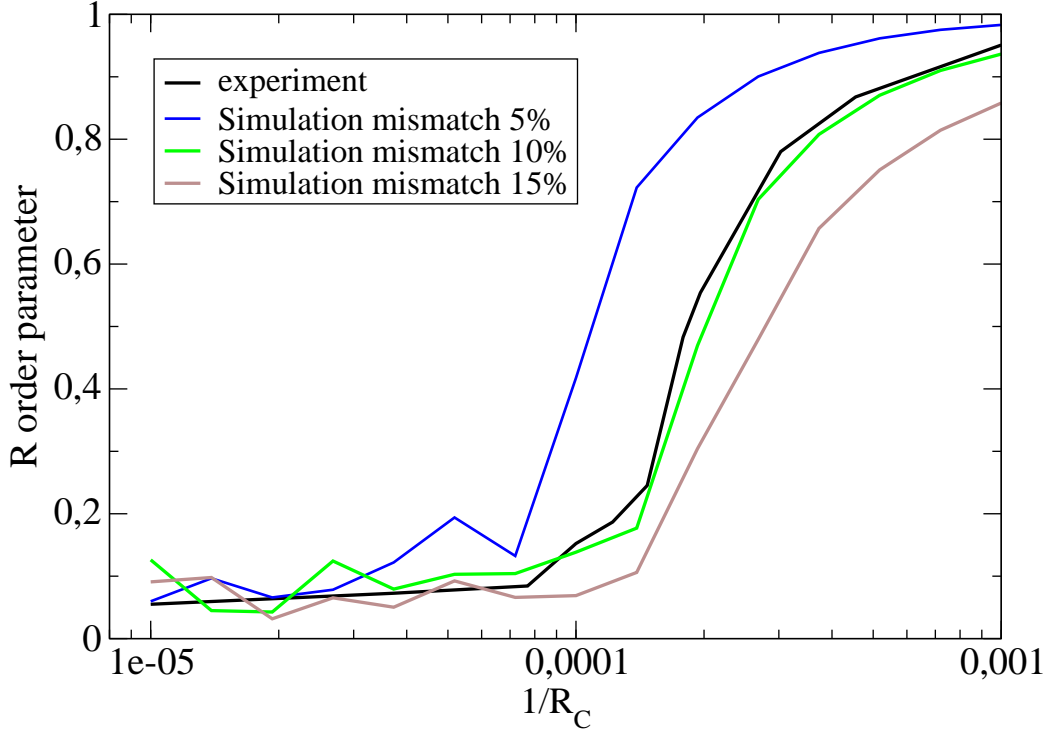


Figure 3.17: *Synchronization curves of the system with 16 units in function of the coupling resistance R_c for the experiments and the numerical simulations.*

It is now straightforward to deduce the ODE of the coupled system:

$$C_2 \frac{dV_2}{dt} = \frac{(V_{cc} - V_2)}{R_2} - i_d(V_2, V_1) \quad (3.25)$$

$$C_3 \frac{dV_3}{dt} = \frac{(V_{cc} - V_3)}{R_3} - i_d(V_3, V_2) \quad (3.26)$$

$$C_1 \frac{dV_1}{dt} = \frac{(V_{cc} - V_1)}{R_1} - i_d(V_1, V_3) + \frac{1}{R_c} \frac{1}{N} \sum_{n=0}^N (V_1^n - V_1) \quad (3.27)$$

The parameters used in the experiments are:

- $R_1 = R_2 = R_3 = 1k\Omega$ with a variability of 10%
- $C_1 = C_2 = C_3 = 1\mu F$ with a variability of 10%

- $V_{cc} = 3V$
- $V_{th} = 2.3V$ with a variability of 10%
- $K = 400 \cdot 10^{-3} \text{ A/V}^2$

Figure 3.17 summarize the experiments with circuits and the numerical simulation with the previous model. Different mismatch on the parameters R , C and V_{th} has been applied to the simulation. It seems that the closest simulation to the experiment is for a 10% mismatch.

References

- [1] F. Jacob and J. Monod, “Genetic regulatory mechanisms in the synthesis of proteins”. *J Mol Biol.* **3**, 318 (1961).
- [2] A-L Barabási and Z. N. Oltvai, “Network biology: understanding the cell’s functional organization”, *Nature Rev. Genetics* **5**, 101 (2004).
- [3] C. Yanofsky, “Attenuation in the control of expression of bacterial operons”, *Nature* **289**, 751 (1981).
- [4] A. Becskei and L. Serrano, “Engineering stability in gene networks by autoregulation”. *Nature* **405**, 590 (2000).
- [5] T. S. Gardner, C. R. Cantor, and J. J. Collins, “Construction of a genetic toggle switch in Escherichia coli”, *Nature* **403**, 339 (2000).
- [6] M.B. Elowitz and S. Leibler, “A synthetic oscillatory network of transcriptional regulators”, *Nature* **403**, 335 (2000).
- [7] J. García-Ojalvo, M.B. Elowitz and S. Strogatz, “Modeling a synthetic multicellular clock: Repressilators coupled by quorum sensing”, *Proc. Natl. Acad. Sci. U.S.A.* **101**, 10955 (2004).
- [8] J. Mason, P.S. Lindsay, J.J. Collins and L. Glass, “Evolving complex dynamics in electronic models of genetic networks”, *Chaos* **14**, 707 (2004).
- [9] D. McMillen, N. Kopell, J. Hasty and J.J. Collins, “Synchronizing genetic relaxation oscillators by intercell signaling”, *Proc. Natl. Acad. Sci. USA* **99**, 679 (2002).

- [10] L. You, R.S. Cox, R. Weiss and F.H. Arnold, “Programmed population control by cell-cell communication and regulated killing”, *Nature* **428**, 868 (2004).
- [11] Y. Kuramoto, “*Chemical Oscillations, Waves, and Turbulence*”, (SpringerVerlag, Berlin, 1984).
- [12] S.H. Strogatz, “From Kuramoto to Crawford: Exploring the onset of synchronization in populations of coupled oscillators”, *Physica D* **143**, 1 (2000).
- [13] I. Z. Kiss, Y. Zhai and J. L. Hudson, “Emerging coherence in a population of chemical oscillators”, *Science* **296**, 1676 (2002).
- [14] H. Kori and A. S. Mikhailov, “Entrainment of Randomly Coupled Oscillator Networks by a Pacemaker”, *Phys. Rev. Lett.* **93**, 254101 (2004).
- [15] D. Bell-Pedersen, V. M. Cassone, D. J. Earnest, S. S. Golden, P. E. Hardin, T. L. Thomas, and M. J. Zoran, “Circadian rhythms from multiple oscillators: lessons from diverse organisms”, *Nature Rev. Genetics* **6**, 544 (2005).
- [16] M. Menaker, “Circadian photoreception”, *Science* **299**, 213 (2003).
- [17] S. Yamaguchi, H. Isejima, T. Matsuo, R. Okura, K. Yagita, M. Kobayashi, and H. Okamura, “Synchronization of cellular clocks in the suprachiasmatic nucleus”, *Science* **302**, 1408 (2003).
- [18] V. Anishchenko, A. Neiman, A. Astakhov, T. Vadivasova, and L. Schimansky-Geier, “*Chaotic and Stochastic Processes in Dynamic Systems*” (Springer Verlag, Berlin, 2002).
- [19] J. Lewis, “Autoinhibition with Transcriptional Delay - A Simple Mechanism for the Zebrafish Somitogenesis Oscillator”. *Current Biology* **13**, 1398 (2003).
- [20] L. Chen, R. Wang, T. J. Kobayashi and K. Aihara, “Dynamics of gene regulatory networks with cell division cycle”. *Phys. Rev. E* **70**, 011909 (2004)

- [21] S. Bernard, B. Ajavec, L. Pujo-Menjouet, M. C. Mackey and H. Herzel, “Modeling transcriptional feedback loops: The role of Gro/TLE1 in Hes1 oscillations”. *Phil. Trans. Roy. Soc. A* **364**, 1155 (2006)
- [22] M. C. Mackey and L. Glass, “Oscillations and chaos in physiological control systems”, *Science* **197**, 287 (1977).

Chapter 4

Synchronization of coupled systems with delay

4.1 Introduction

Chaos synchronization was initially focused in unidirectionally coupled systems [1]. The reason beyond this fact could be that, for technical applications, it is interesting to reproduce the state of a certain chaotic system, no matter the distance or the number of the replica systems. This kind of configuration is commonly known as master-slave configuration [2] and is the most extended technique to synchronize chaotic systems [3]. Most of the applications were achieved in the chaotic communications field, where a chaotic transmitter hides a secret message which is recovered at the receiver when the latter synchronizes with the chaotic part of the received input [4, 5], i.e., reproducing the state of the transmitter. Nevertheless, in Nature the oscillators are essentially bidirectionally coupled.

Without regard to the direction of the coupling, the interaction between two chaotic systems have been deeply studied during the last decade, focusing in the ability of synchronization even in the presence of noise or delay [3]. More recently, the spread of complex networks have dealt with synchronization in large communities of chaotic systems showing the emergence of complex behaviours [6, 7]. Less attention has been paid to the transition from the simplest case, i.e., two bidirectionally coupled systems, to a broad community of chaotic oscillators.

Here we depart from two chaotic systems bidirectionally coupled with de-

lay and show a counter-intuitive phenomenon that arises when a third chaotic element placed between them is considered: *the isochronous synchronization of the two outer chaotic systems*. This fact has been recently reported in bidirectionally coupled semiconductor lasers [8, 9], where a third laser, in this case, is also requested. The present work follows the path opened by Fischer *et al.* [8] and goes one step beyond. First, we analyse the robustness of the phenomenon for different delay times, showing that accurate values of the delay time are not required. Second, we give the first experimental evidence, at the moment of the writing of the Ph.D. thesis, that the relaying system could be different from those to be synchronized at zero-lag. The chapter is organized as follows: In Section 4.2, we study the synchronization of two mutually coupled chaotic circuits, with a certain delay in the coupling path. We show that zero-lag synchronization is not observed in this particular configuration. In Section 4.3, we introduce a relay system between the two chaotic circuits and observe the appearance of isochronous (zero-lag) synchronization between the outer units. Finally, in Section 4.4 we show, with an example, that zero-lag synchronization holds even when a different dynamical system is used as the relay system, ending with some concluding remarks.

4.2 Mutually coupled chaotic circuits

Unidirectional synchronization of chaotic circuits and specifically, Chua circuits, have been deeply studied during the last years. From two circuits to a chain of many of them, synchronization have been reported under different experimental setups.

In a general framework, we can distinguish between different types of synchronization if we consider the system that is leading the dynamics along with the delay between the outputs of the synchronized systems. In lag synchronization [10], for example, the receiver system follows the evolution of the transmitter with a delay τ due to a parameter mismatch. In achronal synchronization, there is a time lapse between the output of the synchronized systems, which is a consequence of a certain delay in the transmission line. More recently, a counter-intuitive phenomenon has been reported, the anticipated synchronization, where the receiver system advances in time the signal of the transmitter [11, 12].

In all cases, when considering unidirectional injection, a leader and fol-

lower role can be distinguished, being the former the system that sends the signal to the other. However, this reasoning does not apply for the case of mutually (bidirectional) coupled systems. In this condition, the leader and follower role can only be inferred from the analysis of the circuit outputs. When two system are considered, both circuits affect each other and eventually synchronize, which lead any of them to assume the role of the leader (or follower).

Here we are interested in the synchronization between two chaotic electronic circuits when bidirectional coupling with delay is considered. Several works have dealt with mutually coupled chaotic circuits [13, 14, 15, 16, 17], nevertheless less attention has been paid to electronic circuits coupled with delay. For the case of two chaotic systems, lasers have been the paradigmatic example of coupled systems with delay [18, 19, 20, 21]. The seminal work of Heil *et al.* [18] has shown the influence of the non-negligible coupling time between two mutually coupled lasers. Specifically, a synchronization between two chaotic lasers was observed with a time delay τ_c , corresponding to the time for the output signal to travel between the two dynamical systems. Furthermore an alternation between the leader and the follower was observed, i.e., there was not a clear leader (follower) in the dynamics.

The experimental setup studied here is schematically represented in Fig. 4.2. The output of two chaotic Chua circuits is connected bidirectionally through a transmission line with a delay τ_c , which means that the output signal needs some time to arrive to the other circuit.

Figure 4.1 shows a detailed description of the Chua's circuit used in this work. A nonlinear resistor is connected to a set of passive electronic components (R, L, C). We have systematically studied the dynamical ranges of the circuit when R_{exc} is modified, observing stable, periodic, excitable and chaotic dynamics. Among all of them, we drive the circuit to have chaotic dynamics by setting $R_{\text{exc}} = 1.73 \text{ k}\Omega$. Under these conditions, the dynamics of the circuit in the phase space given by (V_1, V_2) lies in a double-scroll chaotic attractor [22]. The output of the circuit (V_1 or V_2) is sent to the other circuits (with the same characteristics) via a voltage follower, in order to guarantee unidirectional injection (see Appendix I below for details on the coupling implementation).

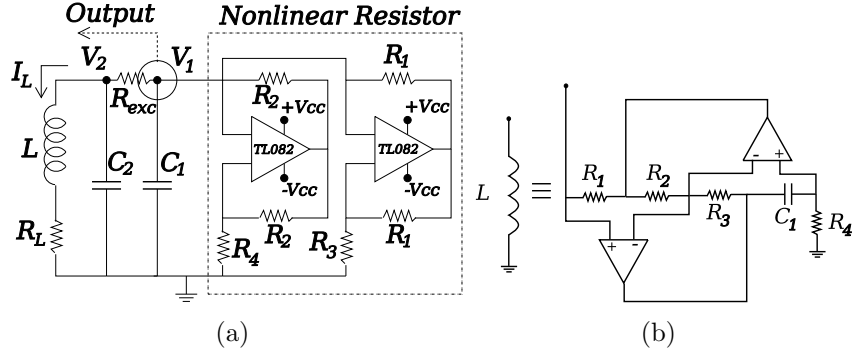


Figure 4.1: (a) Description of the Chua circuit, which is built with two TL082 operational amplifiers and passive electronic components of values: $V_{cc} = 15$ V, $R_1 = 222 \Omega$, $R_2 = 22 \text{ k}\Omega$, $R_3 = 2.2 \text{ k}\Omega$, $R_4 = 3.3 \text{ k}\Omega$, $R_L = 23 \Omega$, $C_1 = 10 \text{ nF}$, $C_2 = 100 \text{ nF}$, $L = 10 \text{ mH}$. We set $R_{exc} = 1.85 \text{ k}\Omega$ in order to have chaotic dynamics. V_1 and/or V_2 correspond to the outputs of the circuit, which are coupled to the other circuits through a voltage follower as shown in the experimental setup. Note that all the components have a 5% tolerance on their values. In the Fig. (b) we show an equivalent of the coil which is called the girator. This circuit emulates the coil behavior. It allows to control the frequency of the circuit easily. The equivalent inductance value is: $L = R_1 R_3 R_4 C_1 / R_2$.

The dynamics of the circuit are described by the equations [22]:

$$C_1 \frac{dV_1}{dt} = \frac{V_2 - V_1}{R_{exc}} - g(V_1, V_{cc}) \quad (4.1)$$

$$C_2 \frac{dV_2}{dt} = \frac{V_1 - V_2}{R_{exc}} + I_L \quad (4.2)$$

$$L \frac{dI_L}{dt} = -V_2 - R_L I_L, \quad (4.3)$$

where the function $g(V_1, V_{cc})$ represents the characteristic curve of the nonlinear resistor, which is piecewise linear and contains a region of negative resistance.

However a more convenient version of the Chua circuit has been proposed without the inductor. The equivalent circuit of the inductor described in [23]. We reproduce here the scheme of the coil that we used for the experiments in the Fig. 4.1 (b). This circuit behave has an inductor, as the input frequency

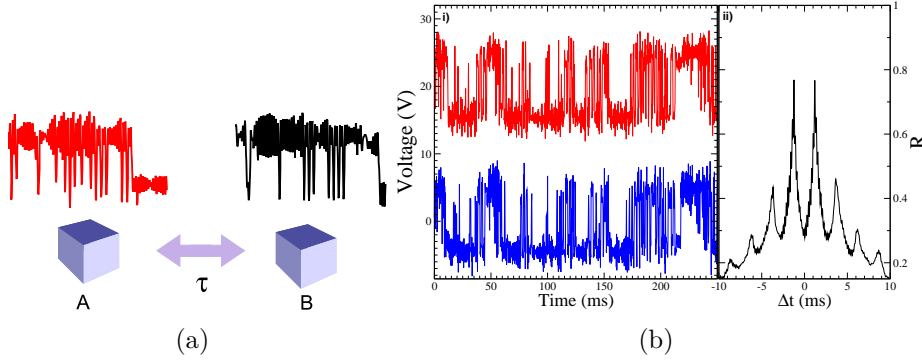


Figure 4.2: (a) Qualitative description of the experimental setup. Two similar chaotic systems (A and B) are coupled through a bidirectional channel with a time delay τ_c . (b) In the inset (i) we plot the output voltage V_1^A (above) and V_1^B (below), which has been vertically shifted to ease comparison. In inset (ii) the cross-correlation function is plotted, showing two maxima of similar value at a time delay $\Delta t = \pm\tau_c$. For this particular example, the internal coupling parameters are: $R_{coup} = 47$ k Ω and $\tau_c = 1.1625$ ms.

increases its equivalent impedance increases linearly. The numerical value of the equivalent inductance depends on the components of the circuit: $L = R_1 R_3 R_4 C_1 / R_2$.

The output of both circuits are chaotic when uncoupled, and keep their dynamics for low to moderate coupling strengths. Nevertheless, when the coupling strength crosses a certain threshold, synchronization arises. Figure 4.2 (b) shows the output voltage of both circuits for a coupling resistance of $R_c = 47$ k Ω , which corresponds to a moderate coupling. We can observe how both signals show a relatively good synchronization. The quality of the synchronization is measured with the cross-correlation function which gives an estimate of the similarity between two time series shifted with a time lag Δt . The cross-correlation function between two output voltages V_1^A and V_1^B (the voltage 1 of the circuit A and B respectively) is defined as:

$$C(\Delta t) = \frac{\langle (V_1^A(t) - \langle V_1^A \rangle)(V_1^B(t + \Delta t) - \langle V_1^B \rangle) \rangle}{\sqrt{\langle (V_1^A(t) - \langle V_1^A \rangle)^2 \rangle \langle (V_1^B(t) - \langle V_1^B \rangle)^2 \rangle}},$$

where Δt is a temporal shift introduced in V_1^B and the brackets represent time averaging. This tool helps to find the delay between two time series,

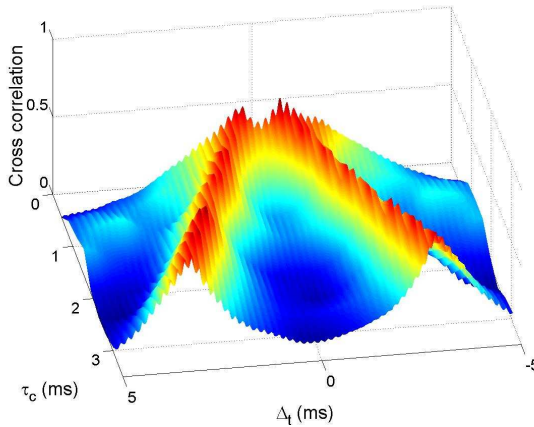


Figure 4.3: *Cross-correlation of Chua circuit A and B, as a function of the time shift Δt between both series and the time delay τ_c . We can observe how the highest correlation ($C_{max} \sim 0.64$) always occurs at $\Delta t = \pm\tau_c$, which indicates that we have lag-synchronization with exchanges in the leader-follower role between both circuits.*

which corresponds to the Δt with the highest correlation ($-1 < C(\Delta t) < 1$). In Fig. 4.2 (b) (right inset) we plot the cross-correlation between the output voltage of both circuits, which has two maxima at precisely the coupling time $\pm\tau_c$. It is worth mentioning that both maxima have similar values ($C \sim 0.6$) indicating that there is not a clear leader or follower in the dynamics, i.e., both circuits alternate their role.

At this point we make a systematic study of the influence of the coupling time in the synchronization of both circuits, since phenomena like amplitude death [24], symmetry breaking [18] or periodic regimes [20] have been previously reported in experiments with mutually coupled systems. With a fixed coupling strength, we sweep the coupling time τ_c and check the quality of the synchronization between both circuits. Figure 4.3 shows the cross-correlation as a function of τ_c . We observe how the highest cross-correlation is always obtained at $\pm\tau_c$, which indicates, first of all, that the delay between both outputs matches the coupling time and, second, that the switching of the leader-follower role is independent of τ_c . Therefore, we can say that the phenomenon is robust against the coupling time and furthermore that isochronous synchronization, i.e., zero-lag between circuit outputs, is not ob-

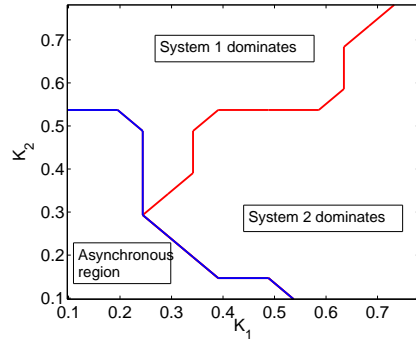


Figure 4.4: *Synchronization region for the two oscillators. In one region one of the oscillators dominates the other, that is the oscillator forces the other to follow its dynamics. In the other region the opposite occurs, the other oscillator dominates. The third region is the region where the coupling is too low for the synchronization to occur.*

served in two bidirectionally coupled circuits with delay, a fact previously reported in chaotic lasers [18].

We further study the influence of the coupling strength on the correlation function as the coupling become asymetrical. The dominant system, the leader, has a correlation peak at $\Delta t = \pm\tau$ higher than the follower. We should stress on the fact that the two peaks of the cross correlation are symetric with respect to $\Delta t = 0$. A good way to check the influence of the coupling strength on this system is to compare de numerical values of this two peaks. As the peak for $\Delta t = \tau$ is lower than the peak at $\Delta t = -\tau$, we consider that the system 1 dominates over the system 2. In the circuit we can control the gain K_1 of the injection from the circuit 1 to the circuit 2. As this gain is very high the circuit 1 dominates the circuit 2. On the other hand, the gain K_2 controls the coupling strength in the direction 2 to 1. In the Fig. 4.4 we span the parameter space K_1, K_2 in order to compare the strength of the two peaks. The diagram determinates which system dominates over the other one depending on the coupling strength. In the figure, three different region appear clearly. The first region in the lower side represent the region for which the correlation is too low to consider that the synchronization arises. The second zone correspond the region where the system 1 dominates and the third zone the region for which the system 2 dominates. The figure is

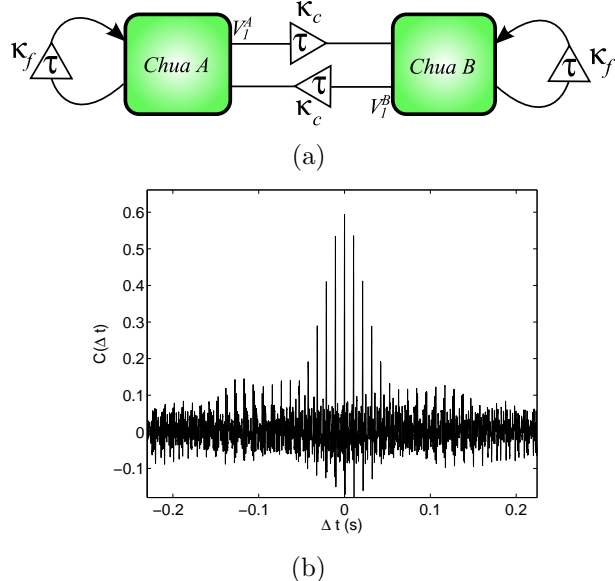


Figure 4.5: (a) In this Figure we show a simplified diagram of the experimental setup which consist in two bidirectionaly coupled Chua circuit with a coupling gain K_i and a delayed feedback signal with a gain K_f . The gains and the delay can be tuned automatically by software. The plot in the Fig. (b) is a example of isochronous synchronization of the circuit for a sufficiently high feedback gain. Notice that the peak located at $\Delta t = 0$ is higher that any other one. This means that globally the zero time-lag synchronization dominates.

symmetrical along the diagonal line which marks the separation of the two domains of influence. Since that along this line the two gains are identical ($K_1 = K_2$) there is no dominant system over the other and both displays the same power, the role of the leade and follower alternates.

An important remark should be made here. There is no isochronous synchronization in this experimental setup. In order to obtain synchronization of the two systems with a zero lag an suplementary ingredient is needed. This synchronization is stable only if we introduce a delayed feedback of the coupling variable in each oscillators.

We extend the previous results by introducing a new element in the system, that is a delayed feedback of the signal. As a matter of fact, the only way to obtain sustained isochronous chaotic oscillations in our experiment is

to introduce a feedback of one of the variable. However, this feedback has to be delayed in order to keep the systems synchronized. This surprising fact is possible only with feedback in this bidirectionally coupled system. The signal and the feedback are delayed by the same time lag. In the Fig. 4.5 (a) we have a simplified diagram of the experimental setup with all the parameter that we control. The gain K_f holds for the gain of the feedback, for all the measures the gain is normalized so that it takes its numerical values in the interval $[0, 1]$. The gain K_i holds for the coupling gain, which remain equals in both direction for all the experiments.

4.3 Isochronous synchronization in three coupled circuit

Arriving to this point the question about if it is possible to obtain zero-lag synchronization in mutually coupled chaotic circuits when a delay is considered in the coupling path is still open. A recent work by Fischer *et al.* [8] has shown that the addition of a relay system between two chaotic lasers can lead to isochronous synchronization between the outer systems. With this idea in mind, we introduce a third Chua circuit between the two previous ones, keeping the bidirectional coupling and the delay in the transmission channels. Figure 4.6 shows the experimental setup, where the intermediate Chua circuit, which acts as the relay system, is drawn in red since it has different internal parameters from those of the outer Chua circuits (see Fig. 4.6 for details). The coupling time and the coupling strength are set to be equal at all paths, leading to a symmetrical system. In Fig. 4.6 (a) we plot the output voltages V_1 of the three circuits for intermediate coupling ($R_c = 1.2 \text{ k}\Omega$). We can observe how circuits A and C are synchronized at exactly the same time despite the delay in the coupling lines, which is the typical signature of isochronous synchronization. An interesting point arises when looking at the output of the relaying system. We can observe how the Chua circuit B is also synchronized with the other two, but in this case it is delayed with a time corresponding to τ_c . In this way, the central system is following the dynamics of the outer circuits and therefore it is not driving them.

Figure 4.6 (b) show the cross-correlation function between pairs of circuits. We can observe how for the case of Chua circuit A and B the correlation

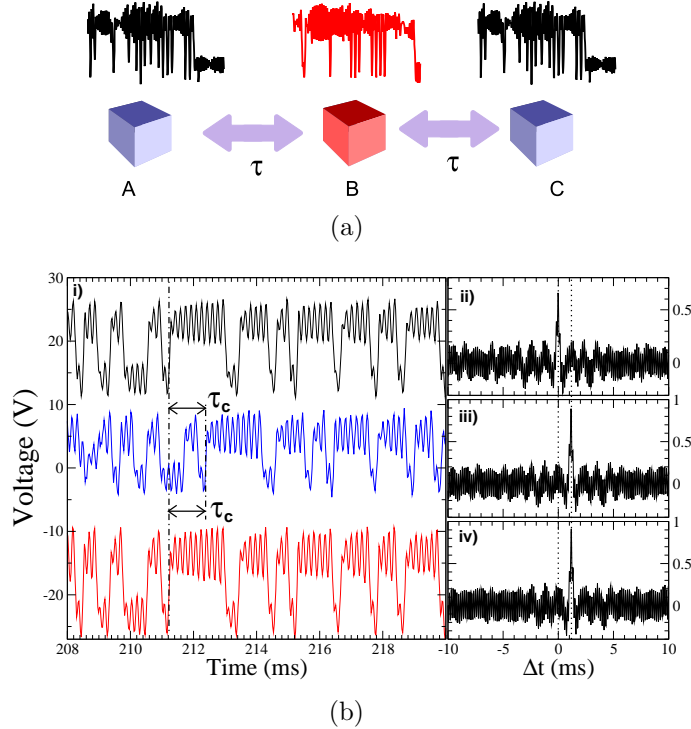


Figure 4.6: (a) Qualitative description of the experimental setup. A third (B) Chua circuit is introduced between A and C. We adjust the internal parameters of the Chua circuit B to be different from those of the outer Chua circuits: for the circuit A and C, $R_{exc} = 1.85 \text{ k}\Omega$ and $L_o = 14 \mu\text{H}$, whereas for circuit B, $R_{exc} = 1.76 \text{ k}\Omega$ and $L_i = 10 \mu\text{H}$. The three circuits are tuned in the double scroll chaotic regime. (b) In (i) we plot the V_1 variable of the circuits (vertically shifted). We can observe how Chua circuit A and C show isochronous synchronization (zero-delay) while the central one (B) is lag-synchronized with its outer counterparts. In the left figure, the cross-correlation function between A-C (ii), A-B (iii) and C-B (iv) is plotted. We can observe how A and C synchronize with zero delay, while B follows the outer circuits with a delay corresponding to the coupling time τ_c .

peak is obtained at zero-delay, indicating isochronous synchronization. As expected, correlations of the external circuits (A and C) with the central one (B) show the achronal synchronization, with a peak at exactly the coupling time τ_c . In this case, there is no alternation between the leader role and the

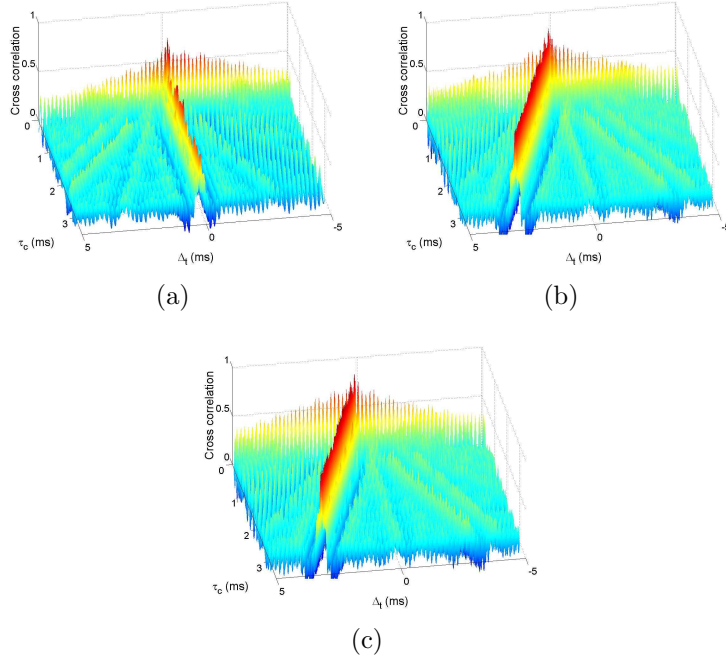


Figure 4.7: Cross-correlation plots of Chua circuits A and C (a), A and B (b) and C and B (c), as a function of the time shift Δt between both series and the delay in the transmission line τ_c . We can observe isochronous synchronization between A and C, since the best correlation is always reported at zero-lag (upper figure). Bottom plots show lag-synchronization between the central and the outer circuits, since the best correlation is always observed with a delay of τ_c , no matter what its value is.

central Chua circuit is always the follower.

In order to show the robustness of the phenomenon versus the coupling time, we repeat the experiment with different delay times from values ranging from near to zero until $\tau_c \sim 3$ ms. The cross-correlation function shows in all cases the zero-lag synchronization for the outer circuits (see Fig. 4.7 (a)) and achronal synchronization with regard to the central one (see Fig. 4.7 (b,c)). It is worth mentioning that the central circuit do not necessarily need to be matched with the outer ones. In fact, as mentioned before, internal parameters of the relay Chua circuit were deliberately detuned.

4.4 Replacing the relay system

Since the isochronous synchronization seems to be dependent on the symmetry of the system, it would be reasonable to obtain the same results with a different dynamical system acting as a relay, since symmetry would be preserved (as long as the outer circuits are identical). With this aim, we replace the central Chua circuit by a Sprott circuit [26] a different nonlinear electronic circuit which, as the Chua circuit, is able to behave chaotically.

The chaotic circuit, named after J.C. Sprott [26], is a simple circuit composed of three linear integrators with a non-linear feedback loop. We adjust the parameters of the circuit to show a chaotic double scroll structure. The schematic representation is shown in Fig. 4.8. The circuit simulates a third degree differential equation which is called a “jerk”. The equations modelling the circuit are:

$$\frac{dV_1}{dt} = \frac{1}{R_3 C_3} V_2 \quad (4.4)$$

$$\frac{dV_2}{dt} = \frac{1}{R_1 C_2} (V_3 - V_2) \quad (4.5)$$

$$\frac{dV_3}{dt} = \frac{1}{C_1} \left(-\frac{1}{R_2} V_2 - \frac{R_5}{R_4 R_6} \frac{1}{R_6} V_1 + \frac{R_5}{R_4 R_7} \frac{1}{R_7} V_{cc} \text{sign}(V_1) \right) \quad (4.6)$$

The numerical values of the components of the circuit are shown in the figure caption of Fig. 4.8.

In Fig. 4.9 we show a schematic description of the experimental setup, where we can see that, despite the different central unit, the system maintains the symmetry. Figure 4.9 (b) shows the time series of the circuit outputs. We observe how the zero-lag synchronization holds for the Chua circuits. At the same time, the Sprott circuit also synchronizes, in this case, advancing the dynamics of the outer ones a time equal to τ_c . Cross-correlation functions between pairs of circuits quantifies the phenomenon observed in the time series, circuits A and B have a maximum at zero delay, while correlations with the central circuit show that, in this case, the relaying system is leading the dynamics.

We have done several experiments (not shown here) with different relaying circuits in order to understand the role of the central circuit in the isochronous synchronization. We have seen that, as long as the central circuit do not filter the signal of the outer ones, isochronous synchronization is observed. Nevertheless, we have observed that it is very sensitive to a mismatch in the

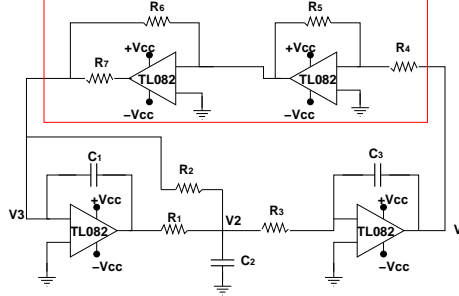


Figure 4.8: Description of the Sprott circuit. The circuit is composed of a linear integrator (lower part) and a non linear feedback loop (red square). The nonlinear function can be written as $f(x) = -A_3x + A_4\text{sign}(x)$. The numerical values of the components are: $R_3 = R_4 = R_5 = 1 \text{ k}\Omega$, $R_1 = 220 \Omega$, $R_2 = 1 M\Omega$, $R_6 = 10 k\Omega$, $R_7 = 31 k\Omega$, $C_1 = 10 nF$, $C_2 = 22 nF$, $C_3 = 10 nF$.

coupling, in the sense that, when we introduce an asymmetry in the coupling time or coupling strength, zero-lag synchronization is lost. Interestingly, similar phenomena have been reported in interconnected cortical areas of the brain, where simulations based on realistic neuroanatomical and physiological properties of the neural architecture have shown the appearance of time lags when asymmetry is considered [25].

4.5 Conclusions

This work is focused on synchronization in mutually coupled circuits with delay in the coupling connections. First, we analyze the synchronization of two chaotic circuits as a function of the delay time. We observe that despite both circuits synchronize when they are similar, a time delay between both outputs appears. The delay is equal to the coupling time between both circuits τ_c , i.e., the time needed by the signal to travel from one circuit to the other. Furthermore, the role of leader and follower in the dynamics is exchanged continuously between both circuits, a phenomenon previously reported in coupled semiconductor lasers [18]. Next, we include a relay circuit between the two chaotic circuits, which is bidirectionally coupled. Under this configuration, exchanges in the leader/follower role disappear and the two outer circuits synchronize with zero-lag. This phenomenon, known as isochronous synchronization holds when the relay circuit is replaced by a

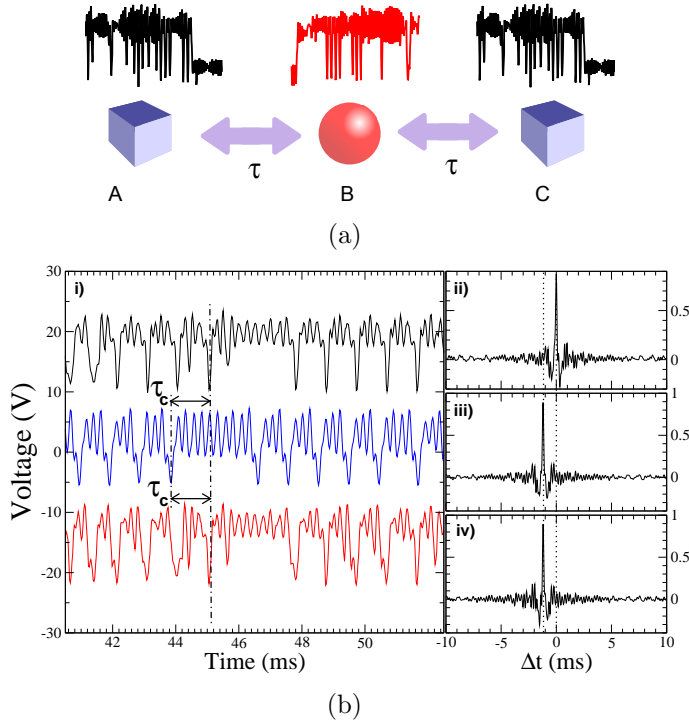


Figure 4.9: (a) Qualitative description of the experimental setup. Two similar chaotic systems A and C (Chua circuits) are coupled through a different chaotic system B (Sprott circuit). (b) In (i) we plot the output voltage of the three circuits showing that despite being different dynamical systems all of them synchronize their dynamics. Furthermore, the two outer circuits keep the zero-lag synchronization as can be observed both in the time series (i) and in their cross-correlation plots (ii). The central circuit B, synchronizes with the outers with a delay equal to the coupling time τ_c , despite being a completely different dynamical system. Figures (iii) and (iv) show the cross-correlation between the central and the outer circuits, where the central circuit is advanced a time interval equal to the coupling time τ_c .

different dynamical unit, in this case a Sprott circuit. In parallel experiments, not shown here, we have observed that the symmetry is the key ingredient of isochronous synchronization, and is lost when asymmetries are introduced in the coupling time or the coupling strength.

Appendix I: Coupling and delay board

The coupling between each circuit is introduced by a digital delay line which samples and buffers the signal before restoring it τ ms later. The circuits are coupled with different input/output variables, depending on the direction of the signal. V_1 is the output variable whereas the input signal is injected into variable V_2 . This mechanism of asymmetric coupling prevents feedback loops in the circuits, and therefore the signals are completely decoupled. The Sprott circuit is coupled in a similar way, the variable V_1 is sent to the other circuits while the variable V_2 receives the incoming signals through the coupling resistance. Details of the coupling scheme are shown in Fig. 4.10. Each signal is buffered with an op-amp in order to preserve the dynamics of the circuit. The experimental setup is made up of several blocks. The first part consists of the chaotic circuit. Each circuit is connected to the digital delay line and to the ADC acquisition board (see blue lines in Fig. 4.10). The dig-

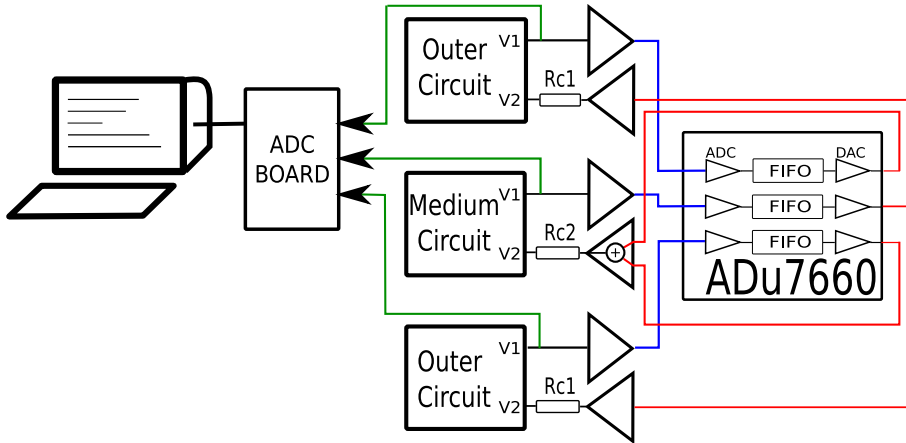


Figure 4.10: *Experimental setup that has been used for the coupling of the circuits. The output voltage V_1 of each signal is sampled in the microcontroller ADu7660 and then buffered into a digital memory before being returned to the circuits. Each triangle represents a signal conditioner in order to adapt the signal to the specification of the ADC inputs. The blue line represents the injected signal and the red lines are the delayed signals reintroduced into the circuit. The central circuit receives the sum of the signals of the outer circuits. Each signal is reintroduced into variable V_2 through a resistance R_c . Note that this resistance might be different for the central circuit.*

ital delay line is composed of an autonomous microcontroller with on-board memory and DAC and ADC converters. The microcontroller is an ADu7660 development board from Analog Devices. The signal is first converted to digital signal and then stored into a FIFO buffer in order to introduce the delay. After a number of clock ticks, the signal is then converted into analog. These converters sample signals up to 50 KHz with 12 bits precision and the delay can be chosen up to $128/f_e$, being f_e the chosen sampling frequency. In the experiments the sampling frequency of the microcontroller is chosen to be $f_e = 50\text{ KHz}$.

The analog signals from the circuits are then sampled with an ADC sampling board connected to a computer and signals are later analyzed with Matlab software. The variable V_1 of each circuit is sampled at ten times their mean frequency, that is above 40 KHz, and with a precision of 12 bits.

References

- [1] L.M. Pecora and T.L. Carroll, “Synchronization in chaotic systems”, *Phys. Rev. Lett.* **64**, 821 (1990).
- [2] A.S. Pikovsky, M.G. Rosenblum and J. Kurths, “Synchronization : A Universal Concept in Nonlinear Sciences”, *Cambridge University Press* (2004).
- [3] S. Boccaletti, J. Kurths, G. Osipov, D. L. Valladares, and C. S. Zhou, “The synchronization of chaotic systems”, *Phys. Rep.* **366**, 1 (2002).
- [4] L. Kocarev, K.S. Halle, K. Eckert, L.O. Chua and U. Parlitz, “Experimental demonstration of secure communications via chaotic synchronization”, *Int. J. Bifurcation Chaos* **2**, 709 (1992).
- [5] K.M. Cuomo and A.V. Oppenheim, “Circuit implementation of synchronized chaos with applications to communications”, *Phys. Rev. Lett.* **71**, 65 (1993).
- [6] F.M. Atay, J. Jost and A. Wende, “Delays, Connection Topology, and Synchronization of Coupled Chaotic Maps”, *Phys. Rev. Lett.* **92**, 144101 (2004)
- [7] C. Masoller and A. C. Marti, “Random Delays and the Synchronization of Chaotic Maps”, *Phys. Rev. Lett.* **94**, 134102 (2005).

- [8] I. Fischer, R. Vicente, J.M. Buldú, M. Peil, M.C. Torrent, C.R. Mirasso and J. García-Ojalvo, "Zero-lag long-range synchronization via dynamical relaying", *Phys. Rev. Lett.* **97**, 123902 (2006).
- [9] A. Cho "Bizarrely, Adding Delay to Delay Produces Synchronization", *Science*, **314**, 37 (2006).
- [10] M.G. Rosenblum, A.S. Pikovsky, and J. Kurths, "From phase to lag synchronization in coupled chaotic oscillators", *Phys. Rev. Lett.* **78**, 4193 (1997).
- [11] H.U. Voss, "Anticipating chaotic synchronization", *Phys. Rev. E* **61**, 5115 (2000).
- [12] C. Masoller, "Anticipation in the Synchronization of Chaotic Semiconductor Lasers with Optical Feedback", *Phys. Rev. Lett.* **86**, 2782 (2001).
- [13] D.Y. Tang and N.R. Heckenberg "Synchronization of mutually coupled chaotic systems", *Phys. Rev. E* **55**, 6618 (1997).
- [14] S. Taherion and Y.C. Lai, "Experimental observation of lag synchronization in coupled chaotic systems", *Int. J. Bifurcation Chaos* **10**, 2587 (2000).
- [15] B. Canna and S. Cincotti, "Hyperchaotic behaviour of two bidirectionally coupled Chua's circuits", *Int. J. Circ. Theor. Appl.* **30**, 625 (2002).
- [16] I. Gomes da Silva, S. Montes, F. d'Ovidio, R. Toral and C. Mirasso, "Coherent regimes of mutually coupled Chua circuits", *Phys. Rev. E* **73**, 036203 (2006).
- [17] I.G. Da Silva, J.M. Buldú, C.R. Mirasso, and J. García-Ojalvo "Synchronization by dynamical relaying in electronic circuit arrays", *Chaos* **16**, 043113 (2006).
- [18] T. Heil, I. Fischer, W. Elsässer, J. Mulet and C.R. Mirasso, "Chaos Synchronization and Spontaneous Symmetry-Breaking in Symmetrically Delay-Coupled Semiconductor Lasers", *Phys. Rev. Lett.* **86**, 795 (2001).
- [19] J. Mulet, C.R. Mirasso, T. and I. Fischer "Synchronization scenario of two distant mutually coupled semiconductor lasers", *J. Opt. B: Quantum Semiclass. Opt.* **6**, 97 (2004).

- [20] H-J. Wünsche, S. Bauer, J. Kreissl, O. Ushakov, N. Korneyev, F. Henneberger, E. Wille, H. Erzgräber, M. Peil, W. Elsäßer and I. Fischer, “Synchronization of delay-coupled oscillators: A study on semiconductor lasers”, *Phys. Rev. Lett.* **94**, 163901 (2005).
- [21] L.B. Shaw, I.B. Schwartz, E.A. Rogers, R. Roy, “Synchronization and time shifts of dynamical patterns for mutually delay-coupled fiber ring lasers”, *Chaos* **16**, 015111 (2006).
- [22] M.P. Kennedy, “Robust OP amp realization of Chua’s circuit,” *Frequenz* **46**, 66 (1992).
- [23] L.A.B. Torres and L.A. Aguirre, “Inductorless Chua’s circuit” *Electronics Letters* **36**, 1915 (2000).
- [24] D.V.R. Reddy, A. Sen and G.L. Johnston, “Time Delay Induced Death in Coupled Limit Cycle Oscillators” *Phys. Rev. Lett.* **80**, 5109 (1998).
- [25] D. Chawla, K.J. Friston and E.D. Lumer, “Zero-lag synchronous dynamics in triplets of interconnected cortical areas”, *Neural Networks* **14**, 727 (2001).
- [26] J.C. Sprott, “A new class of chaotic circuit”, *Phys. Lett. A* **266**, 19 (2000).

Chapter 5

Application of isochronous synchronization to communication

5.1 Introduction

Probably, one of the most promising application of the synchronization of chaotic systems is its use in secure communications. First proposed by Pecora and Carroll in their seminal paper about chaos synchronization [1], the transmission/recovery of an encrypted message using chaotic systems was experimentally demonstrated by Kocarev *et al.* two years later [2]. The message recovery process relies on the chaos-pass filtering properties of the synchronized chaotic systems, *i.e.*, when a message is introduced in the chaotic carrier output of the transmitter system, the receiver synchronizes only with the chaotic part of its input signal and the message can be recovered after a straightforward signal treatment. Therefore, synchronization between chaotic systems is a necessary requirement in communications with chaotic carriers, nevertheless synchronization can have many faces [3]. If we assume a certain delay in the coupling line, which would correspond to the case of real applications, it would be possible to define different kinds of synchronization by taking into account the delay between the synchronized systems. In the most general case, the receiver follows the transmitter output with a lag equal to the coupling time, in what is usually called achronal synchronization [4]. However, if the internal parameters of the coupled systems are adequately

tuned, it is possible to obtain anticipated synchronization [5, 6], where the receiver system advances in time the dynamics of the transmitter. The intermediate case is known as isochronal synchronization [7] (also called zero-lag synchronization) and corresponds to the situation where both chaotic systems have the same dynamics at exactly the same moment, despite the time lost in the transmission line. Isochronal synchronization has been observed in the dynamics of interconnected cortical areas of the brain [8, 9, 10] and it has been recently reproduced in small arrays of coupled chaotic lasers [11, 12] and electronic circuits [13] where bidirectional coupling was introduced. It is within the framework of lasers that isochronal synchronization has been proposed as a technique to bidirectionally encrypt/decrypt a message. Two recent works [14, 15] have shown by means of numerical simulations that it is possible to establish bidirectional secure communication between two independent chaotic lasers and, in addition, messages can be sent simultaneously (*i.e.*, both lasers sending/receiving messages at the same time). More recently, unidirectional message transmission in the framework of isochronal synchronization has been shown experimentally in semiconductor lasers with opto-electronic feedback [16].

In this chapter we present, to the best of our knowledge, the first experimental demonstration of simultaneous bidirectional communication between two chaotic systems by means of isochronal synchronization. First, we synchronize two Mackey-Glass electronic circuits with time-delayed feedback, where, a delay is also introduced in the coupling line. Both systems are coupled bidirectionally and isochronal synchronization arises when feedback and coupling parameters are accurately matched. Then an encrypted message is introduced in both chaotic outputs and recovered at the opposite system. Finally we show how this encryption technique is suitable to negotiate an encryption key between both systems, even in the case that an eventual eavesdropper has access to both transmitted signals.

5.2 Experimental Setup

We have chosen a Mackey-Glass electronic circuit [17, 18, 20] as the chaotic system to encrypt/decrypt the transmitted messages. The electronic circuit, based on the Mackey-Glass model, is shown in Fig. 5.1 (a) and consists in a non-linear oscillator whose oscillations are induced by the feedback loop with delay. Three basic elements can be distinguished. First of all, a nonlinear

function $f(x)$, which processes the signal V_{in} , so that it feeds the analog integrator with the voltage $f(V_{in})$. This integrator is the second element of the system and it is composed of a simple RC circuit, represented by R_4 and C_1 . The voltage at the capacitor C_1 is the dynamical variable V_{out} , which is sent in turn to the third element, a digital delay line represented by a triangle in Fig. 5.1 (a). Along the delay line, a gain κ_f and a delay τ_f is applied to the voltage V_{out} , so that the voltage $V_{in}(t)$ at the output of the delay line is $V_{in}(t) = \kappa_f V_{out}(t - \tau_f)$.

The differential equations that represent this circuit are quite similar to the Mackey-Glass model. The form of the nonlinearity differs slightly with the original Mackey-Glass model [22] as it can be seen in the Fig. 5.2. However these differences do not change the main characteristics of the system. A complete study of the circuit is detailed in the Appendix I along with the description of the Mackey-Glass model. Equations corresponding to the circuit of Fig. 5.1 (a) can be easily deduced by circuit analysis. We obtain the differential equation:

$$R_4 C_1 \frac{dV_{out}}{dt} = -V_{out} + f(\kappa_f V_{out}(t - \tau)), \quad (5.1)$$

where the nonlinear function $f(\kappa_f V_{out}(t - \tau))$ depends on a p-channel JFET (Junction Field Effect Transistor). The details on the implementation can be found in the Appendix I.

Now we describe the communication setup which consists on a coupling line with delay that connects two identical Mackey-Glass electronic circuits [see Fig. 5.1 (b)]. Both circuits are coupled to each other (bidirectionally) by adding the output signals V_{out} to the variables V_{in} of the opposite circuit. The variable V_{out} of each circuit is sent through a digital coupling line with a certain delay and gain. The equations of the coupled system represented in the Fig. 5.1 (b) are:

$$R_4 C_1 \frac{dV_a}{dt} = -V_a + f(\kappa_f V_a^{\tau_f} + \kappa_c (V_b^{\tau_c} + M_b^{\tau_c})) \quad (5.2)$$

$$R_4 C_1 \frac{dV_b}{dt} = -V_b + f(\kappa_f V_b^{\tau_f} + \kappa_c (V_a^{\tau_c} + M_a^{\tau_c})), \quad (5.3)$$

where variables V_a and V_b correspond to the output variable of each circuit, and the superscript τ_c means the delayed variable, *i.e.*, $V_a^{\tau_f} = V_a(t - \tau_f)$. The encrypted messages are M_a and M_b and they are introduced at V_a and V_b , respectively, by means of a voltage adder, in a classical chaos masking

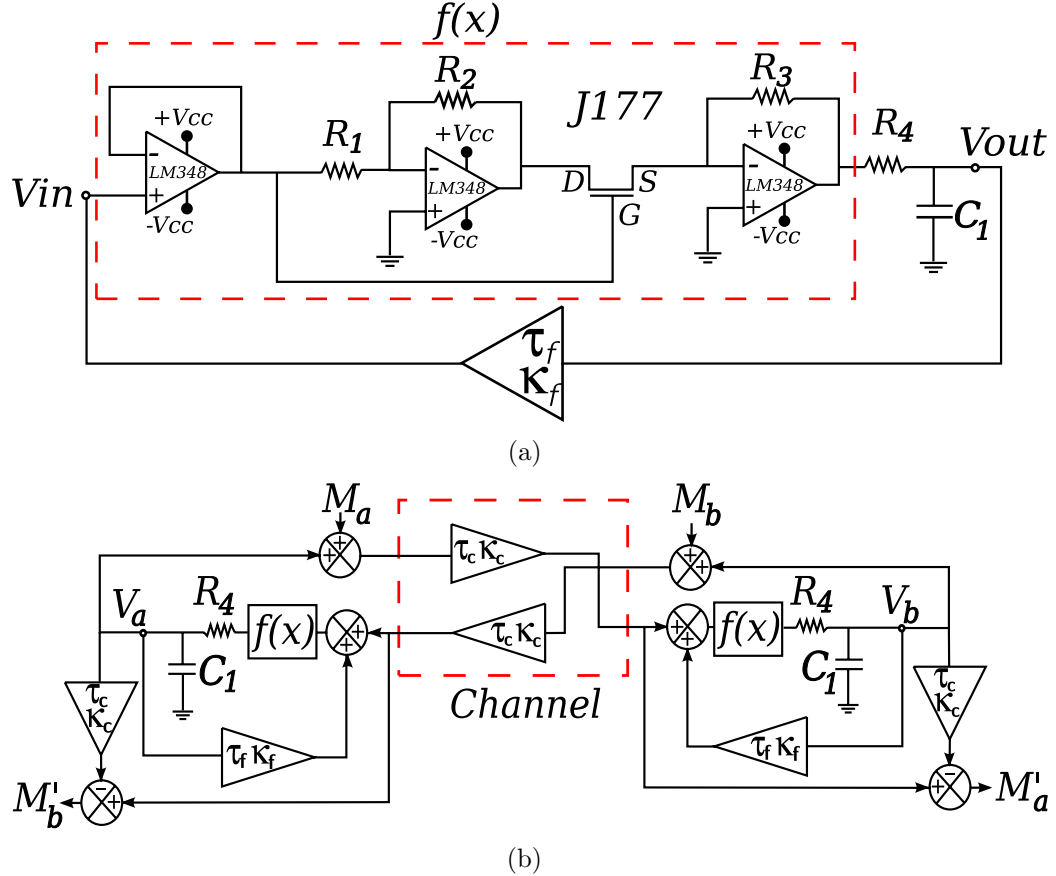


Figure 5.1: In (a) a single Mackey Glass circuit is represented. The circuit is composed of a non-linear function $f(x)$ outlined in the dashed box. At the output of the nonlinear function a simple RC circuit, composed of R_4 and C_1 , integrates the voltage V_{out} . V_{out} is further introduced into a delayed feedback loop, represented by a triangle. The symbols τ_f and κ_f correspond to the feedback delay and feedback strength, respectively. Parameter values are: $R_1 = 1 \text{ k}\Omega$, $R_2 = 0.5 \text{ k}\Omega$, $R_3 = 4 \text{ k}\Omega$, $R_4 = 1 \text{ k}\Omega$, $C_1 = 1 \mu\text{F}$, $J177$ is a JFET transistor and $LM348$ is an operational amplifier. In (b) we plot the schematic setup of the experiment corresponding to the transmission of a message with chaotic masking. The outputs of two identical Mackey-Glass circuits are coupled through a digital delay line and then, they are added to the feedback signal of the opposite circuit.

encryption way. A parallel method of introducing the message through the feedback loop has been recently proposed [19], however, a third dynamical unit is required in this case.

The digital delay line is composed of an autonomous microcontroller with on-board memory and DAC (Digital to Analog Converter) and ADC (Analog to Digital Converter) converters. The signal is first converted to a digital signal and then stored into a FIFO buffer and after a number of clock ticks, the signal is then converted back into analog. The gain κ_f y κ_c and the delay τ_c of each channel can be adjusted by software, so that we can make automated measurement for several gains and delays. The delay ranges from 0 to 20 ms. The gains κ_f and κ_c have values in the interval [0, 1].

Finally, the output signals of both circuits are sampled with an ADC sampling board connected to a computer and signals are later analyzed with Matlab software. The setup for the delay line is similar to the one described in Chap. 4 as described in the Appendix I.

5.3 Isochronal synchronization

Figure 5.2 shows the dynamics of one of the circuits in the absence of coupling, which behaves chaotically for a sufficient feedback and delay. The output voltage V_a exhibits a single extremum dynamics when plotted in the phase space defined by $[V_a, V_a(t - \tau_f)]$, which reflects its chaotic behaviour. Both circuits behave similarly, since the only difference between them is introduced by the tolerance of their electronic components.

At this point, we couple together both circuits through a delay line of gain κ_c and delay τ_c . When the bidirectional coupling is introduced different scenarios arise, as it can be observed in the bifurcation diagram of Fig. 5.3 (a). From low to moderate coupling strengths, both circuits behave chaotically, although windows of N-period oscillations arise for intermediate and high couplings.

Since we are interested in communicating through chaotic masking, we set the coupling strength to $\kappa_c = 0.3$ which sets the system to lie within the chaotic region. Figure 5.3 shows the outputs of both circuits corresponding to the mentioned value of κ_c and a coupling delay time of $\tau_c = 18\text{ms}$. We can observe how the system is highly synchronized without a delay between both outputs, despite the time lost in the transmission line. This is the typical signature of isochronal synchronization.

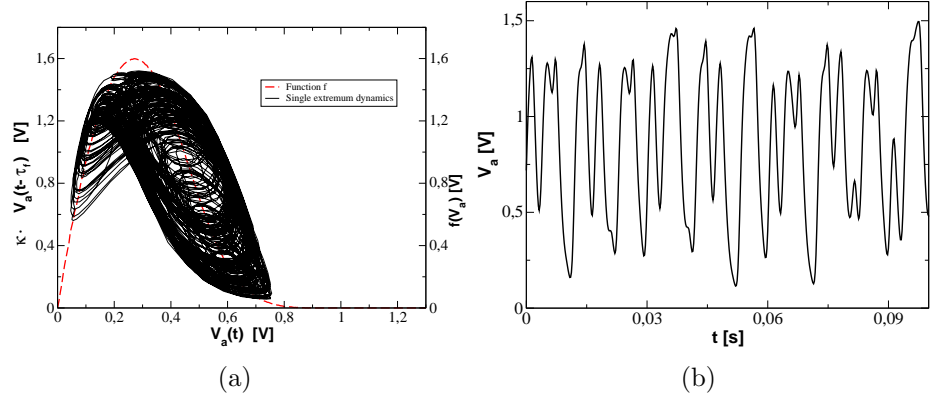


Figure 5.2: (a) Chaotic attractor of the system in the phase space given by $[V_a, V_a(t - \tau_f)]$ and the corresponding time series in (b) for an uncoupled Mackey-Glass circuit. The overall aspect of the attractor reflects the non-linear function f which is plotted in red dashed line. The maximum value of this function is $V_{max} = 1.605\text{V}$ which scale the dynamics of the circuit. The parameters of the system for this experiment are: $\tau_f = 8\text{ms}$, $\kappa_f = 1$. The threshold for the feedback strength which undergoes a Hopf bifurcation is $\kappa_f = 0.55$, below these values the system cannot oscillate. However this threshold depends on the delay τ_f of the feedback loop.

In order to characterize the quality of the synchronization and to evaluate the delay between the output of both circuits we compute the Cross-Correlation function (CC) between the V_a and V_b . The CC function is defined as:

$$C(\Delta t) = \frac{\langle (V_a(t) - \langle V_a \rangle)(V_b(t + \Delta t) - \langle V_b \rangle) \rangle}{\sqrt{\langle (V_a(t) - \langle V_a \rangle)^2 \rangle \langle (V_b(t) - \langle V_b \rangle)^2 \rangle}},$$

where the brackets indicate time averaging. In this way we compute the correlation between time series for different shifts in the time-axis, obtaining the quality of the synchronization ($-1 < C(\Delta t) < 1$) and the delay between the time series, indicated by the position of the maximum of the CC function. In Fig. 5.3 (b), we plot the CC function, which confirms that we are dealing with isochronal synchronization since: a) The maximum of the CC (~ 0.99) function has a value close to the unity, indicating the synchronized behaviour and b) the maximum is placed at $\Delta t = 0$, which reflects that there is no delay

between both outputs despite the time taken in the transmission line. Note that similar to Ref. [12], the bidirectional coupling and the inclusion of the feedback loops lead to a stable zero-lag synchronization, i.e. leader-laggard

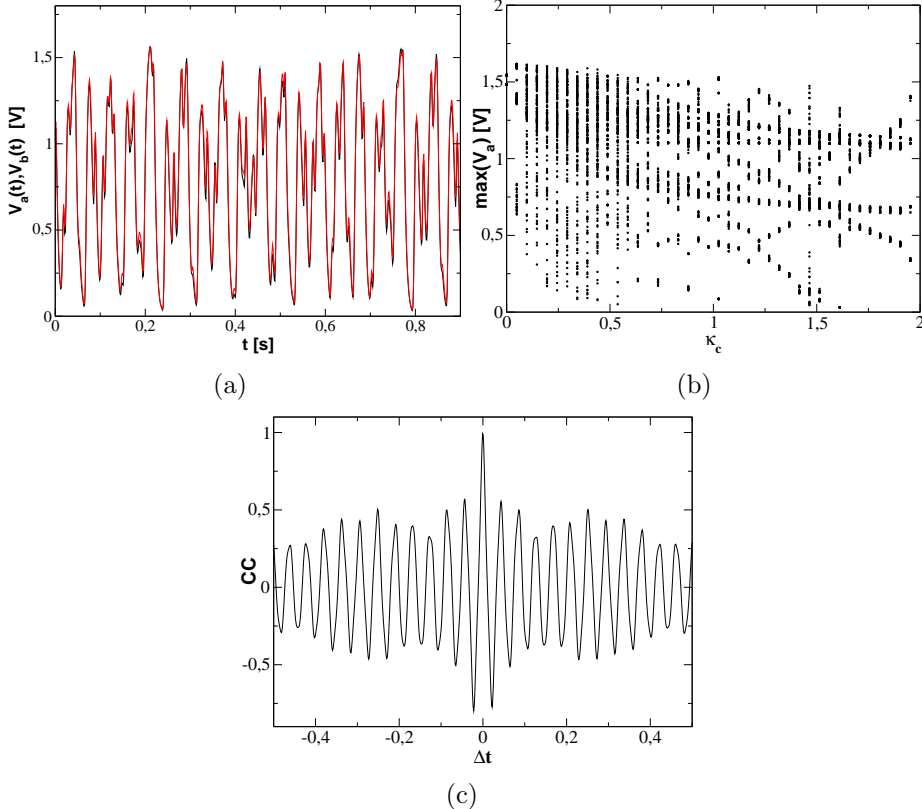


Figure 5.3: (a) Time series of both circuit outputs V_a (black line) and V_b (red line) under isochronal synchronization ($\kappa_c = 0.3$). Figure (b) on the left shows the bifurcation diagram of the coupled system as a function of the coupling strength κ_c with a fixed coupling delay of $\tau_c = 18\text{ms}$. (c) represent the cross-correlation function under isochronal synchronization. A maximum of 0.99 is observed at $\Delta t = 0$, which indicates that there is no delay between both outputs. Time series and cross-correlation function plot here are obtained for $\kappa_c = 0.3$. The time window used for the computation of the cross-correlation is 1.3s. Feedback parameters (equal for both circuits) are $\tau_f = 18\text{ms}$ and $\kappa_f = 0.4$. The rest of the internal parameters are those given in Fig. 5.1

alternation between both outputs is not observed.

We have repeated the experiment for different values of κ_c and τ_c , obtaining similar results. The only requirement to obtain isochronal synchronization with high cross-correlation values is to accurately match the feedback and the coupling delay, i.e. $\tau_c = \tau_f$, as previously reported in [12].

5.4 Bidirectional communication

Since the synchronization is a necessary condition to communicate by means of chaotic masking, the next step is the evaluation of the ability of the system to encrypt/decrypt a message.

We introduce a binary message with a bit rate of 80 b/s . In the frequency domain, the message is hidden by the broad spectrum of the circuit dynamics, which has a peak at $\sim 120\text{ Hz}$. The transition between the 0/1 state has been filtered since we have observed that drastic jumps worsen synchronization. The amplitude of the message must be as low as possible to guarantee a good encryption, but it is also limited by the amplitude of the intrinsic noise of the system, which hinders the message recovery for low values of the message amplitude. Taking into account both restrictions, we have selected a message amplitude of 0.4 V for the clarity of the results. It corresponds to a 25% of the RMS value of the circuit output.

Figures 5.4 (a,b) show the input and output signals of both circuits, where a message has been already added to both chaotic signals. A message $M_b(t)$ is encrypted by chaos masking with the $V_b(t)$ signal, while at the opposite circuit a message $M_a(t)$ is masked by $V_a(t)$. In order to recover the message, the input signal has been shifted a time τ_c , since it is the time taken by the output signal to arrive at the opposite circuit. We can observe how, by subtracting the output to the input signal, it is possible to decrypt the transmitted message, whose quality can be improved further by filtering and reshaping. Note that thanks to the bidirectional coupling both systems are sending/receiving a message simultaneously, something that can not be achieved in unidirectional communication.

It is worth to distinguish from two similar but different bit-recovery scenarios. When both circuits are sending and receiving the same bit, we obtain identical synchronization, which can be analytically demonstrated by substituting $V_a = V_b$ and $M_a = M_b$ in Eqs. (2)-(3). Intuitively, we can argue that if both outputs are synchronized, and the same signal ($M_a = M_b$) is

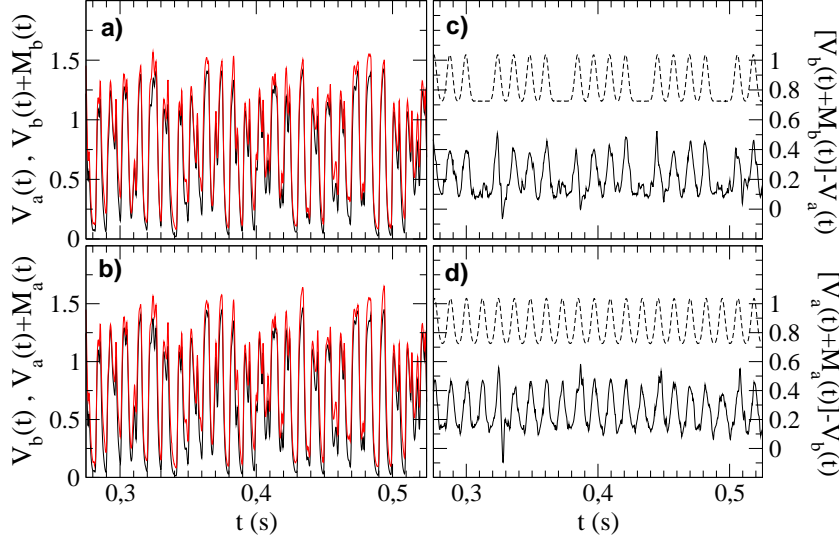


Figure 5.4: (a) and (b) show the input at output signals of circuit A and B, respectively. Message can be recovered by subtraction of both signals. Plots (c) and (d) show the transmitted (dashed line) and recovered (solid line) message at both circuits.

perturbing both inputs, we are helping the coupling to synchronize both outputs thanks to a common external signal (i.e. the message). A different, but also efficient, bit-recovery process occurs when circuits are sending different bits. In this case, the added message, whose amplitude should be low enough to be hidden by the chaotic signal, is treated by the receiving circuit as additive noise, which is filtered due to the chaos-pass filtering properties of the synchronized system [14]. In both cases, the intrinsic noise of the electronic circuits, and the tolerance of the electronic components, lead to the appearance of noisy fluctuations at the recovered message, which translates into a similar quality in the recovered bit. Finally, an appropriate filtering together with a threshold-passing treatment lead to a satisfactory recovery of the message.

Arriving at this point it is worth discussing the security of this kind of transmission. Since the signal of both circuits is accessible to a potential eavesdropper, it would be reasonable to think that the eavesdropper could be able to recover the encrypted messages by subtracting both signals (note

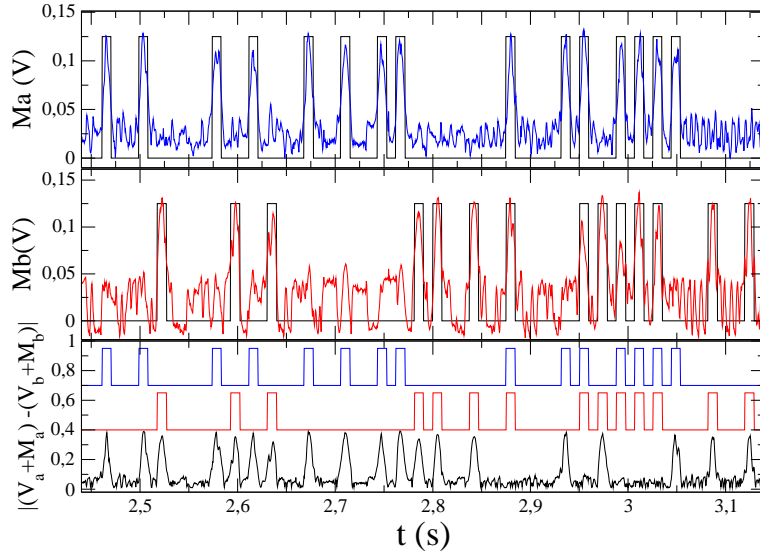


Figure 5.5: Transmitted bits (solid lines) and recovered signals at circuit A (blue lines) and B (red lines). The bottom figure corresponds to the absolute value of the signal recovered by an eavesdropper. We can observe that only when two bits do not coincide, the transmitted signal can be recovered.

that in unidirectional communication only one signal is accessible). Nevertheless, as it has been proposed in Refs. [14, 15], it is a suitable technique to negotiate a secret key between the users. Figure 5.5 shows the message recovered by a possible eavesdropper (bottom time series) when both users are communicating. We can observe that when a bit “1” (or “0”) is sent by the two systems at the same time, the eavesdropper does not detect its presence, since the bit is suppressed when doing the signal subtraction. Only when two bits do not coincide the eavesdropper recovers the bit. In this way both users could send a certain number of bits randomly distributed and take the first N bits that coincide as the secret key to communicate. Note that each receiver system knows which are the right bits by simply comparing the received signal with the sent signal.

5.5 Conclusions

We have shown that two bidirectionally coupled Mackey-Glass electronic circuits can exhibit isochronal synchronization despite the delay existing in the transmission line. Isochronal synchronization appears for a wide ranges of coupling time and is robust against the intrinsic noise of the electronic systems. We have used the isochronal synchronization in order to transmit, bidirectionally and simultaneously, an encrypted message. Finally, we have shown the ability of this kind of communication to negotiate secret keys between users. When a potential eavesdropper has access to both transmitted signals he/she is not able to recover the whole chain of transmitted bits, since bits that coincide are not detected. Despite this type of secure communication has been recently proposed, we give here the first experimental implementation.

Appendix I: Bifurcations of the Mackey-Glass model

In this appendix we describe the bifurcation conditions for the Mackey-Glass model and we apply the same analysis technique to our electronic circuit.

The chaotic Mackey-Glass system is a nonlinear system with a delayed feedback. We present here the details of the bifurcation analysis for the delayed system. The Mackey-Glass model writes:

$$\frac{dx}{dt} = -\gamma x + f(x(t - \tau)). \quad (5.4)$$

With τ a discrete delay and f a nonlinear function with the following form:

$$f(x) = \frac{\alpha x}{1 + \left(\frac{x}{\theta}\right)^n}. \quad (5.5)$$

When there is no delay in the feedback loop the system has two stable states, which are easily obtained as the derivative is equal to zero:

$$0 = -\gamma x^* + f(x^*) \quad (5.6)$$

$$\frac{\alpha x^*}{1 + \left(\frac{x^*}{\theta}\right)^n} = \gamma x^*. \quad (5.7)$$

The first steady state $x_1^* = 0$ is obvious. The second one depends on the parameters of the system:

$$x_2^* = \theta \left(\frac{\alpha}{\gamma} - 1 \right)^{(1/n)}. \quad (5.8)$$

A standard analysis is possible for discrete delay in order to study the stability of the fixed point as the delay evolves. First of all, a function F is defined such as:

$$\left. \frac{dx}{dt} \right|_{x^*} = F(x^*) = -\gamma x^* + f(x^*) = 0. \quad (5.9)$$

To evaluate the behaviour around this stable state a small perturbation δx is added to x^* . With a simple analysis, we can determine if this perturbation will be amplified or suppressed, that is, the system gets back to its stable state.

$$F(x^* + \delta x) = -\gamma(x^* + \delta x) + f(x^* + \delta x) = 0, \quad (5.10)$$

with $\delta x \rightarrow 0$, we can remark that the derivative of the function f writes:

$$\frac{df(x^*)}{dt} = \lim_{\delta x \rightarrow 0} \frac{f(x^* + \delta x) - f(x^*)}{\delta x}. \quad (5.11)$$

With this equation, the previous function is transformed as:

$$F(x^* + \delta x) = -\gamma(x^* + \delta x) + f'(x^*)\delta x + f(x^*). \quad (5.12)$$

Equation (5.9) gives $-\gamma x^* + f(x^*) = 0$ and the equation simplifies to:

$$F(x^* + \delta x) = -\gamma\delta x + f'(x^*)\delta x = \delta x(-\gamma + f'(x^*)). \quad (5.13)$$

We have to evaluate the derivative at x^* to know if this perturbation is amplified or shrinked:

$$f'(x) = \frac{\alpha(1 + (x/\theta)^n) - (n\alpha(x/\theta)^n)}{(1 + (x/\theta)^n)^2}. \quad (5.14)$$

This function is evaluated at the two fixed points of the system:

$$\begin{array}{c|c} x^* & f'(x^*) \\ \hline 0 & -1 \\ \theta(\frac{\alpha}{\gamma} - 1)^{(1/n)} & \gamma(1 - n(1 - \frac{\gamma}{\alpha})). \end{array} \quad (5.15)$$

We can derive the condition of stability for the second fixed point with the sign of the quantity $(-\gamma + f'(x^*))$. If this sum is negative then the fixed point is stable, otherwise the fixed point is unstable. The conditions on the parameters of the system:

$$-\gamma + \gamma(1 - n(1 - \frac{\gamma}{\alpha})) < 0, \quad (5.16)$$

as $n > 0$ and $\gamma > 0$, the stability is reduced to the simple expression:

$$\frac{\gamma}{\alpha} < 1. \quad (5.17)$$

However the instability of the fixed point do not assure the oscillation of the system around this unstable fixed point.

Without the delay the system cannot oscillate. The way to determine the sufficient time delay of the feedback loop is through analysis of the eigenvalues of the system. The delay variable is linearized around the steady state and

the eigenvalue corresponding to this variable is $\exp(-\lambda\tau)$. The behavior of the system around the steady state is ruled by the following linearized equation:

$$\frac{d\delta x}{dt} = -\gamma\delta x + f'^*\delta x(t - \tau). \quad (5.18)$$

We are looking for the eigenvalues of the system, the characteristic equation writes:

$$0 = -\gamma - \lambda + f'^*e^{-\lambda\tau}, \quad (5.19)$$

with f'^* the value of the derivative of the function f evaluated at the fixed point. This equation is transcendental and needs a numerical algorithm to be solved. The equation to be solved is:

$$\gamma + \lambda = f'^*e^{-\lambda\tau}. \quad (5.20)$$

However, since we are looking for a change of stability, the eigenvalue in this region should be imaginary. The system undergoes a Hopf bifurcation when the delay increases and the eigenvalue of the system is $\lambda = i\omega$ with ω the frequency of the system

$$\gamma + i\omega = f'^*e^{-i\omega\tau_c}. \quad (5.21)$$

We can separate the imaginary part and the real part to get two equations:

$$\gamma = f'^* \cos(\omega\tau_c) \quad (5.22)$$

$$\omega = -f'^* \sin(\omega\tau_c), \quad (5.23)$$

and since $\sin^2 + \cos^2 = 1$ the equations can be combined:

$$\omega\tau_c = \arccos(\gamma/f'^*) \quad (5.24)$$

$$\omega = \sqrt{(f'^*)^2 - \gamma^2}. \quad (5.25)$$

Finally the condition on the delay τ_c to get a Hopf bifurcation is:

$$\tau_c = \frac{\arccos(\gamma/f'^*)}{\sqrt{(f'^*)^2 - \gamma^2}}. \quad (5.26)$$

Furthermore we can use the previous expression of the derivative at the fixed point to express the critical delay in function of the parameter of the equation:

$$\tau_c = \frac{\arccos(1/(1 + n(\gamma/\alpha - 1)))}{\gamma\sqrt{(1 + n(\gamma/\alpha - 1))^2 - 1}}. \quad (5.27)$$

The circuit also exhibits oscillations, stable and chaotic regimes as the delay of the feedback loop is changed as shown in Fig. 5.6

The nonlinearity of the circuit does not exactly match the analytical form of the Mackey-Glass equation. The nonlinearity is homomorphic and has the same properties. If we call the nonlinearity f the function implemented in the circuit of Fig. 5.6 (a) we can write the equations of the circuit as:

$$R_4 C_2 \frac{dV_{out}}{dt} = -V_{out} + f(\kappa_f V_{out}(t - \tau)), \quad (5.28)$$

with κ_f a gain depending on the delay line. The nonlinear function depends on the characteristics of the JFET transistor. The current I_d flowing through the transistor depends on the input V_{in} . The current I_d is the following:

$$i_d = \begin{cases} 0 & \text{for } V_{in} > V_{th} \\ -K\left(\frac{R_2}{R_1}\right)V_{in}\left(-\left(\frac{R_2}{R_1}\right)V_{in} - V_{th} + V_{in}\right) & \text{for } V_{in} < \frac{V_{th}}{1 + \frac{R_2}{R_1}} \\ K(V_{in} - V_{th})^2 & \text{for } V_{in} > \frac{V_{th}}{1 + \frac{R_2}{R_1}}, \end{cases} \quad (5.29)$$

with V_{th} the threshold the pinch-off point of the transistor and K a parameter depending on the device. However we can use an ad-hoc function that is enough for our purpose which is evaluate the fixed point and the stability of the system. We use a function f that relates the voltage V_{in} to V_{out} :

$$f(x) = p_1 \left(\frac{x}{1 + (\frac{x}{p_2})^6} \right) (\text{step}(p_3 - x)^2), \quad (5.30)$$

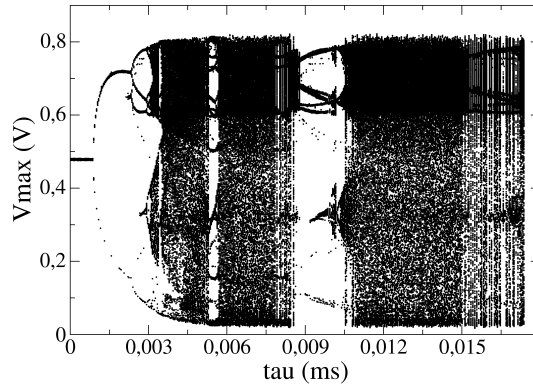


Figure 5.6: Experimental bifurcation diagram of the circuit in function of the time delay of the feedback loop.

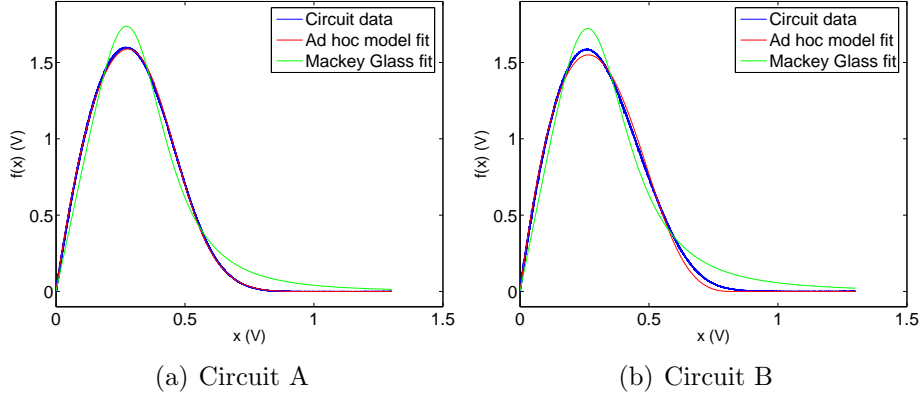


Figure 5.7: *Experimental measurements of the nonlinearity $f(x)$.*

for $x > 0$ and the function step is the Heavyside function with $\text{step}(x) = 0$ for $x < 0$ and $\text{step}(x) = x$ for $x > 0$. In order to estimate the parameter of the system, the data of the nonlinearity has been sampled and later fit with a minimum square method implemented in Matlab. For the particular system that we are considering, the obtained parameters are:

Circuit a	Circuit b	
$p_1 = 13.53$	$p_1 = 19.686$	
$p_2 = 0.514$	$p_2 = 0.633$	
$p_3 = 0.935$	$p_3 = 0.811.$	

(5.31)

The fit is shown in Fig. 5.7 along with the experimental data.

For this particular form of the nonlinearity we can repeat the calculation of the fixed point. The principle is the same, it is assumed that the system is in a steady state:

$$R_4 C_2 \frac{dx}{dt} = -x^* + f(\kappa_f x^*) = 0, \quad (5.32)$$

so that we have to solve the equation:

$$-x^* + p_1 \left(\frac{\kappa_f x}{1 + (\frac{\kappa_f x}{p_2})^6} \right) (\text{step}(p_3 - \kappa_f x)^2) = 0. \quad (5.33)$$

An assumption can be done to simplify the expression: $p_3 - \kappa_f x^* > 0$. This assumption is verified since that the fixed point is generally situated below

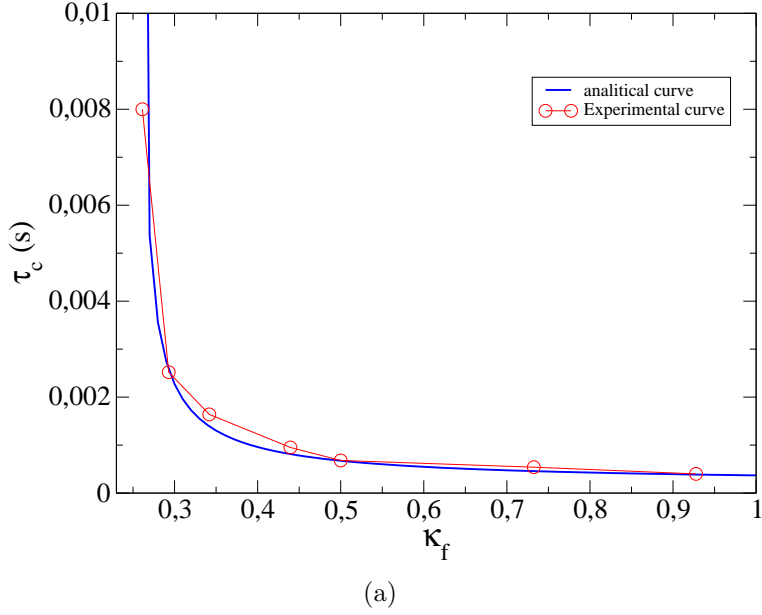


Figure 5.8: Critical delay τ_c for different feedback strengths κ_f . The cross represent the experimental values obtained with the analog circuit. The solid line represent the analytical values obtained from the bifurcation analysis.

the pinch point p_3 . The equation after transformation becomes:

$$\kappa_f p_1 (p_3 - \kappa_f x)^2 = \left(1 + \left(\frac{\kappa_f x}{p_2}\right)^6\right), \quad (5.34)$$

this algebraic equation can be solved analytically however a simple numeric algorithm is enough for our purpose, that is, find the steady states of the system.

In order to evaluate the stability of these fixed points we have to compute the derivative of f at the steady state points. For $x \in [0; p_3[$ the derivative is well defined and smooth. Its expression is given by:

$$f'^* = (f(x\kappa_f))' = f'(x\kappa_f)\kappa_f = \frac{1 - 5\left(\frac{\kappa_f x}{p_2}\right)^6}{1 + \left(\frac{\kappa_f x}{p_2}\right)^6} - \frac{2\kappa_f x}{(p_3 - \kappa_f x)}. \quad (5.35)$$

The stability of the steady state does not depend on p_1 .

Since this stability analysis is only valid when there is no delay we can apply the analysis described before in order to find the critical delay τ_c which

will allow the circuit to oscillate. In this particular case, we have $\gamma = 1/R_4C_2$ and the derivative is normalized by γ

$$\tau_c = \frac{\arccos(1/f'^*)}{\sqrt{(\gamma f'^*)^2 - \gamma^2}} = (R_4 C_2) \frac{\arccos(1/f'^*)}{\sqrt{(f'^*)^2 - 1}}. \quad (5.36)$$

For example with $R_4 = 1k\Omega$, $C_2 = 1\mu F$ and $\kappa_f = 1$ the critical delay is $\tau_c = 0.2$ ms which is in good agreement with the experimental data. In Fig. 5.8 the experimental critical delay necessary to obtain the oscillations are compared with the curve obtained from the previous discussion. The experimental results are in good agreement with the theoretical calculation, and therefore it validates the proposed model.

References

- [1] L.M. Pecora and T.L. Carroll, “Synchronization in chaotic systems”, *Phys. Rev. Lett.* **64**, 821 (1990).
- [2] L. Kocarev, K.S. Halle, K. Eckert, L.O. Chua and U. Parlitz, “Experimental demonstration of secure communications via chaotic synchronization”, *Int. J. Bifurcation Chaos* **2**, 709 (1992).
- [3] A.S. Pikovsky, M.G. Rosenblum and J. Kurths, “Synchronization : A universal concept in nonlinear sciences”, *Cambridge University Press* (2004).
- [4] T. Heil, I. Fischer, W. Elsässer, J. Mulet, and C. R. Mirasso, “Chaos synchronization and spontaneous symmetry-breaking in symmetrically delay-coupled semiconductor lasers”, *Phys. Rev. Lett.* **86**, 795 (2001).
- [5] H.U. Voss, “Anticipating chaotic synchronization”, *Phys. Rev. E* **61**, 5115 (2000).
- [6] C. Masoller, “Anticipation in the synchronization of chaotic semiconductor lasers with optical feedback”, *Phys. Rev. Lett.* **86**, 2782 (2001).
- [7] I.B. Schwarz and L. Shaw, “Isochronal synchronization of delay-coupled systems”, *Phys. Rev. E* **75**, 046207 (2007).

- [8] A.K. Engel, P. König, A.K. Kreiter and W. Singer, “Interhemispheric synchronization of oscillatory neuronal responses in cat visual cortex”, *Science* **252**, 1177 (1991).
- [9] P.R. Roelfsema, A.K. Engel, P. König and W. Singer, “Visuomotor integration is associated with zero time-lag synchronization among cortical areas”, *Nature* **385**, 157 (1997).
- [10] D. Chawla, K.J. Friston, and E.D. Lumer, “Zero-lag synchronous dynamics in triplets of interconnected cortical areas,” *Neural Networks* **14**, 727 (2001).
- [11] I. Fischer, R. Vicente, J.M. Buldú, M. Peil, C.R. Mirasso, M.C. Torrent, and J. García-Ojalvo, “Zero-lag long-range synchronization via dynamical relaying”, *Phys. Rev. Lett.* **97**, 123902 (2006).
- [12] E. Klein, N. Gross, M. Rosenbluh, W. Kinzel, L. Khaykovich and I. Kanter, “Stable isochronal synchronization of mutually coupled chaotic lasers”, *Phys Rev E* **73**, 066214 (2006).
- [13] A. Wagemakers, J.M. Buldú and M.A.F. Sanjuán, “Isochronous synchronization in mutually coupled chaotic circuits”, *Chaos* **17**, 023128 (2007).
- [14] E. Klein, N. Gross, M. Rosenbluh, W. Kinzel, L. Khaykovich and I. Kanter, “Public-channel cryptography based on mutual chaos pass filters”, *Phys Rev E* **74**, 046201 (2006).
- [15] R. Vicente, C.R. Mirasso and I. Fischer, “Simultaneous bidirectional message transmission in chaos-based communication scheme”, *Optics Letters* **32**, 403 (2007).
- [16] M. Peil, L. Larger, I. Fischer, “Versatile and robust chaos synchronization phenomena imposed by delayed shared feedback coupling” *Phys. Rev. E* **76**, 045201 (2007).
- [17] M.C. Mackey and L. Glass, “Oscillation and chaos in physiological control systems”, *Science* **197**, 287 (1977).
- [18] M.-Y. Kim, C. Sramek, A. Uchida and R. Roy, “Synchronization of unidirectionally coupled Mackey-Glass analog circuits with frequency bandwidth limitations” *Phys. Rev. E* **74**, 016211 (2006).

- [19] B. Zhou and R. Roy, “Isochronal synchrony and bidirectional communication with delay-coupled nonlinear oscillators” *Phys. Rev. E* **75**, 026205 (2007).
- [20] A. Namajunas, K. Pyragas and A. Tamasevicius, “An electronic analog of the Mackey-Glass System” *Phys. Lett. A* **201**, 42 (1995)

Chapter 6

Conclusions

In this Ph.D. thesis we studied and developed a method for the simulation of complex systems by means of analog electronic circuits. We summarize here the main results of the work:

1. We presented the modelling with electronic circuits of a simple neuron model based on the Morris-Lecar model. A complex structure of bifurcations have been revealed with the electronic circuit and confirmed by the numerical simulations. We also proposed a method to design bursters based on the two-dimensional bifurcation diagrams. The burster is based on the analysis of the different bifurcations as one of the parameter is varied. We present the experimental results obtained with the circuit.
2. We introduce a bottom-up approach for the design and the analysis of the synthetic genetic networks. We have shown that the dynamics of the genetic networks can be simulated with analog electronic circuits. More in particular, we analyzed the paradigmatic genetic network called the repressilator which is a transcription oscillator designed in the laboratory. The synchronization of a population of repressilator has been achieved with the electronic circuit for a global coupling between units. Moreover, we have shown the possibility to control the population with a common external forcing. As an additional demonstration of the method we present two different genetic networks that can be also simulated with the same basic bricks of the circuit. These two networks are a genetic toggle switch, *i.e*, a bistable switch, and a delay oscillator based on the self-repression of one promoter.

3. We achieved an experimental investigation of synchronization of coupled systems with delay. We show that when a delay is present on a communication line, two chaotic oscillators cannot synchronize. However a singular regime appears. As a feedback is added to each unit the synchronization is achieved and we obtain the same dynamics at the same time despite the delay on the transmission line. This peculiar synchronization is explored more in detail as three oscillators are connected in line. In some of the dynamical regime the synchronization of the outer units is achieved while the third chaotic circuit is in advance. The isochronous state is obtained without the feedback, which is normally necessary to maintain synchronized the two circuits. The same result has been obtained if we change the nature of the third oscillator. We show experimentally the surprising fact that the isochronous state is obtained with a different chaotic oscillator in the middle.
4. We proposed a possible practical application of the phenomenon of isochronous synchronization of two coupled chaotic circuits with delay. We demonstrated how a bidirectional communication is possible when two chaotic circuits exchange signals over a communication channel. The chaotic masking scheme allows to send information within the spectrum of the chaotic carrier. This communication is shown to be practically feasible since we present the first experiment of this nature at the moment of the writing of the Ph.D. thesis.

Curriculum Vitae

PUBLICACIONES

- Isao Tokuda, Alexandre Wagemakers, and Miguel A. F. Sanjuán. “Synchronization prediction in a coupled electronic genetic network”. *Int. J. Bifurcation and Chaos* In preparation.
- Alexandre Wagemakers, Javier M. Buldú, Miguel A. F. Sanjuán, Oscar de Luis, Adriana Izquierdo and Antonio Coloma. “Entrainig synthetic genetic oscillators”. *J. Theor. Biol.*, (submitted).
- Alexandre Wagemakers, Javier M. Buldú, and Miguel A. F. Sanjuán. “Experimental demonstration of bidirectional chaotic communication by means of isochronal synchronization”, *Europhys. Lett.* **81**, 40005 (2008).
- Javier M. Buldú, Alexandre Wagemakers, Miguel A. F. Sanjuán, Antonio Coloma, and Oscar de Luis. “Redes genéticas sintéticas: De lo simple a lo complejo”. *Revista Española de Física* **21**, 10 (2007).
- Isao Tokuda, Alexandre Wagemakers, and Miguel A. F. Sanjuán. “Predicting synchronization of an electronic genetic network”. *Bussei Kenkyu* **87**, 550 (2007).
- Javier M. Buldú, Alexandre Wagemakers, Miguel A. F. Sanjuán, and Jordi García-Ojalvo. “Electronic design of synthetic genetic networks”. *Int. J. Bifurcation and Chaos* **17**, (10), 3507 (2007).
- Alexandre Wagemakers, Javier M. Buldú, and Miguel A. F. Sanjuán. “Isochronous synchronization in mutually coupled chaotic circuits”. *Chaos* **17**, 023128 (2007).

- Alexandre Wagemakers, Javier M. Buldú, Jordi García-Ojalvo, and Miguel A. F. Sanjuán. “Synchronization of electronic genetic networks”. *Chaos* **16**, 013127 (2006).
- Alexandre Wagemakers, José M. Casado, Miguel A. F. Sanjuán, and Kazuyuki Aihara. “Building electronic bursters with the Morris-Lecar neuron model”. *Int. J. Bifurcation and Chaos* **16**, 3617 (2006).
- Alexandre Wagemakers and Miguel A. F. Sanjuán, editors. Physics of Complex Systems and Life Sciences. Research Signpost, India, (2008). Note: ISBN:978-81-308-0170-4.
- Alexandre Wagemakers and Miguel A. F. Sanjuán. “Simulation of a genetic oscillator with electronic circuits” in Physics of Complex Systems and Life Sciences, 193. Research Signpost, India, ISBN:978-81-308-0170-4, (2008).

PRESENTACIONES EN CONGRESOS

- **Conferencia:** Nolineal 2004

Presentación tipo Póster: Diseño de un circuito electrónico para la modelización de una neurona

Autores: Alexandre Wagemakers , Borja Ibarz y Miguel A. F. Sanjuán

Lugar y Fecha: Toledo, del 1 al 4 de Junio de 2004

- **Conferencia:** La 8e Rencontre du Non Linéaire 2005

Presentación tipo Póster: Bifurcations dans un circuit électronique du neurone de Morris-Lecar

Autores: Alexandre Wagemakers, Miguel A. F. Sanjuán, José Manuel Casado y Kazuyuki Aihara.

Lugar y Fecha: Paris, Francia, del 9 al 11 de marzo de 2005

- **Conferencia:** Dynamic Days Berlin 2005

Presentación tipo Póster: Modelling synthetic genetic networks

Autores: Alexandre Wagemakers, Miguel A. F. Sanjuán, Javier Martín Buldú y Jordi García Ojalvo.

Lugar y Fecha: Berlin, Alemania, del 24 al 28 de julio de 2005

- **Conferencia:** Encuentro de Física de Sistemas Complejos y Ciencias de la Vida.
Ponencia: Alexandre Wagemakers, Miguel A. F. Sanjuán, José Manuel Casado y Kazuyuki Aihara.
Autores: Alexandre Wagemakers, Miguel A. F. Sanjuán, Javier Martín Buldú y Jordi García Ojalvo.
Lugar y Fecha: Aranjuez, del 21 al 22 de septiembre de 2006

- **Conferencia:** ECCB Madrid 2005
Presentación tipo Póster: Synthetic genetic networks: From genes to electronic circuits
Autores: Alexandre Wagemakers, Javier Martín Buldú, Jordi García Ojalvo y Miguel A. F. Sanjuán.
Lugar y Fecha: Madrid, del 28 de septiembre al 1 de octubre de 2005

- **Conferencia:** 9e Rencontre du Non-linéaire.
Ponencia: Des Circuits et des Gênes.
Autores: Alexandre Wagemakers, Javier Martín Buldú, Jordi García Ojalvo y Miguel A. F. Sanjuán.
Lugar y Fecha: Paris, del 9 al 11 de marzo 2006

- **Conferencia:** 14th Nonlinear Dynamics in Electronic Systems.
Ponencia: Entrainment by the cell cycle in genetic oscillator with delay
Autores: Alexandre Wagemakers, Javier Martín Buldú y Miguel A. F. Sanjuán.
Lugar y Fecha: Dijon, Francia, del 6 al 9 de junio de 2006

- **Conferencia:** Noise in Life.
Ponencia: Noise-induced frequency locking in a simple genetic oscillator.
Autores: Alexandre Wagemakers, Luonan Chen, Miguel AF Sanjuan y Kazuyuki Aihara.
Lugar y Fecha: Barcelona, del 15 al 17 de junio de 2006

- **Conferencia:** Encuentro Sobre Modelización de Sistemas Complejos.
Ponencia: Simulación de redes genéticas mediante circuitos electrónicos.
Autores: Alexandre Wagemakers, Miguel A. F. Sanjuán, Javier Martín Buldú y Jordi García Ojalvo.
Lugar y Fecha: Aranjuez, del 22 al 23 de septiembre de 2006

- **Conferencia:** International Workshop on synchronization: Phenomena and analyses.
Presentación tipo Póster: Predicting Synchronization of an Electronic Genetic Network
Autores: Isao Tokuda, Alexandre Wagemakers y Miguel A.F. Sanjuán
Lugar y Fecha: Tokio, Japón, del 2 al 3 de octubre de 2006

- **Conferencia:** Nolineal 2007.
Presentación tipo Póster: Sincronización isócrona de circuitos caóticos acoplados con retardos.
Autores: Alexandre Wagemakers, Javier Martín Buldú y Miguel A.F. Sanjuán.
Lugar y Fecha: Ciudad Real, del 6 al 9 de junio de 2007

- **Conferencia:** Nolineal 2007.
Presentación tipo Póster: Forzamiento de redes genéticas.
Autores: Alexandre Wagemakers, Javier Martín Buldú, Antonio Coloma, Oscar de Luís y Miguel A. F. Sanjuán.
Lugar y Fecha: Ciudad Real, del 6 al 9 de junio de 2007

- **Conferencia:** XXXI Encuentro Bienal de la Real Sociedad Española de Física.
Ponencia: Forzamiento de redes genéticas.
Autores: Alexandre Wagemakers, Javier Martín Buldú, Antonio Coloma, Oscar de Luís y Miguel A. F. Sanjuán.
Lugar y Fecha: Granada, del 10 al 14 de septiembre de 2007.

- **Conferencia:** Nolineal 2008.
Ponencia: Sincronización de una Población de Osciladores Genéticos

con Choques Térmicos.

Autores: Alexandre Wagemakers, Javier Martín Buldú, Miguel A. F. Sanjuán, Oscar de Luís, Adriana Izquierdo y Antonio Coloma.

Lugar y Fecha: Barcelona, del 16 al 19 de junio de 2008.

- **Conferencia:** XXXI congreso de la Sociedad Española de Bioquímica y Biología Molecular.

Presentación tipo Póster: Sincronización de redes genéticas sintéticas.

Autores: Oscar de Luís, Adriana Izquierdo, Javier Martín Buldú, Alexandre Wagemakers, Miguel A. F. Sanjuán y Antonio Coloma.

Lugar y Fecha: Bilbao, del 10 al 13 de septiembre de 2008.

ESTANCIAS DE INVESTIGACIÓN

- **Lugar:** Tokio, Japón

Centro y Departamento: Institute of Industrial Sciences, University of Tokyo, Aihara Laboratory.

Fecha: Octubre-Diciembre de 2004

Financiación: Propia

- **Lugar:** Tokio, Japón

Centro y Departamento: Institute of Industrial Sciences, University of Tokyo, Aihara Laboratory.

Fecha: Octubre-Diciembre de 2005

Financiación: Beca de ayuda a la movilidad de la URJC 2005

- **Lugar:** Boston, EEUU

Centro y Departamento: Applied Biodynamics Laboratory, Boston University.

Fecha: Octubre-Diciembre de 2006

Financiación: Beca de ayuda a la movilidad de la URJC 2006

- **Lugar:** Dijon, Francia

Centro y Departamento: Laboratoire LEII, Université de Bourgogne

Fecha: Abril de 2006

Financiación: Acción Integrada Hispano-Francesa HF04-173.

• **Lugar:** Dijon, Francia

Centro y Departamento: Laboratoire LEII, Université de Bourgogne

Fecha: Junio de 2006

Financiación: Acción Integrada Hispano-Francesa HF04-173.

• **Lugar:** Túnez, Túnez

Centro y Departamento: ETSI, Universidad del 7 de noviembre

Fecha: Junio de 2007

Financiación: PCI-Mediterraneo España-Túnez.

Resumen y objetivos de la tesis en castellano

Introducción

El presente trabajo de tesis doctoral propone una metodología de estudio de los sistemas dinámicos mediante el empleo de circuitos electrónicos analógicos. El creciente interés de la comunidad científica por los sistemas complejos es uno de los motores de esta tesis. Actualmente, se observa cada vez más una colaboración entre científicos de distintos campos debido a la necesidad de utilizar herramientas nuevas destinadas a problemas nuevos. Se detalla aquí una alternativa a las simulaciones numéricas clásicas: es decir al uso de ordenadores. Presentamos varios ejemplos de simulaciones con circuitos analógicos de sistemas complejos tan distintos como de una neurona o un oscilador genético.

La base de la modelización de los sistemas estudiados son las ecuaciones diferenciales ordinarias. Estas ecuaciones deterministas pueden representar la dinámica de los sistemas estudiados, su evolución temporal y los diferentes tipos de comportamientos en función de sus parámetros. Existen numerosas herramientas analíticas y computacionales para analizar el comportamiento de estos objetos. Presentamos y aplicamos algunos de estos métodos de simulación. Proponemos la simulación de las ecuaciones diferenciales de un sistema dado con el uso de circuitos electrónicos analógicos. Existe una analogía que permite pasar de un sistema de ecuaciones diferenciales a un conjunto de elementos electrónicos cuyos voltajes y corrientes representan las variables dinámicas originales. Muchos de los sistemas lineales y no lineales tienen su equivalente en circuitos electrónicos.

Objetivos

Los objetivos de esta tesis doctoral son múltiples y de naturaleza interdisciplinar. Como principales objetivos destacamos los siguientes puntos:

- Se propone el estudio de sistemas dinámicos complejos mediante el uso de circuitos electrónicos analógicos. Los modelos presentados aquí se basan en ecuaciones diferenciales de tres tipos: ecuaciones diferenciales ordinarias, ecuaciones diferenciales no autónomas y ecuaciones diferenciales con retardo. Estas tres clases de ecuaciones modelizan sistemas dinámicos procedentes de varias áreas de conocimiento como la dinámica neuronal, la biología sintética y la sincronización de osciladores caóticos.
- En el contexto de la dinámica neuronal se presenta un estudio exhaustivo de la dinámica de un modelo de neurona basado en el modelo de Morris-Lecar. Los diagramas de bifurcaciones del modelo se exploran para varios parámetros de control del sistema. Introducimos además una metodología para la construcción de una neurona de tipo burster a partir de los diagramas de bifurcación obtenidos.
- Dentro del ámbito de la biología sintética se propone un método para diseñar y simular redes de transcriptores genéticos. Se simula primero un oscilador genético llamado represilador, y se estudia la sincronización de una red de osciladores mediante los circuitos analógicos. Se introduce luego una perturbación periódica externa con el fin de sincronizar la población con y sin acoplamiento. Demostramos también la validez del método simulando otros dos ejemplos de red genética.
- El estudio de la sincronización de redes de osciladores caóticos acoplados con retardo es uno de los objetivos. Se presenta un estudio de los fenómenos de sincronización cuando existe un retardo en la línea de transmisión para dos y luego tres osciladores caóticos acoplados.
- Una vez estudiada la sincronización de dos osciladores con retardos se presenta la aplicación de estos fenómenos a las comunicaciones personales encriptadas. Se usan los circuitos caóticos con retardo para la transmisión de un mensaje de manera segura sobre un canal de comunicación no seguro.

Metodología

Hay varias definiciones de sistema complejo en la comunidad científica y existen diferentes definiciones de la complejidad en función del campo científico. En nuestro caso, un sistema complejo se compone de unidades elementales sencillas que pueden ser modeladas y simuladas individualmente. Estos componentes tienen dinámicas diferentes, y pueden incluso llegar a tener comportamientos sofisticados, tales como oscilaciones caóticas. Pueden ser estudiados con todas las herramientas disponibles de la dinámica lineal y no lineal. Sin embargo, una vez acopladas, estas unidades elementales interactúan unas con otras de forma muy compleja y no lineal. Los comportamientos colectivos pueden ser radicalmente diferentes cuando los componentes están conectados en una red. En ese caso, el estudio del sistema en su conjunto también es necesario, ya que comportamientos que no estaban presentes en los elementos individuales pueden aparecer ahora en un sistema conectado.

La metodología seguida en este trabajo consiste en el estudio o diseño de las partes individuales para luego ganar en complejidad a la hora de la interconexión de los diferentes elementos entre ellos. Este método se adapta perfectamente al empleo de circuitos electrónicos. El primer paso es construir los elementos básicos y estudiarlos a fin de caracterizar su comportamiento. Estos elementos básicos se reproducen y se interconectan entre sí con el fin de estudiar la dinámica en un nivel de complejidad superior.

Es preciso subrayar aquí que el método de diseño de un sistema de la parte más sencilla a la más compleja y organizada se llama el enfoque “de abajo hacia arriba” o “bottom-up approach”. Este es el procedimiento habitual en la ingeniería a la hora del proceso de diseño. El procedimiento científico tradicional está en el lado opuesto. Consiste en el estudio de un objeto de desde el mayor nivel de detalle hasta el más pequeño. Aquí proponemos un enfoque diferente que ha dado resultados fructíferos en campos tan diversos como la sincronización de osciladores caóticos o incluso en la ingeniería genética.

Resultados y Conclusiones

El estudio de la dinámica de sistemas complejos es un tema central de mi tesis doctoral. Hemos propuesto un planteamiento novedoso para su estudio con circuitos electrónicos. El uso de estos dispositivos presenta ventajas

en varios aspectos. Primero la simulación resulta muy modular, ya que se trata de ensamblar bloques para observar el resultado. La computación con electrónica analógica es mucho mas rápida que con un ordenador convencional. De esta forma se podrían simular redes de tamaño más grande. Por otra parte la simulación de sistemas con retardos es mucho más fiable con circuitos electrónicos. A continuación presentamos los resultados para cada parte obtenidos a lo largo del proceso de esta tesis doctoral realizada en el Departamento de Física de la Universidad Rey Juan Carlos:

- **Dinámica Neuronal**

En el Cap 2. presentamos la modelización electrónica de un modelo de neurona simple basado en el modelo de Morris-Lecar. Se ha hallado una estructura de bifurcación compleja con el circuito electrónico y luego confirmada con las simulaciones numéricas. También propusimos un método de diseño de neuronas de tipo burster basado en los diagramas de bifurcación en dos dimensiones. El “burster” es neurona especial cuyo comportamiento dinámico consiste en la alternancia de periodos de actividad breves espaciados por periodos de silencios. La esencia de la dinámica de éstas reposan sobre una biestabilidad del sistema. El método se basa en el análisis de las diferentes bifurcaciones cuando los parámetros del sistema varían y se apuntan los comportamientos biestables. Se presentan los resultados experimentales obtenidos con el circuito.

- **Simulación analógica de redes genéticas**

Se introduce un enfoque “de abajo hacia arriba” en el Cap. 3 para el diseño y el análisis de redes genéticas sintéticas. Hemos mostrado que la dinámica de las redes genéticas se pueden simular con los circuitos electrónicos analógicos. Más precisamente, hemos analizado la red genética paradigmática llamada represilador. Es un oscilador de transcripción diseñado en laboratorio con componentes procedentes de varios organismos y ensamblados en una bacteria. La expresión de los genes oscila en el tiempo en las bacterias individuales. La sincronización de una población de represiladores se ha logrado con circuitos electrónicos mediante un acoplamiento global entre las unidades. Además se demostró la posibilidad del control de la población con un forzamiento externo común. Como una demostración más del método, se presentan dos redes génicas diferentes que también pueden ser simuladas con los mismos bloques de base del circuito. Estas dos redes son

un interruptor biestable genético, y la otra un oscilador basado en el retardo de la auto-represión de un promotor.

- **Sincronización de osciladores con retardos**

En el Cap. 4 estudiamos la sincronización isócrona (es decir, sin retraso entre los sistemas sincronizados) de circuitos caóticos acoplados bidireccionalmente. Cuando dos circuitos caóticos se sincronizan mediante acoplamiento mutuo, se observa que no hay sincronización a tiempo cero debido al tiempo que tarda la señal en ir de un circuito a otro. Como consecuencia, aparece una alternancia en la sincronización, es decir uno de los dos circuitos avanza al otro y transcurrido un cierto tiempo los papeles se intercambian. Sin embargo, cuando se introduce un tercer circuito entre los dos sistemas anteriores podemos observar como las dos unidades externas se sincronizan sin retraso alguno. Curiosamente, el sistema intermedio puede tener una dinámica distinta de los dos sistemas entre los que está mediando. Finalmente, demostramos experimentalmente que también es posible sincronizar dos circuitos si se les añade también una realimentación con retraso.

- **Aplicación de la sincronización con retardos a las comunicaciones**

Se propone en el Cap. 5 una posible una aplicación práctica del fenómeno de la sincronización isocrona de dos sistemas caóticos acoplados con retraso. En este capítulo investigamos la posibilidad de una comunicación bidireccional cuando dos circuitos caóticos intercambian señales en un canal de comunicación. El enmascaramiento caótico permite enviar información escondida en el espectro de la portadora caótica. Este tipo de comunicación se puede llevar en la práctica. Además presentamos aquí el primer experimento de esta naturaleza hasta el momento de la redacción.